UNIVERSITY OF OKLAHOMA

GRADUATE COLLEGE

DIFFERENTIAL CONTRIBUTIONS OF OUTER MEMBRANE PERMEABILITY AND ACTIVE EFFLUX IN PHYSIOLOGY AND DRUG SUSCEPTIBILITY OF GRAM-NEGATIVE BACTERIA

A DISSERTATION

SUBMITTED TO THE GRADUATE FACULTY

in partial fulfillment of the requirements for the

Degree of

DOCTOR OF PHILOSOPHY

By

DAVID WOLLOSCHECK
Norman, Oklahoma
2017

DIFFERENTIAL CONTRIBUTIONS OF OUTER MEMBRANE PERMEABILITY AND ACTIVE EFFLUX IN PHYSIOLOGY AND DRUG SUSCEPTIBILITY OF GRAM-NEGATIVE BACTERIA

A DISSERTATION APPROVED FOR THE
DEPARTMENT OF CHEMISTRY AND BIOCHEMISTRY

BY

_____
Dr. Helen Zgurskaya, Chair

_____
Dr. Valentin Rybenkov

_____
Dr. Anthony Burgett

_____
Dr. Michael Ashby

_____
Dr. Marc Libault

Dedicated to my family, who has supported me through this journey, loved me, and always gave me the advice I needed to succeed.

Acknowledgements

I sincerely enjoyed my time at OU and I would like to thank everyone that was part of my time here. This includes first and foremost all the members of the Zgurskaya lab. You guys have always been there with good advice and have become truly great friends to me. I will miss each and every one dearly and the time we spent together. Especially the fun times during lunch breaks of course ("lunch, lunch, lunch?!"). I also would like to thank my committee for their advice and guidance during my time in graduate school. You helped me to grow as a scientist and to always be critical. It also includes the undergraduates I was lucky enough to mentor and guide in the lab. You showed me the joy and rewarding experience of teaching.

I would like to specifically thank Dr. Ganesh Krishnamoorthy who was actively involved in several experiments and for his work in creating some of the strains used in this study. Furthermore, I want to thank Jennifer Nguyen for her help with antibiotic susceptibility testing and in carrying out some of the physiology assays.

Of course, I would not have been able to finish this journey without the help of my parents. I am so thankful for your words of encouragement and the love you show me every day. Thank you for always pushing me forward and being the moral compass in my life. You encouraged me to ask questions and to always be curious.

Special thanks have to go to my mentor, Dr. Helen Zgurskaya. You have developed me into the best possible scientist I could become and taught me to ask the right questions. You always guided me with warmth and humor, and showed me when to question or trust a result. I am so grateful to have had such a great mentor who is truly passionate about her work.

Most importantly though, I have to thank my wife Jessica. Without your help, this wouldn't have been possible, and I'm eternally grateful for your support and love. Thank you for celebrating the good times with me and lifting me up during bad times. I love and cherish you every day.

Table of Contents

List of Tables

List of Figures

Abstract

The increased frequency of antibiotic resistant bacterial isolates is of great concern for public health. It is currently estimated that infections caused by multidrug resistant pathogens will surpass cancer as a leading cause of death by 2050 (1). Of particular concern are gram-negative bacteria, due to their robust intrinsic resistance provided by a low permeability outer membrane barrier in combination with active efflux. Active efflux is mainly mediated by Resistance-Nodulation cell Division (RND) transporters, which associate as tripartite complexes that facilitate the export of substrates across the outer membrane. These two mechanisms of resistance work in synergy to efficiently limit intracellular accumulation of antibiotics. This directly results in very low hit rates during antimicrobial screenings and presents unique challenges in the development of antibiotics.

In addition to providing resistance, RND transporters are also involved in the physiology of bacteria. *Pseudomonas aeruginosa* possesses twelve RND transporters of which three are indicated to be involved in its quorum sensing networks. Overexpressing or deleting the genes of these transporters has a great physiological impact and can result in a loss of virulence or extended lag phases during growth. In many cases, the endogenous substrates of these transporters are not known and their impact on the physiology of the cell is not well understood.

This dissertation focuses on the interplay between the low permeability outer membrane and active efflux in drug resistance and their contribution to physiology of *P. aeruginosa*. Current methods to investigate the contributions of the outer membrane barrier in drug resistance, like the use of polymyxins to permeabilize the outer

membrane, have many disadvantages. Here, we developed a novel approach to separate the contributions of efflux and the outer membrane in antimicrobial susceptibility by introducing a genetically modified pore that non-selectively increases the permeability of the outer membrane. In combination with the removal of efflux transporters, this hyperporination approach highlights the synergy of the outer membrane and efflux, and has potential implications for the development of new antibiotics. It could provide the means to discover new rules in drug design that predict the uptake of a compound into the gram-negative cell according to its structural features.

Furthermore, this dissertation will characterize the contributions of the RND transporter MexGHI-OpmD from *P. aeruginosa* in the physiology and antimicrobial resistance of the bacterium. Our results suggest that the transporter is involved in establishing the steady-state concentrations of the important virulence factor pyocyanin. In addition, we showed that the unusual fourth component MexG physically interacts with the transporter and that its presence results in inhibition of the efflux activity towards certain substrates. Our results suggest that the activity of RND transporters are masked by the presence of the outer membrane and that hyperporination highlights the actual transport efficiencies of these pumps. RND transporters heavily rely on the outer membrane barrier, and this hyperporination approach could be used to re-evaluate their substrate specificities.

I: Introduction

Bacterial infections are as old as mankind itself. From the bubonic plaque, to leprosy, to malaria, and tuberculosis bad bugs have been the cause of many epidemics and millions of lives lost. Alexander Fleming discovered penicillin in the mid-1900s and with it the ultimate weapon to fight bacteria. As antibiotic discovery accelerated it seemed like only a matter of time until these diseases would disappear forever. With the onset of antibiotic resistance, however the idea of eradicating these pathogens has become less likely. Decades of misuse of antibiotics in farming and overprescribing by doctors constantly put selective pressure on bacteria to develop sophisticated resistance mechanisms. Today, the threat of multidrug resistant (MDR) superbugs is more real than ever. A recent discovery in a US hospital of a *Escherichia coli* strain resistant to carbapenems as well as the last resort antibiotic colistin shows how close we are to bacteria that are completely resistant to all conventionally used antimicrobials (2). In the US alone, current estimates range from a $21 to $34 million in health care costs, and even a decrease in the GDP by 0.4% to 1.6% due to the increased recovery time of patients (3). A report by the UK government estimated that by 2050 as many as 10 million people will die from diseases caused by multidrug resistant bacteria, passing even cancer with a projected 8.1 million deaths (1). To make matters worse, current antibiotic discovery has slowed down dramatically with the last class of antibiotics, the cyclic lipopeptides, discovered in the late 1980s (3). It has become clear that we will lose the race against fast evolving superbugs without any significant innovations in the field.

There are several mechanisms by which cells can become drug resistant. Bacteria can modify the target of a particular antimicrobial through a single point mutation and this way reduce binding of the drug to its target (4). In addition to mutations of the target, bacteria also modify them by, for example, methylation which can prevent binding of the drug (4). Another clinically relevant mechanism of drug resistance is modification of the antibiotic itself (4). Bacteria express enzymes that can hydrolyze or acetylate antibiotics rendering them ineffective. Genes expressing these enzymes are often rapidly spread to entire populations through horizontal gene transfer and are a major area of research. However, arguably the most effective way for cells to become resistant against multiple classes of antibiotics is by decreasing the permeability of the cell envelope by modifying the cell membrane in combination with active drug efflux.

This is especially true for gram-negative bacteria and their highly impermeable outer membranes (5). In contrast to gram-positive bacteria, the cell envelope of gram-negatives is made up of two distinct membranes. The inner membrane and the inner leaflet of the outer membrane are mainly made up of phospholipids that provide good protection for hydrophilic molecules to enter the cell. The outer leaflet of the outer membrane consists of lipopolysaccharides (LPS), which due to the presence of large polar sugar groups is highly hydrophilic. LPS reduces the permeation of hydrophobic molecules, which encompasses a large part of antibiotics. This combination makes it incredibly difficult for drugs to reach their target and carry out their activity.

In addition to this low permeability of the outer membrane, gram-negative bacteria also have several efflux transporters. The class of transporters that is most

commonly associated with antibiotic resistance in bacteria are RND type transporters. They are tripartite protein complexes that span the entire cell envelope, allowing them to export substrates across the outer membrane and out of the cell. This feature leads to a synergistic effect with the low permeability barrier of the outer membrane and makes infections of gram-negative bacteria incredibly hard to treat.

It is no surprise that the three bacterial species that make up the priority one group for the development of new antibiotics of the World Health Organization are highly resistant gram-negative bacteria (6). The most critical species are *Acinetobacter baumannii*, *Pseudomonas aeruginosa*, and some carbapenem resistant *Enterobacteriaceae* (6). Drug development for gram-negatives specifically also provides extra challenges. The low permeability of these bacteria poses a big challenge in drug screening, decreasing the hit rate of compounds by up to a staggering 1,000-fold (7). Taken together, multidrug resistant gram-negative pathogens represent a tremendous challenge for the scientific community, and new ways to treat such infections are desperately needed.

This dissertation will focus on understanding the interplay of outer membrane permeability and active efflux of the gram-negative, opportunistic pathogen *P. aeruginosa*, and on characterization of the *P. aeruginosa* RND transporter MexGHI-OpmD and its impact on drug resistance and physiology. *P. aeruginosa* most infamous for nosocomial diseases and lung infections in cystic fibrosis patients (8). Infections can be acute or chronic and are difficult to treat due to the high intrinsic resistance of the bacterium. Acute infections are caused by planktonic cells, which typically invoke a severe immune response in the patient (9). The most effective class of antibiotics used

against these infections are fluoroquinolones (10, 11). In cases of multidrug resistant strains, patients undergo either a continuous infusion of meropenem, treatment with colistin, or polymixin B (12), all of which are considered last resort antibiotics. Chronic infections are caused by colonization of *P. aeruginosa* grown as biofilms, which are made up of exopolysaccharides, extracellular DNA, and proteins (9, 13). This structure provides an additional layer of resistance for the pathogen due to the high rate of persister cells and the slow mode of growth (14). The increased frequency of multidrug resistant isolates of *P. aeruginosa* is of great concern and necessitates the discovery of new approaches to combat the pathogen (6, 15-17).

I.1: Structure and properties of the bacterial outer membrane

Intrinsic resistance in gram-negative pathogens is mainly mediated by the structure and composition of the outer membrane and active efflux. The bacterial outer membrane is quite different from the inner membrane (Fig. I.1). The inner leaflet of the outer membrane, like the bacterial inner membrane, consists mainly of phospholipids. What makes the outer membrane distinctly different is the outer leaflet, which is made up of lipopolysaccharides (LPS). LPS is well known for its toxic effects, as it is sometimes referred to as endotoxin. It can invoke severe immune responses in mammalian hosts and lead to septic shock (18). However, it also plays a big role in the structure of the cell envelop of gram-negative bacteria. The asymmetric bilayer of LPS and phospholipids makes gram-negative bacteria uniquely impermeable (5). The structure of LPS has been studied extensively (19-28). LPS consists of lipid A, an inner and an outer core, as well as a large stretch of polysaccharides referred to as O-antigen.

Lipid A typically consists of two phosphorylated glucosamine moieties that are N- and O-acylated (26). The exact structure of lipid A can vary between bacterial species. In *P. aeruginosa*, the major forms are hexa- and penta-acylated lipid A (19, 21). Variations in the acylation occurs as a result of different growth conditions, such as the amount of available Mg^{2+} in the environment (19). The acyl chains are either 10 or 12 carbons in length and form the hydrophobic portion of the molecule (26). The acylation pattern and length of the acyl tails differ in other species. *E. coli*, for example, utilizes 12 to 14 carbon acyl chains and is typically hexa-acylated (25).

The inner core of LPS is generally comprised of two α-3-deoxy-D-manno-oct-2-ulosonic acid (Kdo) and two L-glycero-D-manno-heptose (Hep) residues covalently linked to the glucosamine residues of lipid A (26). The second Hep residue of the inner core of *P. aeruginosa* has a carbamoyl group attached at the O-7 position, which appears to be unique to pseudomonads (24). In addition, the Hep residues are extensively phosphorylated by mono-, di-, and even triphosphate groups, which have been implicated in intrinsic resistance of *P. aeruginosa* (27, 28). The outer core consists mainly of D-galactosamine, D-glucose, and L-rhamnose residues with a characteristic L-alanyl group acylation at the D-galactosamine for *P. aeruginosa* (26).

The O-antigen is a relatively large structure of different amino saccharides and can vary significantly between different isolates of *P. aeruginosa*. There are currently 20 accepted serotypes of *P. aeruginosa* strains based on variability of the O-antigen (22, 23). Notably, *P. aeruginosa* isolates found in cystic fibrosis lungs largely lack the O-antigen altogether (20). LPS lacking the O-antigen are commonly referred to as “rough” LPS.

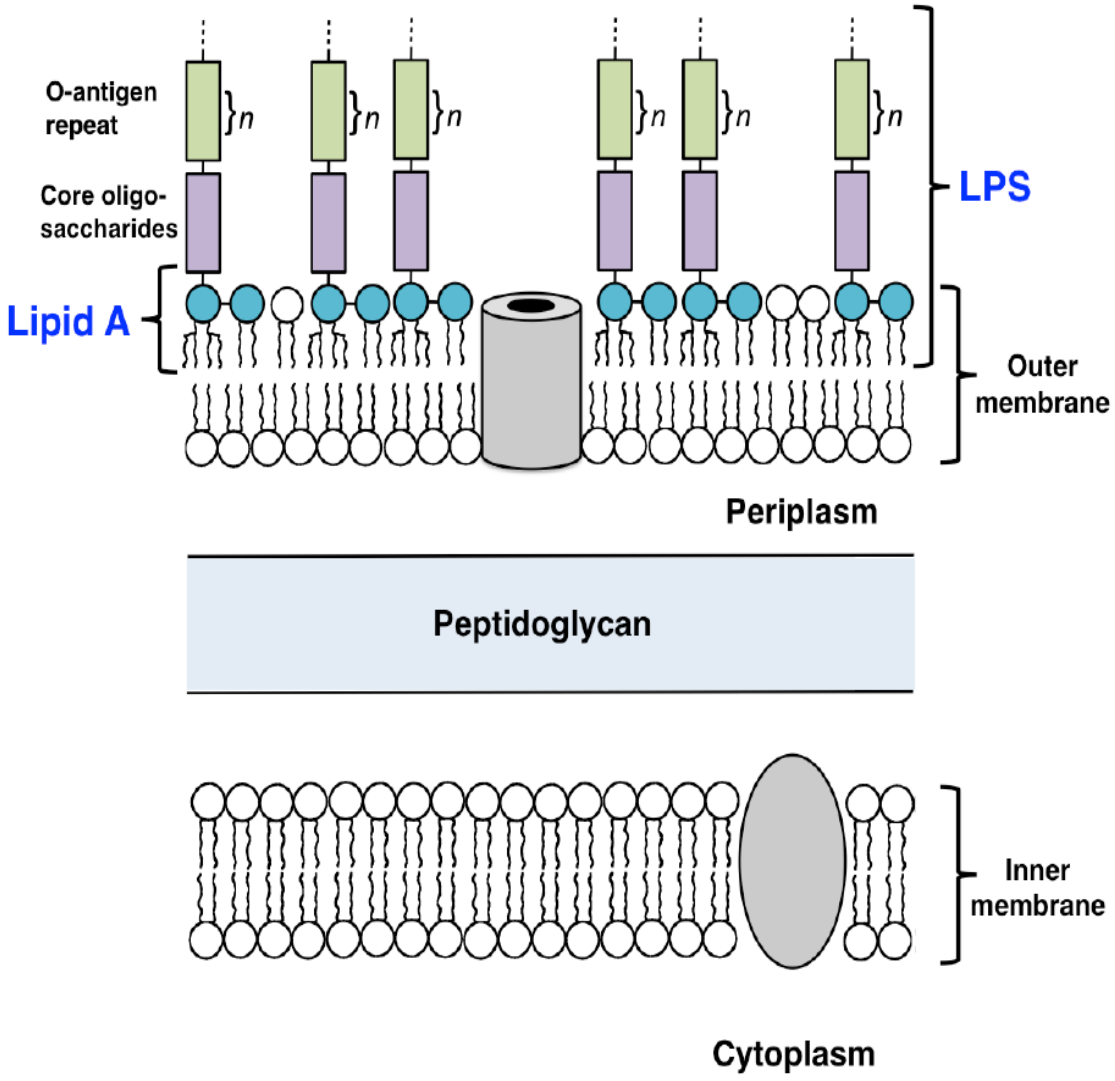

Figure I.1 - The gram-negative cell envelope.

Illustration of the cell envelope of gram-negative bacteria. Transmembrane structures in grey represent integral membrane proteins. Figure modified from Metzger et al., 2012 (29).

Taken together, LPS is a large and mostly polar structure that provides significant protection from hydrophobic molecules, which are thought to enter the cell through passive diffusion across the cell envelope. The outer membrane, with its asymmetric arrangement of LPS on the outer leaflet and phospholipids on the inner leaflet, forms a formidable barrier for a wide range of compounds and is one of the main reasons why gram-negative bacteria possess such high levels of intrinsic resistance.

I.2 Outer membrane porins of gram-negative bacteria

Despite this low permeability of the outer membrane, gram-negative cells are still able to take up nutrients for their metabolism. This is mainly achieved through passive diffusion through outer membrane porins (30). These porins can be specific, like the maltoporin LamB from *E. coli*, or general porins that have no substrate binding site (31). Specific porins usually have a binding site for their respective substrate whereas general porins do not (30). The most well-known general porins are OmpF and OmpC from *E. coli*. Their exclusion size largely dictates the permeability of the cell envelope for hydrophilic molecules and for OmpF is estimated to be about 600 Da (5, 31). In contrast to *E. coli*, *P. aeruginosa* largely lacks general porins. It expresses so-called "slow porins" that are non-specific but with much smaller exclusion limits (5, 30). The main slow porin in *P. aeruginosa* is OprF with an estimated exclusion size of about 200 Da (5, 30). The differences in outer membrane porins has a dramatic effect on permeability. It is estimated that the relative permeability of the cell envelope of *P.*

aeruginosa is only 1-8% when compared to *E. coli* (32). This underlines the stark differences between these bacteria and highlights the difficulties in designing antipseudomonal drugs.

I.3 MDR transporters in bacteria

In bacteria, multidrug resistance transporters generally belong to one of five superfamilies of proteins: the Major Facilitator Superfamily (MFS), the Multidrug Toxic Compound Extrusion (MATE) superfamily, the Small Multidrug Resistance (SMR) superfamily, the ATP-Binding Cassette (ABC) superfamily, and the Resistance Nodulation cell Division (RND) superfamily (33). These transporters differ in their structure, energy dependence, composition, and substrate specificities (34-38). They are all located in the inner membrane and generally follow the same mechanistic principles of substrate binding, reorienting of the substrate towards the periplasm, and releasing the substrate based on reduced affinity to the transporter after the conformational change. The families are broken down into primary and secondary transporters. ABC transporters are the only primary transporters and utilize ATP to facilitate efflux (34). MFS, SMR, MATE, and RND transporters all use a chemical gradient, mostly protons and sodium ions, to drive their conformational changes (33). In gram-negative bacteria, MDR transporters can associate with so called membrane fusion proteins (MFP) and outer membrane factors (OMF) to form a complex that spans the entire cell envelope.

RND transporters are the most commonly associated with clinical drug resistance in gram-negative bacteria. This is mostly due to their very broad substrate specificity and because they are almost always found in complexes with MFPs and

OMFs, allowing them to translocate substrates across the outer membrane into the extracellular space (33, 38). Transport across the outer membrane coupled with its low permeability leads to powerful and synergistic resistance mechanism.

The chromosome of *P. aeruginosa* specifically encodes for at least twelve RND transporters, many of which are constitutively expressed (39). The most clinically relevant transporters are MexAB-OprM(40), MexCD-OprJ (41), MexEF-OprN (42, 43), and MexXY (43). They generally have a very broad substrate specificity and are frequently found to be overexpressed in clinical isolates (43). MDR transporters contribute tremendously to the resistance of *P. aeruginosa* and, consequently, considerable effort is dedicated to finding inhibitors of efflux pumps (44). Some efflux pump inhibitors (EPIs) like PAβN have already been described and show promising results (45). However, EPIs are not available in clinical settings yet and more work is necessary to discover new targets and mechanisms of EPIs.

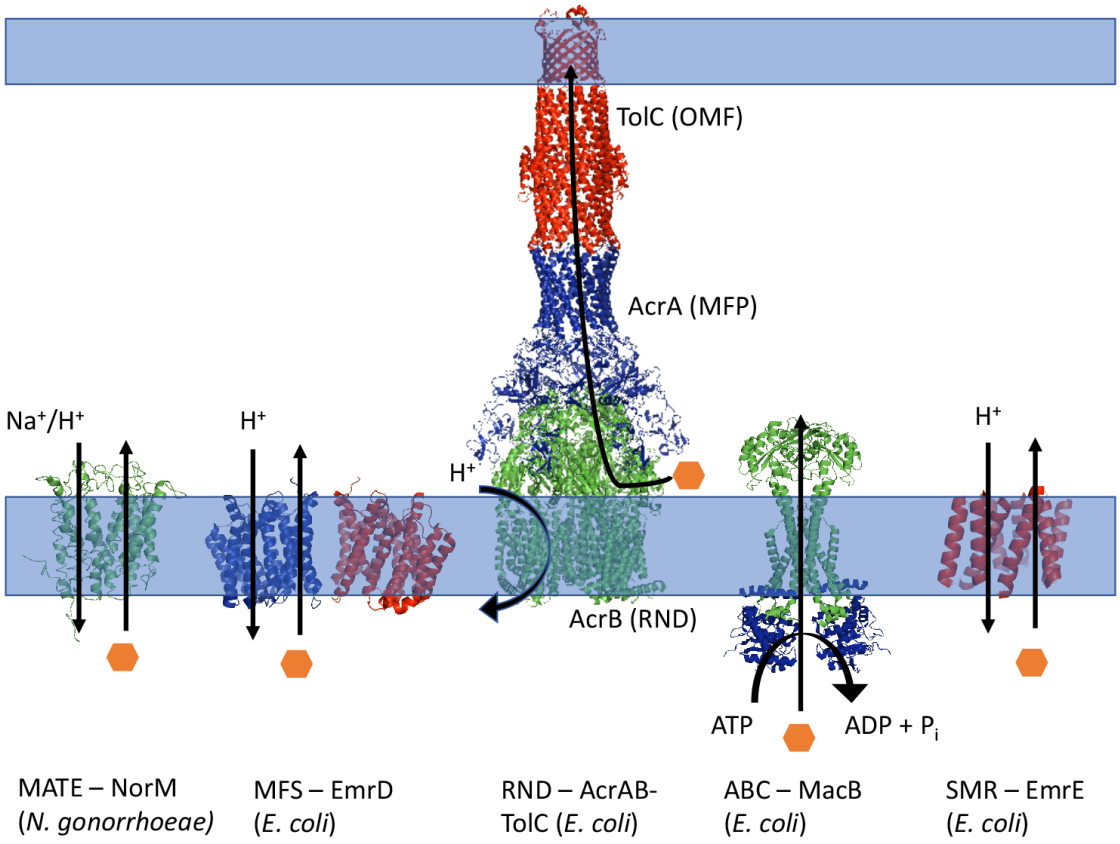

Figure I.2 - Types of bacterial MDR transporters.

Representatives of the five MDR superfamilies from gram-negative bacteria. Although only AcrB is shown in complex with MFP and OMF, MFS and ABC transporters can also form tripartite complexes (46, 47). MFS transporters are thought to act as monomers, however are sometimes found as dimers (48). Areas shaded in blue indicate the inner and outer membrane, and substrates are indicated as orange hexagons. Structures modified from PDB files 4HUK (NorM, Lu et al. (49)), 2GFP (EmrD, Yin, et al. (50)), 5O66 (AcrAB-TolC, Wang, et al. (51)), 5NIK (MacB, Fitzpatrick, et al. (52)), and 2I68 (EmrE, Fleishman, et al. (53)).

I.4 Mechanism of RND transporters

RND transporters work in concert with membrane fusion proteins (MFPs) and outer membrane channels (OMFs) to expel their substrates out of the cell. This tripartite complex is critical to provide efflux across the bacterial outer membrane. Every part of the complex is essential, and a deletion of one component completely abolishes the activity of the transporter (54, 55). Interactions between the transporter, the MFP, and the OMF are strong, so that the components are frequently co-purified together (56, 57). The fully assembled complex spans the entire cell envelope, allowing it to expel substrates from the inner membrane, or the interphase between the periplasm and the inner membrane, across the outer membrane (58). This is cause for significant synergy between the efflux pump and the low permeability outer membrane. RND transporters are secondary transporters and use the proton motive force to supply the energy needed to translocate substrates (38). The most well-known members of this family are AcrAB-TolC from *E. coli* and MexAB-OprM from *P. aeruginosa*. They share a high sequence homology and both provide resistance to a broad spectrum of antibiotics (59).

The RND component of the complex is located in the inner membrane. It associates as a trimer, with each monomer containing 12 transmembrane α-helices (TM) and two large periplasmic loops (38). The RND protein is usually divided into the transmembrane domain, the porter domain, and the docking domain (Fig. I.3) (60). The transmembrane domain anchors the transporter into the inner membrane and contains the residues needed for the proton relay network. There are typically two highly conserved aspartic acid residues and one lysine residue on TM4 and TM10, which facilitate the movement of protons from the periplasm to the cytoplasm (38). This

results in a conformational change in the transmembrane domain, which ultimately facilitates the transport reaction. The porter domain is subdivided into PN1, PN2, PC1, and PC2 domains, each of which contains four to five β-strands forming an antiparallel β-sheet and two α-helices (60). It contains the proximal and the distal binding pockets that are separated by a switch-loop (61). Both pockets are typically rich in phenylalanines and other hydrophobic residues, making them ideal to non-specifically bind many different hydrophobic antibiotics and other compounds (62). The docking domain forms a funnel like structure which guides the substrates towards the OMF for transport out of the cell (60).

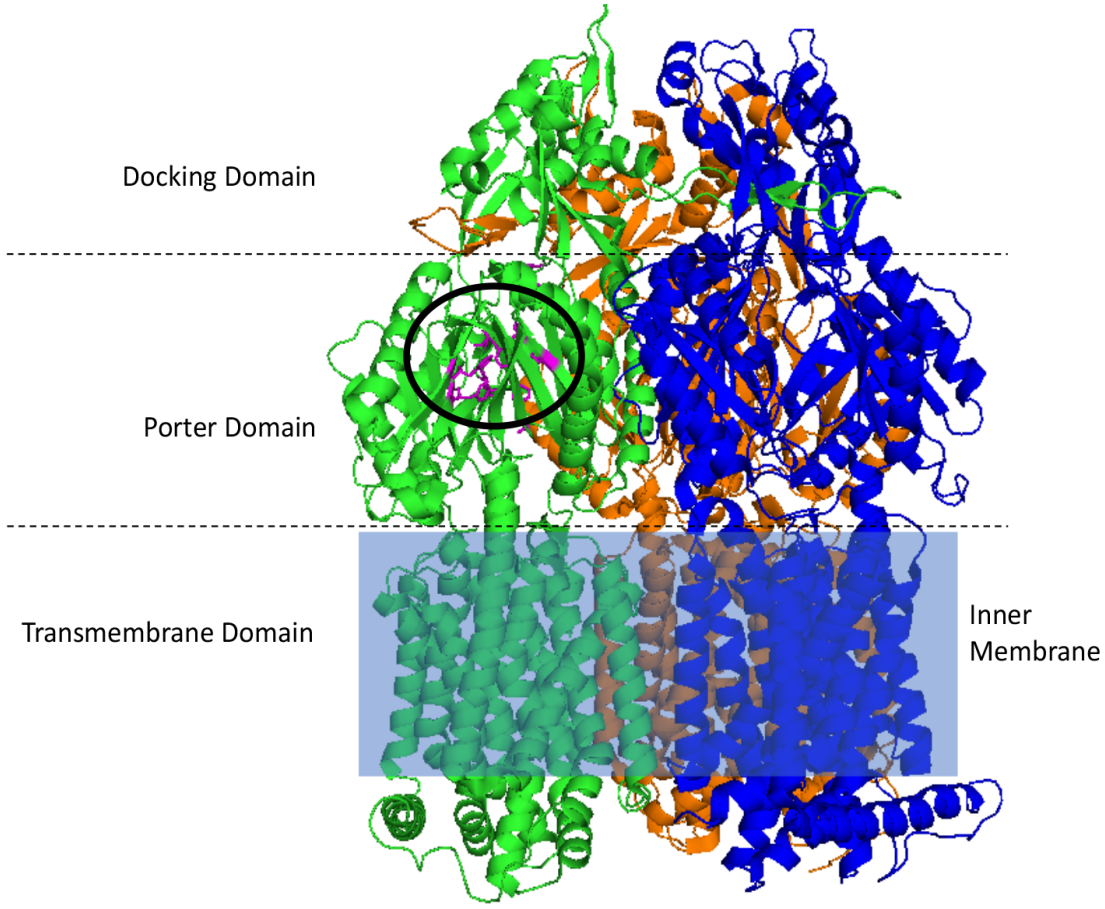

Figure I.3 - Structure of RND transporters.

Side view of the RND transporter AcrB from *E. coli*. Each monomer is shown in a different color. Dotted lines separate the three different domains. Inner membrane is indicated by the blue shaded area. Residues of the substrate binding pocket are shown in magenta and circled. Modified from PDB 2GIF (Seeger, et al. (63)).

RND transporters facilitate the transport reaction through an asymmetric functional rotating mechanism (60). Each protomer is generally present in one of three conformations and will switch between the “loose” or “access” form, the “tight” or “binding” conformation, or the “open” or “extrusion” form (38). Each conformer differs slightly in the structure of the binding pockets and the protonation state of the proton relay network in the transmembrane domain. The changes in the binding pockets effectively guide the substrate from the proximal pocket to the distal pocket and ultimately out of the transporter through the docking domain (62). Substrates are thought to enter the binding pockets close to or at the interphase between the periplasm and the inner membrane via an access tunnel and are moved through the transporter by a peristaltic pump like mechanism, which is energized by the movement of protons in the transmembrane domain (60).

I.5 Membrane fusion proteins connect the RND transporter to the OMF

MFPs, also sometimes called periplasmic adaptor proteins, form a link between the RND transporter and the OMF. They consist of four distinct domains and like RND transporters are a peptide strand folded onto itself, which is likely the result of a gene duplication event. MFPs consist of a membrane proximal domain, a β-barrel domain, a lipoyl domain, and a α-hairpin domain (Fig. I.4) (64). Additionally, some MFPs, like MexH of MexGHI-OpmD, possess a lipid modification at the membrane proximal domain embedding the peptide into the inner membrane (65). The membrane proximal domain and the β-barrel domain are thought to interact with the RND transporter, whereas the α-hairpin domain binds to the OMF (64). Between domains is a stretch of

unstructured amino acids, making the overall structure of MFPs highly flexible (66). It is thought that they transfer the energy from conformational changes in the RND transporter during transport to the OMF (67). This ultimately causes the OMF to open, allowing for substrates to leave the cell (68). There was much debate on whether MFPs associate as timers or hexamers. To date, the most widely accepted quaternary structure is a trimer of dimers or a hexamer (69-71). In the oligomeric state, MFPs are thought to form a funnel like structure that surrounds the docking domain of RND transporters and parts of the OMF (70).

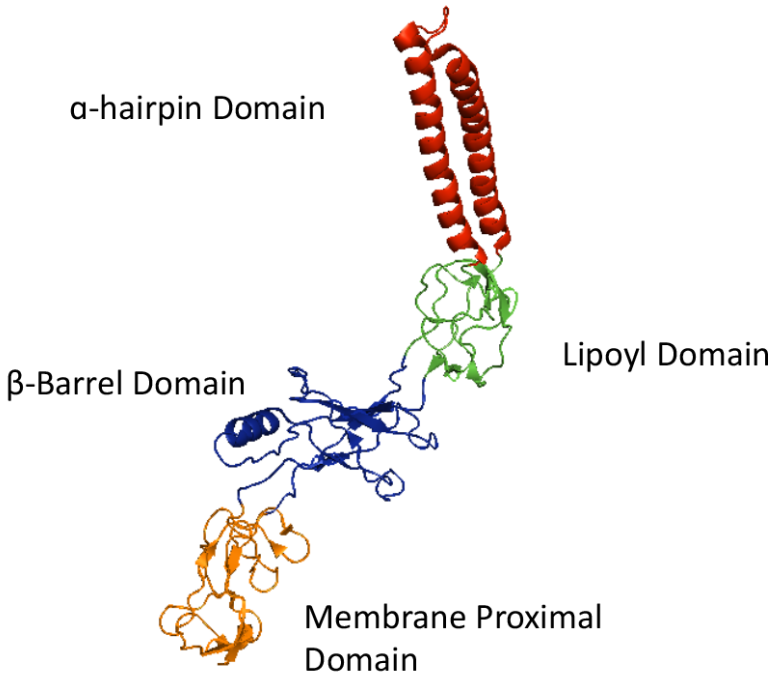

Figure I.4 - Four domains of membrane fusion proteins (MFPs).

Crystal structure of the membrane fusion protein AcrA from *E. coli*. Each domain is shown in a different color. Unstructured stretches of amino acids between the four domains result in a highly flexible structure. Structure modified from PDB 5O66 (Wang, et al. (51))

I.6 Outer membrane factors guide substrates out of the cell

OMFs are channel proteins that are inserted into the outer membrane of gram-negative bacteria. They are typically promiscuous and can interact with different types of transporters. *E. coli*'s main OMF TolC, for example, interacts with at least nine transporters, making a *tolC* mutant highly susceptible to many different antibiotics (72). OMFs are not unique to RND transporters. They can also be found in transporters from the major facilitator and ATP binding cassette families, usually accompanied by MFPs to facilitate the interaction (72). OMFs consist of three domains and associate as a homotrimer (Fig. I.5) (70). The β-barrel domain is embedded into the outer membrane and forms the pore that allows substrates to leave the cell (73). This directly follows the α-barrel domain, which stretches far into the periplasm (70). Each protomer forms four large α-helices that are interrupted briefly by short β-strands that make up the equatorial domain in the center of the α-barrel domain (70). The end of the α-barrel domain forms a type of iris that is closed when the OMF is not engaged by a transporter (73). It is thought that interaction of the docking domain of RND transporter engages and opens the channel, allowing for substrates to be expelled (55, 73). However, other studies suggest that the RND transporter and the OMF do not directly contact each other (74). Furthermore, ABC and MFS transporter lack large periplasmic domains that could contact the OMF, suggesting that the opening of the OMF is mediated by the MFP (75).

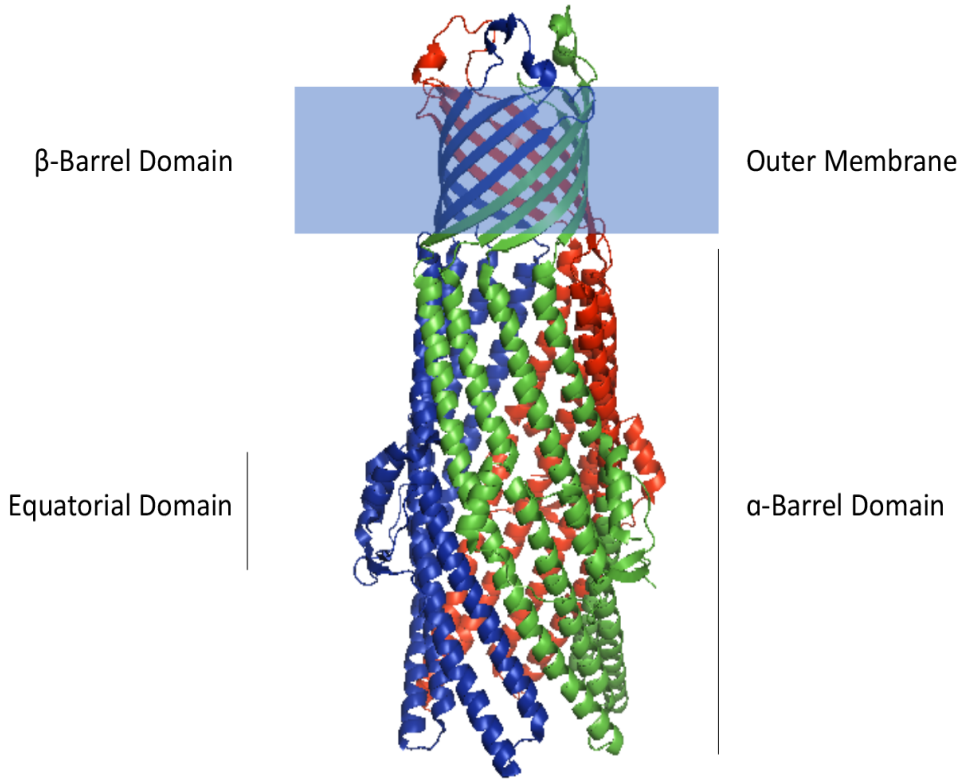

Figure I.5 - Structural features of outer membrane factors.

Outer membrane factors associate as trimers and consist of three different domains. Each monomer is shown in a different color. TolC is shown in the open conformation. Outer membrane is indicated by the blue shaded area. Structure modified from PDB 5O66 (Wang, et al. (51)).

I.7 Quorum sensing and the role of efflux pumps in virulence of *P. aeruginosa*

In *P. aeruginosa*, genes responsible for virulence and biofilm formation are tightly regulated by a complex network of transcription factors and transcriptional activators that are activated once a certain cell density is reached (Fig. I.6) (76). This type of cell-to-cell communication, which is commonly referred to as quorum sensing, is critical to orchestrate gene expression across a cell population and to initiate the production of virulence factors like pyocyanin, rhamnolipids, and elastase (13, 76). Quorum sensing signaling pathways are hierarchically ordered and start with the *las* and *rhl* systems, which are homologous to the LuxI/LuxR signaling mechanism in *Vibrio fischeri* (Fig. I.6) (76, 77). The family of LuxI type proteins are acyl homoserine lactone (AHL) synthases, which synthesize AHLs by catalyzing the acylation of S-adenosylmethionine via an acyl carrier protein (76, 77). The synthesized AHLs are typically excreted into the extracellular space and serve as signaling molecules (76). Once the extracellular concentration is high enough, they will bind to their respective cytoplasmic LuxR type receptors which, in turn, upregulate expression of certain genes (78). In *P. aeruginosa*, the *las* and *rhl* system synthesize the signaling molecules N-(3-oxododecanoyl)-L-homoserine lactone (3OC12-HSL) and N-butanoyl-L-homoserine lactone (C4-HSL) respectively (76). The other major signaling pathway of *P. aeruginosa* is through the Pseudomonas Quinolone Signal (PQS). PQS is synthesized by *pqsABCDH* and its corresponding receptor is PqsR (77). The *las* system upregulates PQS synthesis, whereas the *rhl* pathway downregulates it (Fig. I.6) (77). This highlights the complexity and the way these pathways are interconnected. Activation of PqsR results in the expression of many virulence factors including pyocyanin (76).

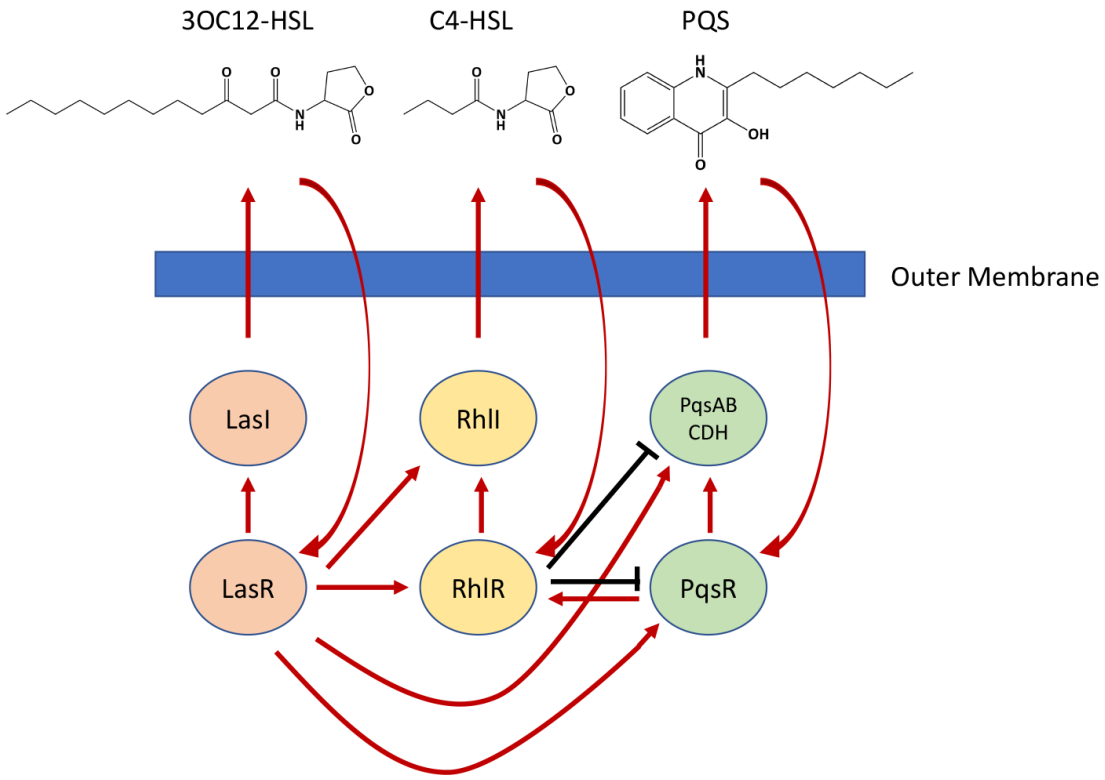

Figure I.6 - Quorum sensing network in *P. aeruginosa*.

The major quorum sensing pathways in *P. aeruginosa* and their corresponding signaling molecules. Arrows in red indicate upregulation and black lines repression.

Quorum signaling molecules are of great importance for virulence and biofilm formation, and cells require careful regulation of these molecules. Some RND transporters were found to be involved in excretion of these molecules, highlighting the importance of these efflux pumps outside of the removal of toxic compounds. So far, MexAB-OprM (79, 80), MexEF-OprN (81, 82), and MexGHI-OpmD (83, 84) are indicated to be involved in maintaining quorum sensing signal homeostasis. Overexpression of MexAB-OprM, for example, was found to result in a dramatic decrease of the production of the important virulence factors elastase, casein protease, and pyocyanin (79), as well as a loss of virulence in a mouse infection model (85). It was found that MexAB-OprM transports 3OC12-HSL and is, thus, involved in the *las* signaling pathway (80). The loss of virulence in MexAB-OprM overproducers is explained by the decreased intracellular concentration of 3OC12-HSL due to excessive efflux (80). Since 3OC12-HSL is no longer able to reach its receptor at high enough concentrations, the *las* pathway is essentially turned off and virulence factors are no longer produced (86). This also means that *P. aeruginosa* strains that acquired multidrug resistance through overexpression of MexAB-OprM are deficient in the production of virulence factors (79). Hence, MexAB-OprM expression is carefully regulated by the *rhl* signaling pathway, which shows the interconnectedness of quorum sensing pathways (87).

Another important RND transporter that is involved in signaling is MexEF-OprN. It was found to transport the PQS precursor HHQ and kynurenine (81, 82). Since PQS is required for the expression of several virulence factors (76), overexpression of MexEF-OprN was found to result in the loss of virulence, presumably due to the low

intracellular concentrations of these PQS precursors (82). Interestingly, this transporter was also found to be upregulated in drug resistant clinical isolates of *P. aeruginosa* (42).

Lastly, MexGHI-OpmD is also indicated to translocate quorum sensing related molecules. Aendekerk et al. found that a disruption in either *mexI* or *opmD* resulted in reduced levels of key virulence factors like pyocyanin, rhamnolipids, and elastase, as well as reduced virulence in a mouse infection model (83, 88). The authors attributed these effects to the transporter's involvement in efflux of the PQS precursor anthranilate (83). Another group found that MexGHI-OpmD transports the phenazine 5-methylphenazine-1-carboxylate (5-Me-PCA), a direct precursor of pyocyanin and indicated to be involved in biofilm formation (84). Although RND transporters are most notorious for their involvement in multidrug resistance, they play key roles in establishing homeostasis of several important molecules. More research has to be dedicated to elucidate the involvement of the twelve RND transporters of *P. aeruginosa* in the physiology of the cell and the establishment of virulence.

Transporters in *P. aeruginosa*		
RND Transporter	**Substrates**	**References**
MexAB-OprM	FQ, ML, TET, LM, CF, NB, PEN, 3O12-HSL (QS)	(89, 90)
MexXY-OprM	FQ, ML, TET, LM, CF, AG	(89)
MexCD-OprJ	FQ, ML, TET, LM, CF, NB, PEN, CEF	(89)
MexEF-OprN	FQ, CF, TMP, TET, HHQ (QS), KY (QS)	(81, 82, 91, 92)
MexGHI-OpmD	FQ, EtBr, ACR, Va^{2+}, AN (QS), 5-Me-PCA (QS)	(83, 88, 93)
MexJK-OprM/OpmH	FQ, ML, TET, TRI	(94, 95)
MexMN-OprM	CF, TML	(96)
MexPQ-OpmE	FQ, ML	(96)
MexVW-OprM	ACR, CF, EtBr, ML, FQ, TET	(97)
MuxABC-OpmB	NB, ATM	(98)
TriABC-OpmH	TRI, SDS	(68, 99)
CzcCBA	Cd^{2+}, Zn^{2+}	(100, 101)

Table I.1 - Substrate specificities of RND transporters in *P. aeruginosa*.

3OC12-HSL N-(3-oxododecanoyl)-L-homoserine lactone (QS), 5-Me-PCA 5-methylphenazine-1-carboxylate (QS), ACR acriflavine, AG aminoglycosides, AN anthranilate (QS), ATM aztreonam, CEF cephalosporins, CF chloramphenicol, FQ fluoroquinolones, KY kynurenine, LM lincomycin, ML macrolides, NB novobiocin, PEN penicillins, SDS sodium dodecyl sulfate, TET tetracycline, TML thiamphenicol, TMP trimethoprim, TRI triclosan

I.8 Specific aims and goals of this dissertation

Outer membrane permeability represents one of the biggest hurdles in the drug screening process (5). Potential hits are often overlooked due to their inability to cross the cell envelope. This results in a dramatically reduced amount of chemical structures with potentially good antibiotic activity that could be refined to improve their permeability. Some methods exist to permeabilize the outer membrane, for example, the use of polymyxins. Polymyxins are cyclic peptides attached to a fatty acid chain (102). The peptides are basic and, under physiological conditions, carry a positive charge (103). This allows them to intercalate into the outer membrane, thereby replacing calcium and magnesium ions, disrupting and, effectively, permeabilizing the outer membrane (103). At higher concentrations, polymyxins further insert themselves into the inner membrane, which results in leakage of essential cytoplasmic components leading to cell death (102). Polymyxins were found to potentiate the activity of some antibiotics, although this effect is mostly seen in hydrophobic antimicrobials (102). In addition to only selectively increasing permeability, they also change the physical properties of the outer membrane through their high charge density (102). This makes them less ideal in a drug screening approach, where non-selective permeability with an intact outer membrane is required.

One aim of this dissertation is to describe and characterize a new approach to permeabilize the outer membrane using a genetically engineered outer membrane pore from *E. coli*. The gene expressing this pore was inserted into the chromosome of *E. coli* and *P. aeruginosa* strains and leads to non-selective increase in the permeability of the outer membrane. Expression of the pore does affect some of the phenotypes controlled

by quorum sensing in *P. aeruginosa* and increases the uptake of several compounds and antibiotics. Furthermore, this dissertation aims to classify groups of antibiotics by whether their accumulation into the cell is limited by active efflux, outer membrane permeability, or a combination of both. To achieve this, antibiotic susceptibilities were tested in strains expressing the pore, lacking efflux, or both and are compared to wild type strains. This approach highlights the differences in outer membrane permeability of *E. coli* and *P. aeruginosa* and defines antimicrobial characteristics that lead to better uptake into cells.

Furthermore, this dissertation aims to characterize the RND transporter MexGHI-OpmD from *P. aeruginosa* on its contribution to antibiotic resistance and physiology. MexGHI-OpmD is an unusual transporter due to its fourth component MexG. MexG is a small about 16 kDa protein that is proposed to be located in the inner membrane. The function of MexG and whether or not it physically associates with the transporter is unknown. MexGHI-OpmD has been indicated to be involved in the transport of quorum sensing molecules, and was also found to export the toxic pyocyanin precursor 5-methylphenazine-1-carboxylate (5-Me-PCA) (83, 84, 88). Pyocyanin is one of the most important virulence factors in *P. aeruginosa* and is responsible for the characteristic blue-green color of *P. aeruginosa* cultures. A disruption in *mexI* or *opmD* was also shown to result in a complete loss of virulence in PA14; however the mechanism by which MexGHI-OpmD is involved in virulence is not known (83). This dissertation aims to elucidate whether MexG is part of the MexHI-OpmD complex and to understand the transporters role in physiology of *P. aeruginosa*.

II. Materials and Methods

Table II.1 - List of bacterial strains used in these studies

Escherichia coli		
Strains	**Description**	**Source**
BW 25113	Wild-type strain Δ(araD-araB)567 Δ(rhaD-rhaB)568 ΔlacZ4787 (::rrnB-3) hsdR514 rph-1	(104)
GD102	BW25113 Δ*tolC-ygiBC*	(105)
GKCW101 (WT)	BW25113 *att*Tn7::mini-Tn7T -Km^{r} -*araC*-P_{araBAD}-MCS	(106)
GKCW102 (WT-Pore)	BW25113 *att*Tn7::mini-Tn7T-Km^{rr} -*araC*-P_{araBAD}-*fhuA*ΔC/Δ4L	(106)
GKCW103 (ΔTolC)	GD102 *att*Tn7::mini-Tn7T-Km^{r}-*araC*-P_{araBAD}-MCS	(106)
GKCW104 (ΔTolC-Pore)	GD102 *att*Tn7::mini-Tn7T-Km^{r}-*araC*-P_{araBAD}-*fhuA*ΔC/Δ4L	(106)
GKCW111	BW25113 *att*Tn7::mini-Tn7T-Km^{r} - *lacI*^{q}-pLAC -MCS	(106)
GKCW112	BW25113 *att*Tn7::mini-Tn7T-Km^{r}-*lacI*^{q}-pLAC-*fhuA*ΔC/Δ4L	(106)
GKCW113	GD102 *att*Tn7::mini-Tn7T-Km^{r} - *lacI*^{q}-pLAC -MCS	(106)
GKCW114	GD102 *att*Tn7::mini-Tn7T-Km^{r}-*lacI*^{q}-pLAC-*fhuA*ΔC/Δ4L	(106)

Pseudomonas aeruginosa		
Strains	**Description**	**Source**
PAO1	Wild type	Gift from O. Lomovskaya
PAO1Δ3	PAO1 Δ*mexAB* Δ*mexCD* Δ*mexXY*	Gift from O. Lomovskaya
PAO314	PAO1 Δ*mexAB-oprM* Δ*mexCD-oprJ* Δ*mexJKL*	(95)
PAO325	PAO1 Δ*mexAB-oprM* Δ*mexCD-oprJ* Δ*mexJKL* Δ*mexXY*	(95)
PAO509 (PΔ5S)	PAO1 Δ*mexAB-oprM* Δ*mexCD-oprJ* Δ*mexEF-oprN* Δ*mexJKL* Δ*mexXY*	(99)
PAO1116	PAO1 Δ*mexAB-oprM* Δ*mexCD-oprJ* Δ*mexEF-oprN* Δ*mexJKL* Δ*mexXY ΔtriABC*	(99)
GKCW111 (PAO1)	PAO1 *att*Tn*7*::mini-Tn*7*T-Gm-*lacI*^{q}-pLAC-MCS	(107)
GKCW112 (PΔ3)	PAO1Δ3 *att*Tn*7*::mini-Tn*7*T- Gm^{r}-*lacI*^{q}-pLAC-MCS	(107)
GKCW113 (PΔ4)	PAO325 *att*Tn*7*::mini-Tn*7*T- Gm^{r}-*lacI*^{q}-pLAC-MCS	(107)
GKCW114 (PΔ6)	PAO1116 *att*Tn7::mini-Tn7T-Gm-*lacI*^{q}-pLAC-MCS	(107)
GKCW127 (PΔ3S)	PAO314 *att*Tn*7*::mini-Tn*7*T- Gm^{r}-*lacI*^{q}-pLAC-MCS	(107)

GKCW119 (PAO1-Pore)	PAO1 *att*Tn*7*::mini-Tn*7*T- Gm^r-*lacI*^{q}-pLAC-*fhuA*ΔC/Δ4L	(107)
GKCW 116 (PΔ3-Pore)	PAO1Δ3 *att*Tn*7*::mini-Tn*7*T- Gm^r-*lacI*^{q}-pLAC-*fhuA*ΔC/Δ4L	(107)
GKCW121 (PΔ4-Pore)	PAO325 *att*Tn*7*::mini-Tn*7*T- Gm^r-*lacI*^{q}-pLAC-*fhuA*ΔC/Δ4L	(107)
GKCW122 (PΔ6-Pore)	PAO1116 *att*Tn7::mini-Tn7T- Gm^r-*lacI*^{q}-pLAC-*fhuA*ΔC/Δ4L	(107)
GKCW 128 (PΔ3S-Pore)	PAO314 *att*Tn*7*::mini-Tn*7*T- Gm^r-*lacI*^{q}-pLAC-*fhuA*ΔC/Δ4L	(107)
DW101 (PAO1ΔG)	PAO1 Δ*mexGHI-opmD*-scar	This study.
DW102 (PΔ3ΔG)	PAO1Δ3 Δ*mexGHI-opmD*-scar	This study.
DW103 (PΔ4ΔG)	PAO325 Δ*mexGHI-opmD*-scar	This study.
DW104 (PΔ6ΔG)	PAO1116 Δ*mexGHI-opmD*-scar	This study.
DWBN110	DW104 *att*Tn*7*::mini-Tn*7*T- Gm^r-*lacI*^{q}-pLAC-	This study.

(PΔ6ΔG-Pore)	*fhuA*ΔC/Δ4L	
DW111 (PΔ4ΔG-Pore)	DW103 *att*Tn*7*::mini-Tn*7*T- Gm^r-*lacI^q*-pLAC-*fhuA*ΔC/Δ4L	This study.
DW112 (PΔ5S-Pore)	PAO509 *att*Tn*7*::mini-Tn*7*T- Gm^r-*lacI^q*-pLAC-*fhuA*ΔC/Δ4L	This study.

Table II.2 - List of plasmids used in these studies

Plasmids	**Description**	**Source**
pBSPII (SK-)	Cb^r; broad-host-range cloning vector	(108)
pMexEF-OprN	Cb^r; pBSPII *mexEF-oprN*; Bla^r; expresses MexEF-OprN^{His}	This study.
pMexHI-OpmD	Cb^r; pBSPII *mexHI-opmD*; Bla^r; expresses MexHI-OpmD^{His}	This study.
pMexGHI-OpmD	Cb^r; pBSPII *mexGHI-opmD*; Bla^r; expresses MexGHI-OpmD^{His}	This study.
pMexG	Cb^r; pBSPII *mexG*; Bla^r; expresses MexG^{His}	This study.

pMexGH	Cb^r; pBSPII *mexG*; Bla^r; expresses $MexG^{His}$	This study.
pMexGHI	Cb^r; pBSPII *mexGHI*; Bla^r; expresses $MexGHI^{His}$	This study.
pMexGHI-flag	pMexGHI with additional FLAG tag on N-terminus of *mexG*	This study.
pMexGH-flag	pMexGH with additional FLAG tag on N-terminus of *mexG*	This study.
pMexGΔHW	Cb^r; pBSPII *mexG*; Bla^r; expresses $MexG\Delta HW^{His}$	This study.
pEX18Ap	Ap^r; $oriT^+$ $sacB^+$, gene replacement vector	(109)
pUC18-mini-Tn7T-LAC	Gm^r; mini-Tn7T based suicide vector	(110)
pEX18Ap-Gm	pEX18Ap with FRT-Gm^r-FRT fragment from pUC18-mini-Tn7T-LAC	This study.
pEXdGHI-D	pEX18Ap-Gm with upstream and downstream fragment of *mexGHI-opmD* flanking FRT-Gm^r-FRT	This study.
pFLP2	Cb^r; $sacB^+$ Plasmid carrying FLP recombinase	(109)
pGK-LAC-FhuAΔC/Δ4L	pUC18-mini-Tn*7*T-Gm^r-$lacI^q$-pLAC vector containing *fhuA* Δ*C/*Δ*4L* gene	(106)
pTNS2	Helper plasmid containing transposase complex	(111)

Growth Conditions

Unless otherwise indicated, bacterial cultures were grown in Luria-Bertani (LB) broth (10 g Tryptone, 5 g Yeast Extract, and 5 g NaCl per liter at pH 7.0) at 37°C and shaking at 200 RPM. Optical densities were measured utilizing a UV-1601 (Shimadzu). Cultures with OD_{600} above 1.0 were diluted down before the final OD was determined.

Plasmid construction

Sequences of all primers can be found in Appendix A. Plasmid constructs for the expression of MexEF-OprN and MexGHI-OpmD were constructed using the broad-host-range vector pBSPII (SK-) (108). Genes were PCR amplified from PAO1 genomic DNA, extracted using the GenElute Bacterial Genomic DNA Kit (Sigma Aldrich), and amplified using the primers EFNpbspFWD and EFNpbspREV, or GHIDpbspFWD and GHIDpbspREVhis. PCR fragments and the vector pBSPII were digested with KpnI-HF and HindIII-HF for MexEF-OprN, or HindIII-HF and BamHI-HF for MexGHI-OpmD using the conditions recommended by the manufacturer of the restriction enzymes (NEB), and ligated into the digested vector using T4-Ligase (NEB). Ligation of the vector with PCR fragments was done following the manufactures protocol. The constructs were confirmed by restriction analysis and expression was validated using the methods described below.

Other parts of the MexGHI-OpmD transporter were cloned into pBSPII (SK-) utilizing similar methods utilizing the restriction enzymes HindIII-HF and BamHI-HF (NEB). pMexG, pMexGH, and pMexGHI were constructed using the primers GHIDpbspFWD and GpbspREVhis, GHpbspREVhis, and GHIpbspREVhis

respectively. pMexHI-OpmD was cloned using the primers HIDpbspFWDhis and GHIDpbspREVhis. Constructs containing a N-terminal FLAG tag of *mexG* were created using the forward primer GpbspFWDflag and the reverse primer GHpbspREVhis for MexGH and GHIpbspREVhis for MexGHI. The MexG mutant MexGΔHW was created by site-directed mutagenesis using the QuikChange Lightning Kit (Agilent) and the primers GdHWfwd and GdHWrev as per the instructions given by the manufacturer.

The plasmid pEXdGHI-D was constructed in order to remove *mexGHI-opmD* from the chromosome of *P. aeruginosa*. pEX18Ap was used as the backbone for the construction of the plasmid. The FRT-GM^{R}-FRT cassette from pUC18-mini-Tn7T-LAC plasmid was amplified using the primers SalIfrtGMfrtFWD and SalIfrtGMfrtREV, and inserted into the multiple-cloning site of pEX18Ap using the SalI restriction site. Next, we amplified 500 base pairs directly upstream of MexG using the the primers GHIDupFWD and GHIDupREV from PAO1 genomic DNA, and inserted the resulting PCR fragment into the created pEX18Ap-GM plasmid using the EcoRI and KpnI restriction sites. Similarly, we amplified the last 508 base-pairs of *opmD* using GHIDdownFWD and GHIDdownREV primers and ligated the fragment into the PstI and HindIII sites in the pEX18Ap-GM plasmid containing the upstream fragment. The result is the pEXdGHI-D *P. aeruginosa* suicide vector.

Manipulation of chromosomal DNA

Gene deletion was carried out using established methods (109). Suicide plasmid pEXdGHI-D was transformed into conjugation proficient *E. coli* SM10 λpir donor cells,

and cell cultures of SM10 and *P. aeruginosa* strains were grown overnight to stationary phase in Luria-Bertani (LB) broth (10 g Tryptone, 5 g Yeast Extract, and 5 g NaCl per liter at pH 7.0). Cells were subcultured 1:100 into fresh LB Media. The media for SM10 cells harboring the pEXdGHI-D plasmid was supplemented with 10μg/ml gentamicin. Both cultures were grown to OD_{600} of 1.0 and 1ml of each was centrifuged. The pellets were resuspended in 50 μl LB media and spotted onto a LB Agar plate. Plates were incubated at 37°C overnight to allow for conjugation. Cells were collected, resuspended in a 10 mM $MgSO_4$ solution, and plated onto selective Vogel-Bonner minimal media agar plates (0.2 g/L $MgSO_4$, 2 g/L citric acid, 10 g/L K_2HPO_4, 3.5 g/L $NaNH_4HPO_4$, and 15 g/L agar) (112) supplemented with 15 or 30 μg/ml and 10% sucrose. Colonies resistant to gentamicin and sensitive to carbenicillin were further analyzed by PCR to confirm successful deletion. To remove the gentamicin resistance cassette, cells were transformed with pFLP2 (109) and plated onto 10% sucrose. Colonies were tested for carbenicillin and gentamicin susceptibility, and excision was confirmed by PCR.

Insertion of the pore was carried out using previously published methods (110). *P. aeruginosa* suicide vector pGK-LAC-FhuAΔC/Δ4L(106) and pTNS2 (111) were electroporated into DW104 cells and integration was selected for by plating onto LB Agar plates supplemented with 10 μg/m gentamicin. Colonies were confirmed by PCR and by vancomycin spot assays as described below.

Minimum Inhibitory Concentration (MIC) Testing

MIC determinations were carried out as previously described (113, 114) using the 2-fold broth dilution method. Indicated cells were grown with or without plasmids

in LB media supplemented with 200 μg/ml carbenicillin at 37°C with shaking at 200 RPM. Overnight cultures were subcultured 1:100 into fresh media, with antibiotic where appropriated, and grown to an OD_{600} of 1.0 at 37°C with shaking. If protein expression is under the control of an inducible promoter, cells were induced at OD_{600} of 0.3 with 0.1% L-Arabinose, 0.1 mM, or 2 mM Isopropyl ß-D-1-thiogalactopyranoside (IPTG). Cells were subsequently diluted to OD_{600} of 0.001 into a petri dish containing 10mL of LB broth. A multichannel pipette was used to inoculate $5x10^4$ cells per 100 μL well of a 96-well plate (assuming OD_{600} of 1.0 equals 10^9 cells). The plates themselves were set up by 2-fold broth dilution using a multichannel pipette to a final volume of 100 μL of media with antimicrobial at different concentrations. When induction of protein expression was required, the media was supplemented with inducer. The last row in each plate was left without antibiotic as a control. Once cells were inoculated, the plates were left in the incubator at 37°C for 18 hours. The MIC was read by visual inspection of the wells and, were indicated, OD_{600} was read using a 10M Spark microplate reader (Tecan).

Spot Assays

The spot assays to determine zone of clearance for antimicrobials were carried out as previously published (106). Cells were grown to stationary phase in LB media at 37°C with shaking at 200 RPM and subcultured 1 to 100 into fresh media. The media was supplemented with antibiotic where appropriate to ensure that plasmids were maintained. Soft agar if prepared by mixing 2 mL of LB with 2 mL of LB Agar (10 g Tryptone, 5 g Yeast Extract, 5 g NaCl, and 15 g Agar per liter at pH 7.0) and kept at

55°C to prevent the agar from solidifying. IPTG was added to the soft agar at a concentration of 0.1mM as necessary for protein expression. Where appropriate, cells were induced at OD_{600} of 0.3 with 0.1 mM IPTG and grown to OD_{600} of 1.0. 300 µL of cultures were taken and mixed with the soft agar. The mixture was poured over LB agar plates and allowed to solidify at room temperature. Sterilized filter disks were added to the plates and the antimicrobial was spotted onto the disks. The plates were stored upside down at 37°C for 18 hours. After this time, the plates were taken out and the zones of clearance determined. To confirm the expression of the pore 100 µg of vancomycin was spotted onto the disk. For PMS and pyocyanin assays 0.5 and 0.05 µmoles were spotted respectively.

Determination of Growth Curves and Growth Rates

Stationary phase cells were subcultured 1:100 and grown in LB media with antibiotic to maintain plasmids were required at 37°C with shaking at 200 RPM. When protein induction was necessary, the cultures were induced at OD_{600} of 0.3 with 0.1% L-Arabinose or 0.1mM IPTG. Once cells reached OD_{600} of 1.0 they were diluted to OD_{600} of 0.001 into a petri dish containing 10 mL of LB media. Growth was measured in a 96-well plate by inoculating 10^5 cells (assuming 10^9 cells in 1 ml of OD_{600} of 1.0) into each well containing 200µL of media supplemented with inducer where appropriate. When growth curves were desired in the presence of antimicrobial, the drug was added in 2-fold broth dilution. The plates were read in a Spark 10M microplate reader. The heating unit in the reader was set to 37°C and it was programmed to read OD_{600} every 30

minutes for 18 or 24 hours. Before each reading the plate was shaken for 10 seconds in orbital mode.

The data was imported into Microsoft Excel and each well was normalized to its OD_{600} at time zero hours. Triplicates of each strain were averaged and plotted against time in hours. Growth rates were calculated by taking $LN(OD_{600})$ and plotting it against time. Plots can be found in Appendix D. Six time points were selected for the determination of the rates based on the coefficient of determination (r^2) from the steepest part of the graph.

Quantification of Pyocyanin

Extracellular pyocyanin was quantified using previously published spectroscopic methods with the following modifications (115). Cultures were grown in LB broth supplemented with 50mM HEPES-KOH buffer pH 7.0 to stationary phase. A 1 mL aliquot was taken and cells were removed through ultracentrifugation at 100,000xg at 4°C. 500 µL of chloroform was added to the supernatant and samples were vortexed for 1 min. The two phases were separated by centrifugation and the blue organic phase was transferred to a new tube. Chloroform was evaporated under nitrogen and samples were resuspended in 250 µL LB broth with 50 mM HEPES-KOH pH 7.0. The absorbance was read at 690 nm and the concentration of pyocyanin was calculated using the extinction coefficient (4,310 M^{-1} cm^{-1}).

Quantification of Pyoverdine

Quantification was done using previously described methods (116). Indicated cultures were inoculated into glucose succinate minimal media (GSM) (10mM slucose, 10 mM succinate, 40 mM NH_4Cl, 0.5 mM K_2SO_4 and 0.4 mM $MgSO_4$) buffered with 5mM K_3PO_4 at pH 7.4) and grown overnight at 37°C with shaking. Cells were subcultured 1:50 into fresh GSM and grown for 5 hours, after which time the OD_{600} was determined every 30 min. Pyoverdine was determined by removing cells through centrifugation and reading the OD_{400} of the supernatant. The concentration of pyoverdine was calculated using the extinction coefficient of 20,000 M^{-1} cm^{-1}. The data was divided by the OD_{600} and normalized to PAO1.

Quantification of Biofilm

Biofilm accumulation of cells grown for several days was quantified as previously described (117). Strains were inoculated into LB media and grown overnight to stationary phase. Cells were washed twice with M9 minimal media supplemented with 0.4% glycerol, 0.4% casamino acid, and 0.1 mM IPTG to induce expression of the pore, and subsequently subcultured 1:100 using the same media into a 96-well PVC plate. Plates were incubated at 37°C for 3 days. 20µl of a 0.1% crystal violet was added to each well to stain the biofilms and incubated for 15 minutes. Wells were subsequently washed rigorously with PBS buffer (137 mM NaCl, 2.7 mM KCl, 10 mM Na_2PO_4, 1.8 mM KH_2PO_4) and allowed to dry. 200 µl of 95% ethanol was added and the OD_{600} was determined. The data was normalized to PAO1.

Uptake of Radiolabeled Compounds

Cells grown to stationary phase were subcultured 1:100 into fresh LB media and incubated at 37°C with shaking at 200 RPM. Expression of the pore was induced with 0.1% L-arabinose in *E. coli* and 0.1 mM IPTG in *P. aeruginosa* strains at OD_{600} of 0.3. Cultures were subsequently grown to OD_{600} of 1.0 and collected by centrifugation at 3,220xg for 10 minutes at room temperature. Cells were washed twice in PMG buffer (50 mM potassium phosphate, 1 mM magnesium sulfate, and 0.4% glucose at pH 7.0) and finally resuspended in PMG buffer of one tenth of the original culture volume.

Radiolabeled [14C]-erythromycin was diluted and mixed with cold stock of the antibiotic to achieve the desired stock concentration and specific activity of 0.025 Ci/mmol. The stock was diluted to different concentrations with PMG buffer at 10X the final concentration. 100 µL of each concentration was added to 1mL of cells and aliquots of this reaction mixture was taken at the indicated time points. The aliquots were added to 96-well MultiScreenHTS FB filter plates with 1.0 and 0.65 µm pore sizes (EDM Millipore) that were attached to a MultiScreen HTS vacuum manifold (EDM Millipore) under vacuum. Before cells were added each filter was treated with PMG buffer. The plates were dried overnight and subsequently added to scintillation vials each with 2mL scintillation fluid. Radioactivity was determined with a Tri-Carb 2810TR scintillation counter (PerkinElmer). The samples were normalized to the 0.5-minute time point and intracellular concentration was calculated assuming OD_{600} equals 1×10^9 cells per milliliter and each cell having an average volume of $1 \mu m^3$.

Uptake of Hoechst33342 into Gram-Negative Bacteria

Stationary phase cells were subcultured 1 to 100 and grown at 37°C with shaking at 200 RPM with antibiotic if appropriate. At OD_{600} of 0.3 cells were induced and grown to and OD_{600} of 1.0, at which time they were collected by centrifugation at 3,220xg and room temperature. Pellets were washed twice with HMG buffer (50 mM Hepes-KOH, 1 mM $MgSO_4$, and 0.4% Glucose at pH 7.0). Cells were resuspended in HMG buffer to an OD_{600} of 2.0 equivalent for *E. coli* and 1.0 for *P. aeruginosa*.

The uptake experiment was carried out in a 10M Spark microplate reader (Tecan). For this purpose, 100 µL of Hoechst33342 (HT) was distributed into a low binding F-bottom 96-well plate (Greiner Bio-One, inc) at 2-fold increasing concentrations. The temperature in the plate reader was kept constant at 25°C and 100 µL of cells were injected into each well. The final concentration of cells in the wells were OD_{600} of 1.0 for *E. coli* or 0.5 for *P. aeruginosa*. Fluorescence was measured for HT at 460 nm (excitation at 355 nm) every 20 seconds for 10 minutes. The plates were shaken briefly before each reading in orbital mode.

Analysis of Fluorescence Uptake Data

The data was first plotted in Microsoft Excel and duplicates of an experiment were averaged. Fluorescence was normalized to the last time point before cells were added and the data was inspected for outliers. To calculate initial rates and steady states of fluorophore uptake, the time courses were imported into MATLAB (MathWorks). The fittype function was used to fit the data to an exponential equation in the form of: $y = A_1 + A_2 * (1 - \exp(-k_2 * t))$. The following constraints were used: For A_1 the lower

and upper bounds were set to be within 5% of the first point after addition of cells, for A_2 the lower bound was set to zero and the upper bound to 10% of the last time point taken, for k_2 the lower bound was set to zero and the upper bound set to one. The start point for A_1 was equal to the first time point after injection of cells, for A_2 was set to the last time point, and for k_2 was set to 0.01. The fitted lines were plotted in MATLAB and the quality of the fit was determined by visual inspection and analysis of the confidence intervals as well as the R-squared value of the calculated parameters.

To calculate the concentration of intracellular HT a conversion factor was determined using the fluorophore binding to salmon sperm DNA or phospholipids. These emission coefficients were determined by linear regression of emission of the fluorophore plotted against its total concentration. The experiments were carried out assuming that 1mL of OD_{600} 1.0 cells contain about 17 µg of DNA and 27 µg of total lipids. Once relative fluorescent units (RFU) were converted to the intracellular concentration of fluorophore in µM the steady states were determined by simple addition of A_1 and A_2. The initial rates of uptake were determined by multiplying A_2 by k_2. This is justified according to this simple derivation:

$$y = A_1 + A_2 * (1 - e^{-k_2 * t})$$

$$\frac{dy}{dt} = A_2 * k_2 * e^{-k_2 * t}$$

Since the initial rate is at t = 0:

$$Initial\ Rate = A_2 * k_2$$

Unless otherwise indicated, three independent experiments were averaged and the standard deviation calculated per fluorophore and strain.

Protein Expression and Determination of Concentration of HIS-tagged Membrane Proteins

Expression of membrane proteins was verified by previously published methods (57) with subsequent immunoblotting. Cells grown to stationary phase were subcultured 1:100 into fresh media supplemented with antibiotic where necessary and grown at 37°C with shaking at 200 RPM. When induction of proteins was required, cells were induced at OD_{600} of 0.3 with 0.1 mM or 2.0 mM IPTG and grown for 3.5 hours after induction. If no induction was necessary, cells were grown for 6 hours after subculturing. Cells were collected by centrifugation at 3,220xg and 4°C and pellets were stored at -80°C overnight.

The pellets were thawed on ice and resuspended in lysis buffer (10 mM Tris-Cl, 5 mM EDTA, and 100 µg/mL Lysozyme at pH 8.0). The mixture was incubated on ice for 1 hours. Cells were further lysed by sonication on ice until the solution became clear. Broken cells were separated from whole cells by centrifugation at 3,220xg for 10 minutes. The supernatant was transferred to a new tube and membrane fractions were isolated by ultracentrifugation at 100,000xg for 1 hour at 4°C. The pellet was resuspended in resuspension buffer (10 mM Tris-Cl, 150 mM NaCl, and 1 mM PMSF at pH 8.0). Protein concentration was determined using a Bradford Protein Assay (Bio-Rad). Samples were prepared for SDS-PAGE and subsequent immunoblotting by normalizing the amount of protein loaded into each lane (either 7.5, 15, or 22.5 µg of total protein) of the gel.

Purification of FhuAΔC/Δ4L^{HIS} from *P. aeruginosa* and Determination of Copy Number

Cells with *fhuAΔC/Δ4L* chromosomal integrations were grown to stationary phase and subcultured 1 to 100 into 1 L of fresh LB broth at 37°C with shaking at 200 RPM. Cultures were induced at OD_{600} of 0.3 with 0.1 mM IPTG and grown for 3.5 hours after induction, after which time the OD_{600} was recorded. Cells were collected at 3,220xg at 4°C and washed once in 40 mL of 10 mM Tris-Cl pH 8.0. Cell pellets were stored at -80°C until the next day. Samples were thawed on ice and subsequently resuspended in 50 mM Tris-Cl, 1 mM $MgCl_2$, 100 µg/mL lysozyme, and 100 µg/mL DNaseI. The lysis mixture was incubated on ice for 30 minutes before adding 5 mM EDTA at pH 8.0 and an additional incubation for 30 minutes on ice. Samples were sonicated until the solution became clear and unbroken cells were separated from lysed cells by centrifugation at 3,220xg for 20 minutes at 4°C. Membrane fractions were isolated from the supernatant by ultracentrifugation at 100,000xg for 1 hours at 4°C. To enrich the outer membrane fraction, the membrane pellet was resuspended in 50 mM Tris-Cl, 150 mM NaCl, 1 mM PMSF, 5 mM Imidazole, and 0.2% Triton X-100 at pH 8.0 and incubated at 4°C overnight while rotating. Outer membranes were isolated by centrifugation at 100,000xG and the pellet was solubilized again in 50 mM Tris-Cl, 150 mM NaCl, 1 mM PMSF, 5 mM Imidazole, and 5% Triton X-100 at pH 8.0 overnight with rotating. Insoluble cell debris and proteins were separated from soluble outer membrane fractions by ultracentrifugation at 100,000xG for 1 hour at 4°C.

The supernatant was incubated for 2 hours with His•Bind Resin (Novagen) at 4°C with rotating. The resin was previously charged with 50 mM $CuSO_4$ and

equilibrated with binding buffer (20 mM Tris-Cl, 500 mM NaCl, 1 mM PMSF, 0.2% Triton X-100, and 5 mM Imidazole at pH 8.0). The samples were transferred to a mini gravity flow column and washed with 10 column volumes of binding buffer with 5 mM and 20 mM Imidazole. FhuAΔCΔ4L was eluted with binding buffer containing 400 mM Imidazole at pH 8.0 into 5 fractions of 1 column volume. Elution fractions were concentrated with a Microcon-30 kDa (EMD Millipore) and loaded onto a SDS-Page gel with subsequent immunoblotting. For detection of FhuAΔCΔ4L a primary monoclonal anti-6xHIS antibody (Fisher Scientific) and a secondary anti-Mouse alkaline phosphatase conjugated antibody (Sigma Aldrich) was used.

To determine the copy number of FhuAΔCΔ4L a protein standard of a *P. aeruginosa* membrane protein ($TriC^{HIS}$) was loaded onto the same gel at 2-fold increasing concentrations. To estimate the amount of FhuAΔCΔ4L the Quantity One software (Bio-Rad) was used. After determination of the amount of protein, the copy number was calculated under the assumptions that 1mL of cell culture at OD_{600} contains $1x10^9$ cells and 100% of the pore bound and eluted from the column.

Protein Crosslinking Experiments

For chemical crosslinking assays, PΔ3 cells expressing pMexGHI-flag or pMexGH-flag were harvested by centrifugation. Pellets were washed twice in PBS buffer (8 g/L NaCl, 0.2 g/L KCl, 1.44 g/L Na_2HPO_4, 0.24 g/L KH_2PO_4 at pH 7.4) and, subsequently, 4 mM DSP (dithiobis(succinimidyl propionate)) or DMSO was added to samples and controls respectively. Cells were allowed to incubate for 2 hours at 37°C while rotating. The reaction was quenched with 100 mM Tris-Cl pH 8.0. Cells were

harvested by centrifugation and resuspended in 50 mM Tris-Cl pH 8.0, 1mM $MgCl_2$, 100 μg/ml DNAseI, and 100 μg/ml Lysozyme. The lysis mixture was incubated on ice for 30 min. EDTA was added to the samples to a final concentration of 5 mM and cells were incubated for an additional 30 min on ice. Lysis was completed by sonication and unbroken cells were separated from broken cells by centrifugation. Membrane fractions were isolated by ultracentrifugation at 100,000xg at 4°C for 1 hour. Pellets were resuspended in 50 mM Tris-Cl, 150 mM NaCl, 5 mM Imidazole, 1 mM PMSF, and 5% Triton X-100 at pH 8.0 and incubated at 4°C overnight while rotating. Soluble compounds were separated from insoluble ones by centrifugation at 100,000xg at 4°C for 1 hour. His-tagged proteins were purified with His•Bind Resin (Novagen), previously charged with 50mM $CuSO_4$. Samples were eluted from the column with 20 mM Tris-Cl, 500 mM NaCl, 1 mM PMSF, 0.2% Triton X-100, and 500 mM Imidazole at pH 8.0. Samples were subsequently analyzed by SDS-PAGE and immunoblotting onto polyvinylidene fluoride membranes (Santa Crux Biotechnology) with Anti-His (Invitrogen) or Anti-FLAG (Agilent) primary antibodies followed by secondary Anti-Mouse antibody (Sigma Aldrich) conjugated with alkaline phosphatase. The membranes were developed with 5-bromo-4-chloro-3-indoyl phosphate (BCIP) and nitroblue tetrazolium (NBT).

Purification of MexG^{HIS} from *P. aeruginosa*

PΔ3 cells carrying the pMexG plasmid were grown to stationary phase at 37°C with 200 μg/ml carbenicillin and subsequently subcultured 1:100 into fresh media supplemented with drug. Cultures were grown for 18 hours at 37°C with shaking at 200

RPM and collected by centrifugation at 3,220xg at 4°C for 40 minutes. Pellets were washed once in 10 mM Tris-Cl pH 8.0 and stored at -80°C until the next day. Cells were allowed to thaw on ice and resuspended in lysis buffer (50 mM Tris-Cl, 1 mM $MgCl_2$, 100 µg/ml lysozyme, and 100 µg/ml DNaseI at pH 8.0). The lysis mixture was incubated on ice for 30 minutes, after which time EDTA (pH 8.0) was added to a final concentration of 5mM and samples were incubated for another 30 minutes on ice. To complete lysis, cells were sonicated until the solution became clear and unbroken cells were separated by centrifugation at 3,220xg and 4°C for 10 minutes. Membrane fractions were isolated by ultracentrifugation at 100,000xg and the pellet was resuspended in solubilization buffer (50 mM Tris-Cl, 150 mM NaCl, 1 mM PMSF, 5 mM Imidazole, and 2% n-Dodecyl-β-D-maltoside (DDM) at pH 8.0). The solubilization mixture was incubated at 4°C with rotating for 18 hours. Insoluble cell debris was removed by ultracentrifugation at 100,000xg and 4°C for 1 hour and the supernatant was applied to His•Bind Resin (Novagen) of 500 µL. The concentration was determined by SDS-PAGE with a BSA protein standard and subsequent analysis with Quantity One (Bio-Rad).

Fluorescence Binding Assay

Fluorescence binding assays were carried out with 1µM purified MexG in 50 mM Tris-Cl, 500 mM NaCl, 1 mM PMSF, and 0.03% DDM. We used a RF-5301PC Spectrofluorophotometer (Shimadzu) and took emission spectra from 300 nm to 550 nm with excitation at 290nm. Readings were done in fast mode and excitation and emission slits set to 5 nm. All experiments were carried out at 25°C in triplicates. Pyocyanin

(Sigma Aldrich) was dissolved in ethanol and titrated into the MexG sample. We measured the binding by monitoring the emission at 330 nm.

Analysis of the fluorescence quenching was done assuming a 1 to 1 binding model as described earlier (118, 119). The following sets of equations were used for the fitting:

$$K_a = \frac{[PL]}{[P]_{free} * [L]_{free}} \quad (1)$$

where

$$[P]_{free} = [P]_{total} - [PL] \quad (2)$$

and

$$[L]_{free} = [L]_{total} - [PL] \quad (3)$$

Substituting Eq. 2 into Eq. 1 yields:

$$K_a = \frac{[PL]}{([P]_{total} - [PL]) * ([L]_{total} - [PL])} \quad (4)$$

Solving for [PL] gives:

$$[PL] = \frac{-\sqrt{K_a^2[L]_t^2 - 2K_a^2[L]_t[P]_t + K_a^2[P]_t^2 + 2K_a[L]_t + 2K_a[P]_t + 1} + K_a[L]_t + K_a[P]_t + 1}{2K_a} \quad (5)$$

$$F = F_0 - [PL] * \Delta F \quad (6)$$

where $[P]_{free}$ and $[L]_{free}$ are the free protein and ligand concentrations; [PL] is the concentration of the protein ligand complex; K_a is the association constant; F_0 and F are the initial fluorescence and the observed fluorescence after addition of ligand; and ΔF is the change of fluorescence upon addition of the ligand.

Fluorescence data was first corrected for dilution and inner filter effects as described earlier (119), and subsequently fitted to equation 5 and 6 using OriginPro (OriginLabs).

Chapter 1. Permeabilizing the Outer Membrane of *Escherichia coli* and *Pseudomonas aeruginosa*

1.1 Abstract

Cases of infections caused by multidrug resistant isolates of human pathogens are becoming increasingly more frequent. The current drug discovery pipeline is unable to keep up with the fast-evolving resistance in bacteria, and new ways to improve it are desperately needed. Gram-negative bacteria represent the biggest challenge due to their highly impermeable cell envelope, which results in a considerably lower hit rate during screening (5). Approaches to permeabilize the outer membrane so far have significant disadvantages, including changing the physical properties of the outer membrane and providing a permeability preference to hydrophobic molecules (102). Here, we are describing strains that contain a chromosomally inserted copy of a genetically engineered pore from *E. coli*. The pore is altered to increase its exclusion size and sensitizes the cells to antibiotics traditionally reserved for gram-positive bacteria due to their inability to penetrate the gram-negative cell envelope. We show that the expression of the pore can controllably increase the outer membrane permeability in *E. coli* and *P. aeruginosa* and is a useful tool to discover new antibiotics for "impermeable" gram-negative bacteria.

1.2 Introduction

Pseudomonas aeruginosa is an opportunistic, gram-negative human pathogen that is most commonly associated with nosocomial diseases, especially infections in cystic fibrosis patients. Of particular concern is the increased frequency of multidrug resistant clinical isolates of this bacterium, placing it on the top of the list of priorities for the development of new antibiotics (3, 6). *P. aeruginosa*, like other gram-negative bacteria, possesses high levels of intrinsic resistance through synergistic effects between the low permeability cell envelope and active efflux across the outer membrane. In order to study this synergism, the contributions of efflux and the outer membrane barrier have to be analyzed separately. Chromosomal deletions of RND transporters remove the contributions of efflux to resistance, however there is currently no suitable way to remove the contribution of the outer membrane barrier.

To date, the methods available to permeabilize the outer membrane, including polymyxins, are not ideal for screening, due to the fact that they significantly change the physical properties of the outer membrane and favor the uptake of hydrophobic compounds (102). Polymyxins are acetylated peptides that are highly positively charged. This allows them to displace the divalent ions of the outer membrane, intercalating into the membrane, and effectively permeabilizing it (103). Polymyxins change the physicochemical properties of the membrane and were shown to increase the uptake selectively for hydrophobic molecules (102). This make them less ideal for drug screening, where an outer membrane with native properties is desired.

We developed a novel way to permeabilize the outer membrane of *E. coli* and *P. aeruginosa*, leading to an increased uptake of compounds non-selectively. Our approach

utilizes a genetically modified version of the outer membrane β-barrel protein FhuA from *E. coli* to hyperporinate the cells in an inducer dependent manner. FhuA or ferric hydroxamate uptake component A is a siderophore transporter in *E. coli* involved in iron uptake (Fig. 1.1) (120). The crystal structure of FhuA was solved and it was found to consist of 22 antiparallel β-strands forming a β-barrel, four extracellular loops and a globular N-terminal cork fold (Figure 1.1) (121). Mohammad et al. engineered the pore by deleting the four loops and the cork domain to be used as a biosensor (122). The result is an open pore with an average diameter of about 2.4 nm (123).

Here, we are describing *E. coli* and *P. aeruginosa* strains with a chromosomal copy of *fhuaΔ4L/ΔC* under arabinose or IPTG inducible promoter respectively. This approach allows us to control the permeability of the outer membrane by changing the inducer concentration. Our findings show that the pore non-selectively increases the antibacterial activities of several antibiotics, while not impacting cell viability. We show that expression of the pore sensitizes both species to vancomycin, a drug that is thought to be unable to penetrate the outer membrane, and increases uptake of radiolabeled antibiotics. Furthermore, through a combination of strains expressing the pore, lacking major RND transporters, or both, we are able to determine the extent to which active efflux or outer membrane permeability plays a role in providing antibiotic resistance. Traditionally, it has always been a challenge to isolate the contribution of efflux on the level of resistance it provides due to the presence of and synergy with the outer membrane. Using this approach, we are able to isolate efflux from the outer membrane permeability barrier and individually analyze its contribution on resistance. The strains described here can provide useful tools for drug screening and provide

information needed to help discover molecular characteristics that more easily allow molecules to cross the outer membrane.

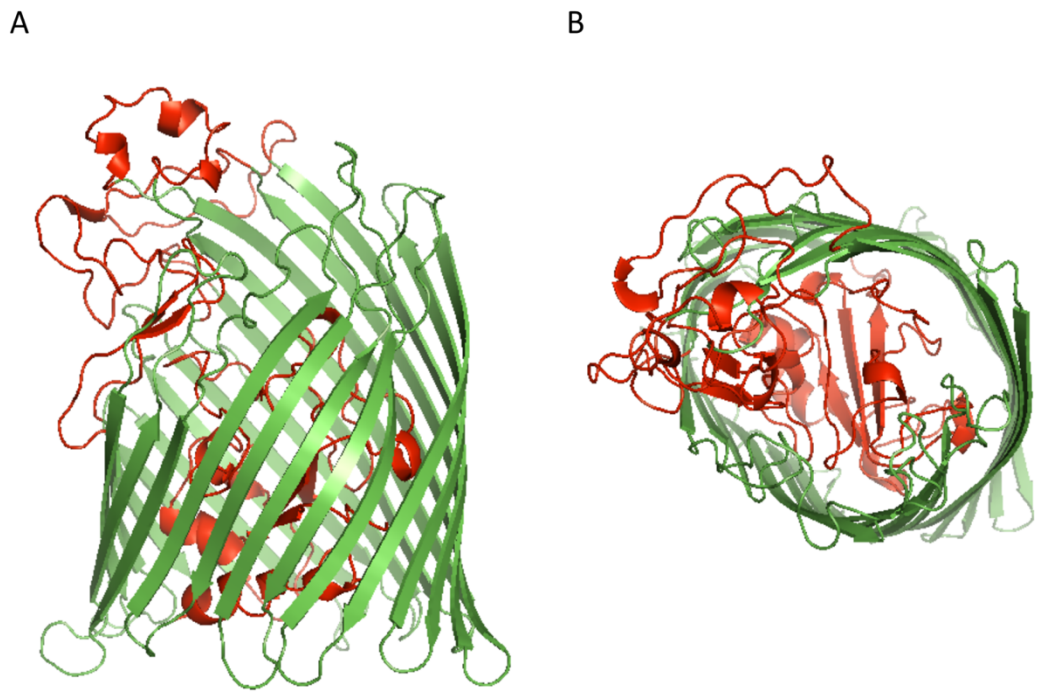

Figure 1.1 - Crystal structure of the siderophore transporter FhuA from *E. coli*.

FhuA crystal structure from PDB: 1BY3 (Locher, et al. (124)). Regions in red show the deleted cork domain and the 4 extracellular loops in the mutant pore FhuAΔ4L/ΔC (122). The mutant pore has an average diameter of 2.4nm (123). **A:** Side view and **B:** periplasmic view of FhuA.

1.3 Results

1.3.1 Controlled expression of the pore permeabilizes the cell envelope of *E. coli* and *P. aeruginosa*

The strains described here expressing the *E. coli* pore mutant FhuaΔ4L/ΔC (from here on referred to as "pore") were cloned as described in the published manuscript for *E. coli* (106) and the submitted manuscript for *P. aeruginosa* (107). The gene *fhuaΔ4L/ΔC* was inserted into several *E. coli* and *P. aeruginosa* strains that differ in their efflux proficiency. For *E. coli*, we used BW25113 as a reference strain and the *tolC* deletion mutant GD102 (105) (referred to as ΔTolC). Deletion of *tolC* in *E. coli* results in the loss of function of at least nine transporters and renders the strain largely efflux deficient (55, 72). For *P. aeruginosa*, we chose several efflux deficient mutants of PAO1 for insertion of the pore. We chose PAO1 as our wild type due to its frequent usage in laboratories and its low virulence compared to other *P. aeruginosa* strains. *P. aeruginosa* contains at least 12 RND transporters on its chromosome and most of them are in an operon together with their own OMF. In contrast to *E. coli*'s TolC, no single OMF is exclusively used by several transporters, making it much more challenging to create an efflux deficient variant of PAO1. To this end we used PAO1 (Gift from Dr. O. Lomovskaya), PΔ3 (Δ*mexAB* Δ*mexCD* Δ*mexXY*) (Gift from Dr. O. Lomovskaya), PΔ4 (95) (Δ*mexAB-oprM* Δ*mexCD-oprJ* Δ*mexJKL* Δ*mexXY*), and PΔ6 (99) (same as PΔ4, but also Δ*mexEF-oprN* Δ*triABC*). Using this step-wise approach of efflux deficient strains, we expect to see the contributions of "minor" efflux pumps on the antibiotic resistance profile of *P. aeruginosa*. In addition, step-wise deletion might also highlight

differences in the production of virulence factors and quorum signals in pore strains when certain transporters are deleted.

We checked the expression of the chromosomal integration in *E. coli* by isolating membrane fractions and subsequent analysis with immunoblotting. The pore carries a C-terminal 6xHis tag allowing us to detect it using primary anti-his antibodies (Fisher Scientific) and subsequent incubation with secondary anti-mouse (Sigma Aldrich) antibodies conjugated with alkaline phosphatase. The immunoblot in Figure 1.2A shows the expression of the mutant pore in WT (BW25113) and the efflux deficient ΔTolC (BW25113 Δ*tolC* Δ*ygiBC*) strain. Furthermore, hyperporination can be controlled by varying the concentration of arabinose as seen in Figure 1.2B and C. We are not able to detect the pore at either zero or 0.0001% of the inducer, suggesting that the pore is under tight control of the promoter. Increasing the arabinose concentration shows a positive correlation with the copy number of the pore. Utilizing the previously purified and quantified membrane protein $TriC^{His}$ as a standard, we were able to calculate the expression of the pore to about 150 copies per cell at 0.1% arabinose in WT.

In the *P. aeruginosa* strains, quantifying the pore protein was more challenging. Since we noticed significant leaky expression from the arabinose promoter, we decided to use strains with the pore under the control of an IPTG inducible promoter. We were unable to detect the FhuA mutant to any significant levels in whole membrane fractions or even enriched outer membranes, suggesting that expression is either much lower than in *E. coli*, the pore is not properly inserted into the outer membrane, or the C-terminal

sequence of the pore, where the Histidine tag is located, is recognized and cleaved as a signal peptide.

To test whether the protein is expressed at low levels, we grew larger culture volumes and added the isolated outer membrane fractions to metal affinity columns to purify and concentrate the pore and remove the bulk of other outer membrane proteins. After purification, we concentrated the elution fractions further using mini centricons and, subsequently, analyzed the samples by immunoblotting. The results can be seen in Figure 1.2D. The immunoblot shows the pore is expressed in PAO1 and all four efflux deficient mutants albeit at low amounts. Quantification with the $TriC^{His}$ standard resulted in roughly 5-7 copies per cell in PAO1-Pore, about 2 copies for PΔ3-Pore, about 1.5 copies for PΔ4-Pore, and about 1 copy per cell of PΔ6-Pore at 0.1 mM IPTG. These calculations were done assuming that the pore binds the affinity resin to 100% and that an OD_{600} of 1.0 equals 10^9 cells per milliliter. These results of the expression in *P. aeruginosa* are in contrast to the relatively high copy number of the pore in *E. coli*.

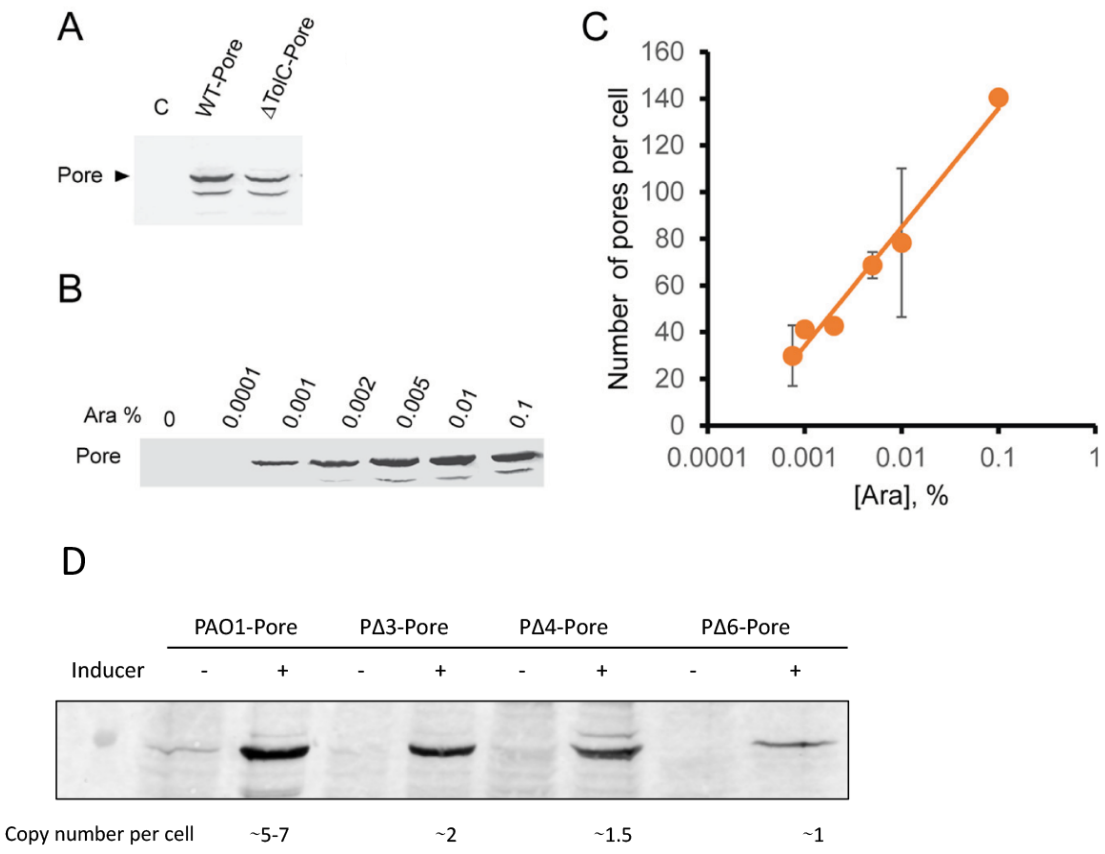

Figure 1.2 - Expression of the Pore in *E. coli* and *P. aeruginosa*.

The expression of FhuAΔC/Δ4L is inducer dependent and higher in *E. coli* than in *P. aeruginosa*. **A:** Expression in *E. coli* WT and ΔTolC induced with 0.1% arabinose. C shows expression of WT without a chromosomal copy of the pore. **B and C:** Arabinose dependent pore expression in *E. coli* WT-Pore cells. The pore was quantified using a His-tagged protein standard, and copy number estimated by assuming OD_{600} of 1.0 equals 10^9 cells per ml. Expression in *E. coli* was done by Dr. Ganesh Krishnamoorthy. **A-C** are modified from published figure (106). **D:** Pore expression is dependent on inducer (IPTG) concentration in *P. aeruginosa*. The pore was purified using metal affinity chromatography.

To check whether the expression of the pore correlates with increased susceptibility and permeability, we tested our constructed strains for vancomycin susceptibility using filter disk assays. Vancomycin is a large antibiotic with a molecular weight of about 1,449.3 Da that inhibits the synthesis of peptidoglycan, and is widely used against infections caused by gram-positive bacteria (Fig. 1.3C). However, its large size typically precludes it from activity in gram-negative bacteria, due to its inability to permeate the outer membrane. The results of the spot assays can be seen in Figure 1.3A and B. As seen by the larger diameters, only pore strains of both *E. coli* and *P. aeruginosa* that were induced by either arabinose or IPTG showed significant susceptibility to vancomycin. The control strains, with insertion of the respective promoter and empty multiple cloning site, did not change susceptibilities with addition of inducer, and the zones are comparable to the pore strains without inducer. This suggests that the pore is functionally expressed and that it sensitizes strains to vancomycin that otherwise is not able to cross the outer membrane. Thus, the FhuA mutant has a significantly larger exclusion size as the general porins in *E. coli* and *P. aeruginosa*, increases susceptibility of the strains tested to antibiotics, and its expression can be tightly controlled.

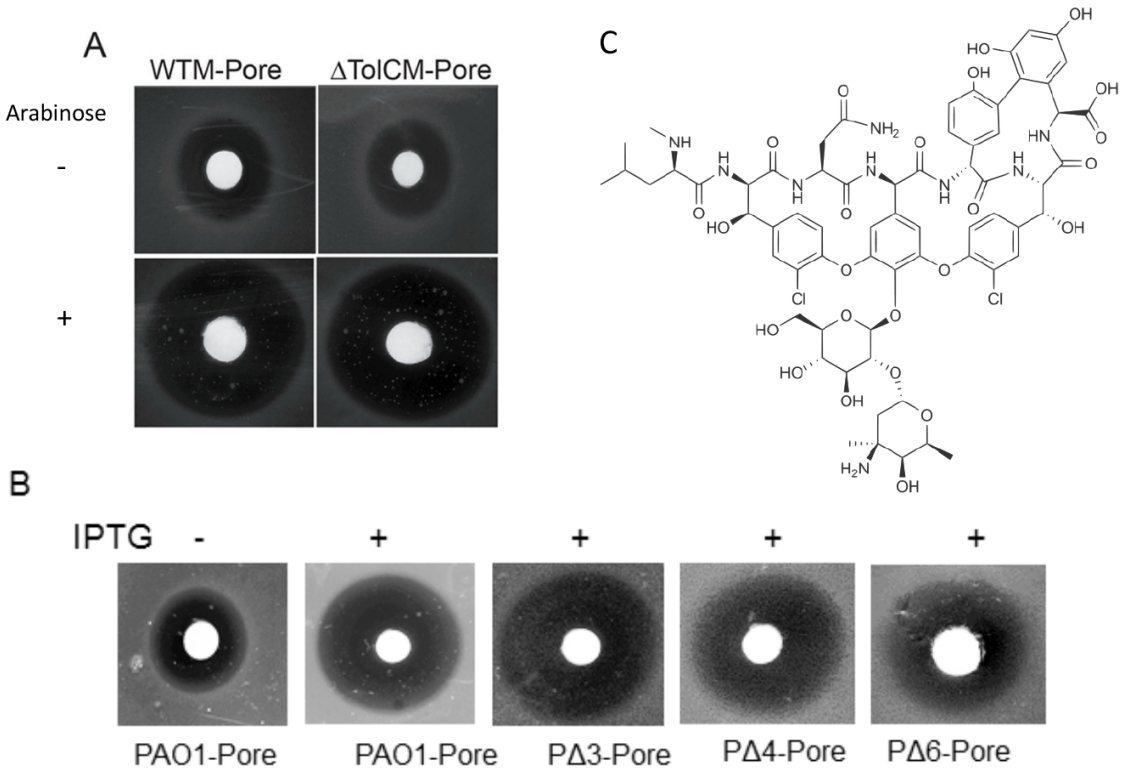

Figure 1.3 - Expression of the pore sensitizes gram-negative bacteria to vancomycin.

The pore increases the susceptibility of *E. coli* (**A**) and *P. aeruginosa* (**B**) to vancomycin. The drug was spotted onto plates that were seeded with the respective strains and incubated for 18 hours at 37°C. Large zones of clearance highlight the increase in susceptibility. **C:** Structure of vancomycin. The susceptibility is controlled by 0.1% arabinose or 0.1 mM IPTG respectively. Experiments were carried out by Dr. Ganesh Krishnamoorthy. *E. coli* results are modified from a published figure (106), and *P. aeruginosa* (107).

1.3.2 Hyperporination has a limited effect on physiology

In order for the constructed strains to be useful tools to study the contribution of the outer membrane to resistance, expression of the pore should not affect the physiology of the bacterium in a significant manner. To check if the presence of the mutant pore has an impact on growth of the strains, we measured growth curves of each strain at increasing concentrations of inducer. In *E. coli*, we compared growth of strains grown in the presence of 0.0001% to 0.1% arabinose in strains with and without the pore. We noticed that all strains prematurely reached stationary phase at arabinose concentrations of 0.001% and higher (Fig. 1.4). Since this effect is also seen in strains that do not have a chromosomal copy of the mutant FhuA, it is not specific to the pore strains. However, it does seem to be more pronounced in hyperporinated strains. When comparing the pore strains to their respective parental strains, we found a slight decrease in the optical densities at 600 nm (OD_{600}) of cell cultures at stationary phase in the pore strains. The final OD_{600} of WT-Pore was about 10% lower compared to WT. This effect was slightly bigger for the efflux deficient ΔTolC strains with about a 20% decrease of the OD_{600} at stationary phase for ΔTolC-Pore compared to ΔTolC. However, we did not find a significant difference in the growth rates, when comparing the hyperporinated to their parental strains. Overall, the *E. coli* pore strains displayed comparable growth phenotypes to the WT strains albeit with a slightly lower OD_{600} at stationary phase.

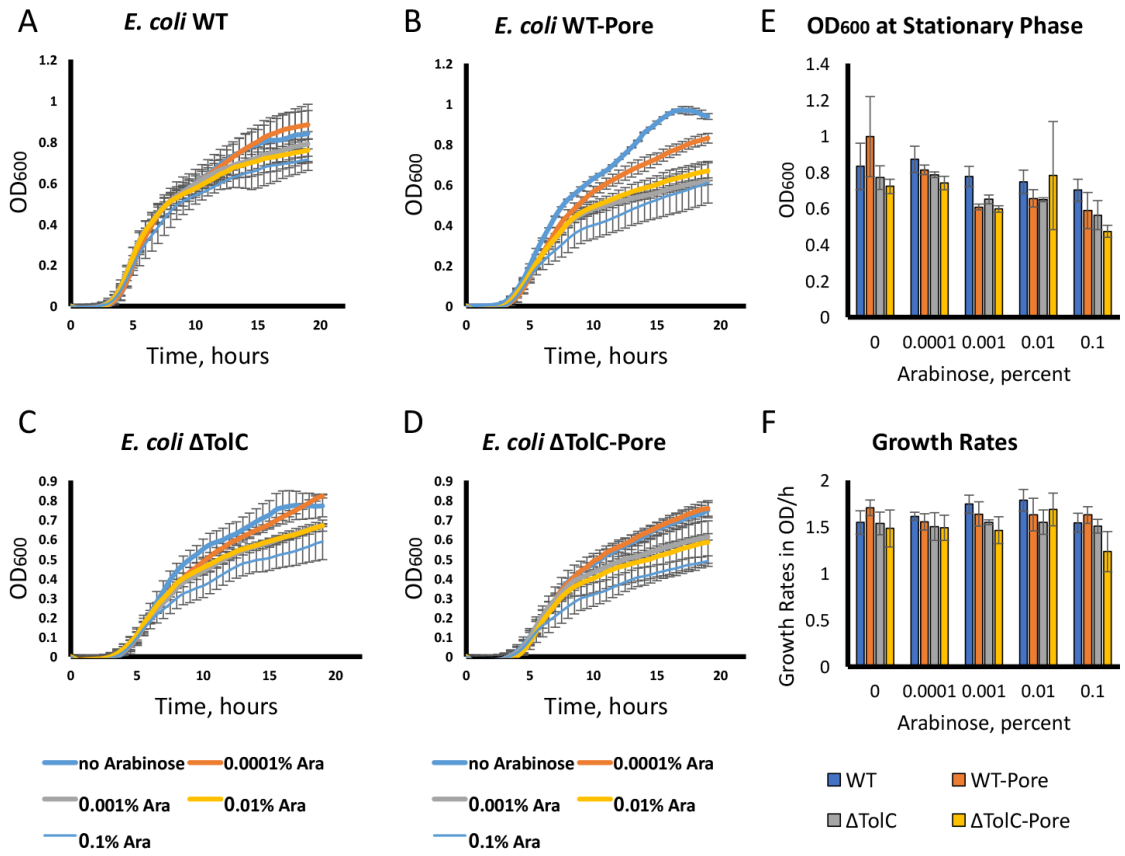

Figure 1.4 - Impact of the pore on growth of *E. coli*.

Growth curves of WT (**A**), WT-Pore (**B**), ΔTolC (**C**), and ΔTolC (**D**) at increasing concentrations of inducer. **E**: Comparison of OD_{600} at stationary phase. Growth rates (**F**) were calculated by plotting $\ln(OD_{600})$ against time and determining the slope of the linear portion. These plots can be found in Appendix D. Error bars are SD (n=4)

For *P. aeruginosa*, we first analyzed at the growth curves of cells without the pore at either no inducer or 0.1 mM IPTG (Fig. 1.5A and B). We noticed a difference in the growth of the deep efflux deletion mutants PΔ4 and PΔ6. Compared to the wild type PAO1 and PΔ3, their OD at stationary phase was significantly lower by about 40%. This difference is likely due to the outer membrane factors which are deleted in PΔ4 and PΔ6 but are still present in PΔ3. Deletion of OMFs were shown to impact the integrity of the outer membrane in *E. coli*, and similar effects could reduce the OD at stationary phase in *P. aeruginosa* (105). Furthermore, deletion of the RND transporters did not seem to have an impact on growth phenotypes when comparing PAO1 and PΔ3, suggesting that any differences for the deep efflux deficient mutants is likely the result of the missing OMFs. IPTG itself did not affect growth of the *P. aeruginosa* strains.

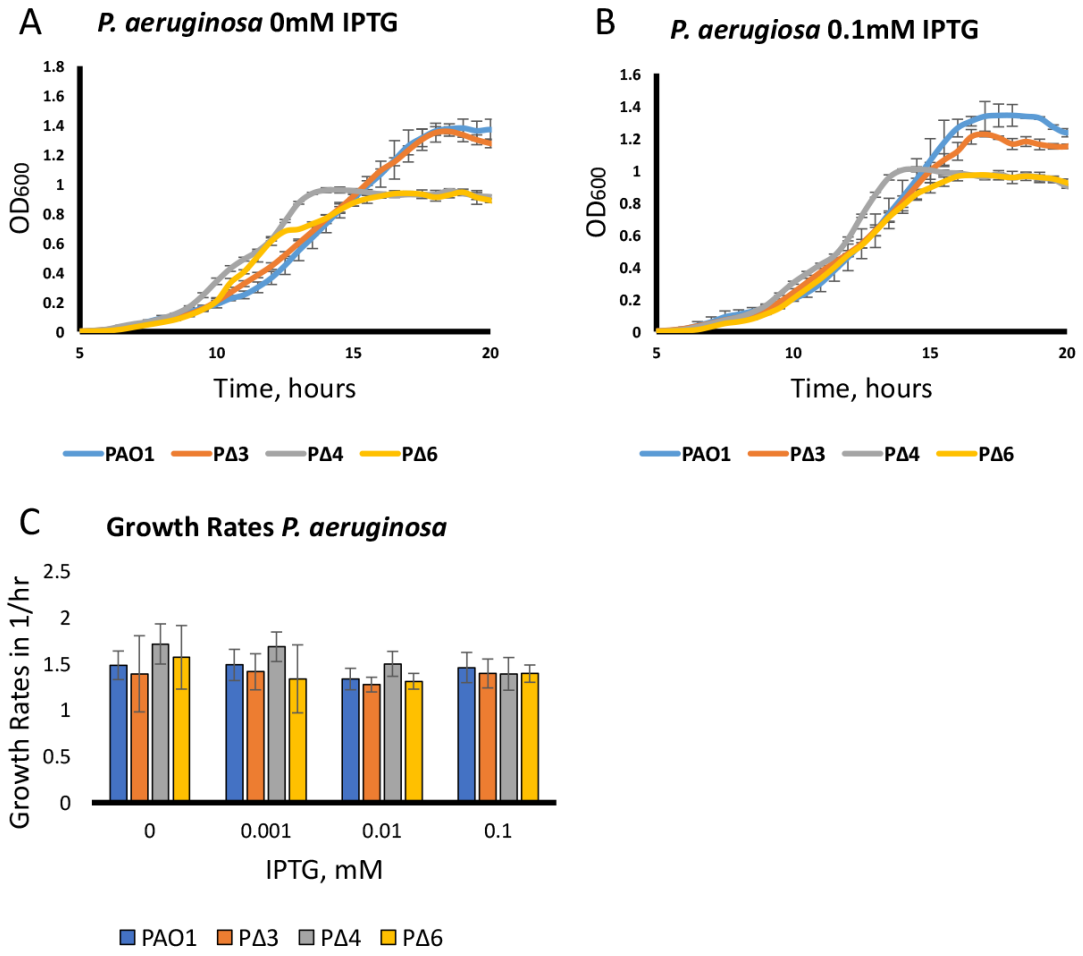

Figure 1.5 - Growth of PAO1 and efflux deficient variants.

Comparison of the growth of PAO1 and efflux deletion mutants with no inducer (**A**) and 0.1 mM IPTG (**B**). There is no significant effect of the inducer on the growth of strains without the pore. **C:** Growth rates of strains at increasing concentration of IPTG. Error bars are SD (n=3).

Next, we analyzed the growth phenotypes of hyperporinated *P. aeruginosa* strains (Fig. 1.6). First, we noticed the same decrease in the OD_{600} at stationary phase when the OMFs are deleted. When titrating the inducer, we saw no significant effect up to a concentration of 0.01 mM IPTG on the OD_{600} or the growth rates (Fig. 1.6E). At higher inducer concentrations, we noticed an effect of hyperporination on the growth of the *P. aeruginosa*. Cells went to stationary phase prematurely and their final OD_{600} was roughly 50% lower when compared to no inducer (Fig. 1.6A-D). However, this did not affect the growth rates of the strains, which remained largely unaffected by the pore (Fig. 1.6E). The only exception to this seemed to be PΔ3, which had a significant decrease in the growth rates at 0.1 mM IPTG. The least affected strain was PAO1 which, presumably, can complement the decreased permeability of the outer membrane with active efflux.

In addition, we noticed that cells expressing the pore started to aggregate at this inducer concentration, which could be related to cell signaling. Cell-to-cell communication requires the presence of a quorum to produce a high enough extracellular concentration of signaling molecules to activate their respective receptors (78). It is likely that increasing the outer membrane permeability could reduce this concentration threshold. This way, a lower cell density could produce enough signaling molecules to activate their respective signaling circuit. Since biofilm formation is directly linked to quorum sensing, it is possible that hyperporinated cells start to form aggregates at lower cell densities (125). This would explain why the pore expressing cells go into stationary phase prematurely and start to form biofilms. To test whether the reduced OD_{600} at stationary phase correlates with a lower number of viable cells, we

measured the colony forming units (CFU) directly following a growth curve experiment (Fig. 1.6F). We normalized the CFUs to the respective OD_{600} of the culture, and noticed no significant difference between the hyperporinated and the parental strain. This suggests that although they go into stationary phase prematurely, the pore expressing strains are still healthy and the growth phenotype is likely due to the premature formation of biofilm.

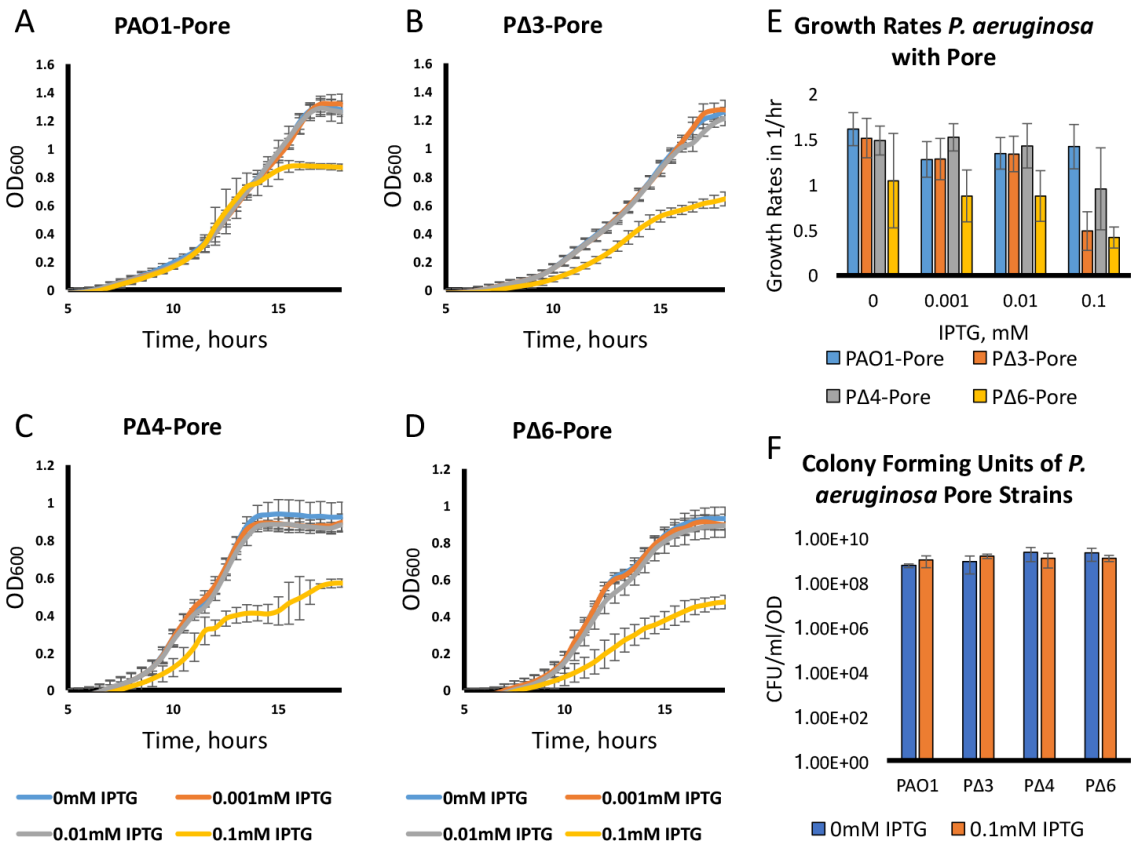

Figure 1.6 - Growth phenotypes of cells expressing the mutant FhuA.

A-D: Growth curves of PAO1-Pore, PΔ3-Pore, PΔ4-Pore, and PΔ6-Pore respectively at increasing concentration of inducer. At 0.1 mM, cells enter into stationary phase prematurely. **E:** Growth rates of *P. aeruginosa* pore strains at increasing concentration of inducer. Plots of LN(OD) vs time can be found in Appendix D. **F:** Colony forming units of pore strains per ml and OD_{600} with and without inducer. Results suggest no significant difference in the number of viable cells when the pore is expressed. Error bars are SD (n=3).

To further analyze the physiological effects of hyperporination in *P. aeruginosa*, we measured the production of pyocyanin, pyoverdine, and the formation of biofilms and compared them to their respective strain without the pore. Pyocyanin is a virulence factor that is responsible for the blue-green color of *P. aeruginosa* cultures. Its production is directly controlled by the *rhl* and PQS quorum signaling pathways, and by itself can act as a signaling molecule (126, 127). Our measurements show that PAO1-Pore produces pyocyanin to the same levels as the control without inducer (Fig. 1.7A). There is a significant difference between the PAO1 strains and the efflux deficient mutants. PΔ3 produces about 73% less pyocyanin when compared to PAO1, with PΔ4 and PΔ6 synthesizing even less of the virulence factor. The difference between PAO1 and PΔ3 is likely due to the deletion of MexAB, since this transporter was already indicated to be involved in quorum sensing (79, 90). Further decrease of the virulence factor suggests that the minor efflux pumps that are absent in PΔ4 and PΔ6 may also contribute to cell signaling. The difference between the levels of pyocyanin of PΔ4 and PΔ6 is likely due to the deletion of MexEF-OprN, since it is also indicated to transport signaling molecules (128). In addition, expression of the pore in efflux deficient strains resulted in a further decrease of about 50% of the pyocyanin levels. This suggests that the presence of the pore does indeed change some of phenotypes controlled by quorum sensing. The fact that we do not observe this decrease in PAO1-Pore suggests that the major transporters can complement hyperporination with regard to the synthesis of this virulence factor.

Pyoverdine is another pigment that is controlled by quorum sensing (129). Pyoverdines are siderophores that are necessary in maintaining iron homeostasis in *P.*

aeruginosa(130). When measuring pyoverdine in PAO1 and PΔ4, we were unable to detect a significant difference in the production of the siderophore between pore expressing strains and their respective parental strains (Fig. 1.7B). Interestingly, we noticeed that PΔ4 produces about 50% more pyoverdine than PAO1.

Lastly, we measured the production of biofilm in PAO1 and PΔ4 strains with and without the pore (Fig. 1.7C). Our results show that PΔ4 produces about 30% more biofilm when compared to PAO1. However, expression of the pore did not seem to affect biofilm formation. This suggests that although the pore variants initially show more cell aggregates and enter the stationary phase prematurely, they ultimately produce equal amounts of biofilm compared to their non-pore expressing counterparts. Overall, it seems that hyperporination affects the quorum sensing signaling pathways of *P. aeruginosa* to an extent, as seen by the differences in pyocyanin production. However, the pathways are not inhibited since other quorum sensing phenotypes are still seen at levels comparable to non-hyperporinated cells.

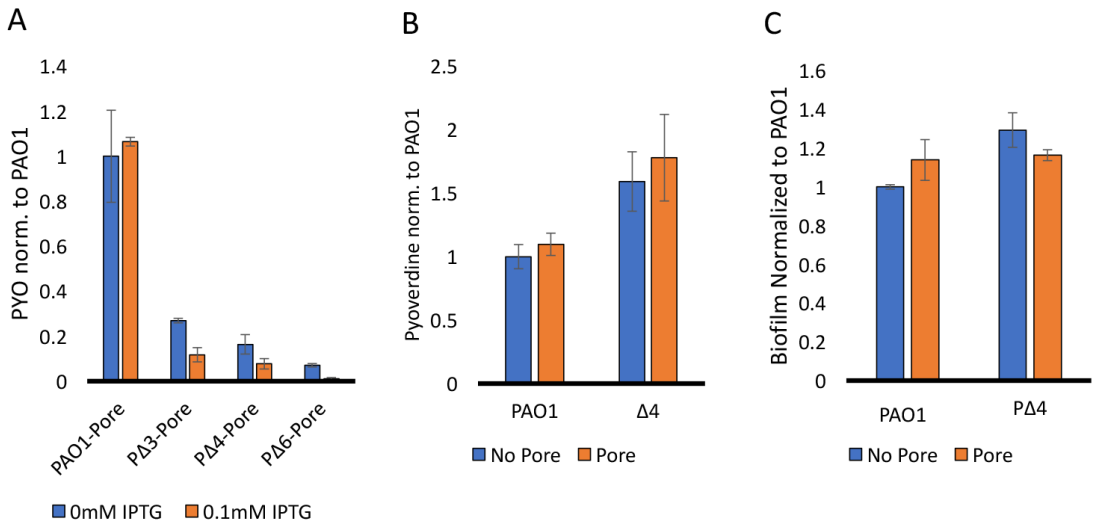

Figure 1.7 - Effect of pore expression on phenotypes controlled by cell signaling.

A: Pyocyanin production in *P. aeruginosa* pore strains with and without 0.1 mM IPTG. Hyperporination decreases pyocyanin synthesis by about 50% in the efflux deficient strains. Furthermore, all efflux deficient variants produce significantly less of the virulence factor. The pore does not affect pyoverdine production (**B**) or biofilm formation (**C**). Error bars are SD (n=3).

Overall, expression of the pore affects both *E. coli* and *P. aeruginosa* in a similar way. Both organisms go into stationary phase early, although the effect is much more pronounced in *P. aeruginosa*. However, growth rates in both organisms do not change significantly and, in the case of *P. aeruginosa*, the reduction in the OD at stationary phase does not affect cell viability. Thus, hyperporination appears to be a much gentler way of increasing the outer membrane permeability when compared to, for example, the use of polymyxins.

1.3.3 Hyperporination sensitizes *E. coli* to antibiotics and increases their intracellular concentration.

Since the presence of the pore increased the sensitivity of all strains to vancomycin, we wanted to see whether it would also potentiate smaller antibiotics. To test this, we grew *E. coli* strains with and without the pore at increasing concentrations of ciprofloxacin and erythromycin (Fig. 1.8). Ciprofloxacin is a fluoroquinolone that inhibits DNA gyrase and topoisomerase IV. Both enzymes are important for DNA replication, by cutting double stranded DNA and relaxing positive supercoils. Ciprofloxacin is a polar molecule that is relatively small at a molecular weight of about about 330 Da. Generally, small polar molecules enter the cells by passively diffusing through general porins. Since the exclusion size of the outer membrane porins OmpF/C in *E. coli* is about 600 Da, it should be able to enter cells readily even without the addition of the pore (30). Our results show significant change in the minimum inhibitory concentration (MIC) between *E. coli* WT and the efflux deficient ΔTolC mutant (Fig. 1.8A). The MIC is defined as the minimum concentration of a compound

required to inhibit visible growth of the bacterium. We determined the MIC of ciprofloxacin in the WT to be 8-fold greater than in ΔTolC, suggesting that efflux is a major contributor of the accumulation of ciprofloxacin into *E. coli*. There is also a slight drop of the optical densities (OD) of the WT-Pore cultures at ciprofloxacin concentrations below the MIC. This decrease is not solely due to the physiological impact of the pore, since the OD of cultures without ciprofloxacin resulted in only a 20% decrease for the pore mutant. However, the actual MIC value only decreased by two-fold in the pore variant, suggesting that the activity of ciprofloxacin is not significantly limited by diffusion across the outer membrane. Furthermore, there was also no significant difference in the efflux deficient ΔTolC strain with and without the pore. Hence, active efflux is the major determinant of the activity of ciprofloxacin in *E. coli* and the outer membrane barrier only has a minimal impact on the MIC, which is likely due to general porins of *E. coli*. However, the pore inhibits the growth of the WT strain at lower, sub-inhibitory concentrations, suggesting that it does increase the uptake of the drug.

Erythromycin is a large, relatively polar antibiotic with a molecular weight of about 700 Da that belongs to the class of macrolides, which bind to the 50S subunit of the ribosome and inhibit protein synthesis. Thus, like fluoroquinolones, macrolides need to penetrate the outer and inner membrane, but, unlike ciprofloxacin, erythromycin is much larger and exceeds the 600 Da cutoff of *E. coli*'s general porins (30). The inhibition curves with erythromycin show a 32-fold change in the MIC when comparing WT to ΔTolC, which highlights that efflux transporters are proficient in transporting this relatively large antibiotic (Fig. 1.8B). When comparing the WT to the WT-Pore

mutant, the MIC decreased from 64µg/ml to 4µg/ml, thus resulting in another 16-fold change. This shows that both the outer membrane barrier and active efflux work in synergy to provide resistance to this antibiotic. Surprisingly, when comparing the efflux deficient ΔTolC to the pore expressing ΔTolC-Pore, we noticed another 4-fold reduction of the MIC. A change in the MIC of ΔTolC strains when hyperporinated suggests that there is still some efflux present in ΔTolC. Since TolC largely controls efflux across the outer membrane, this efflux likely occurs through the inner membrane. When comparing the MIC of WT to ΔTolC-Pore, we measured the most significant change of 128-fold. Overall, hyperporination and the depletion of efflux affect both antibiotics differently. Ciprofloxacin is small and can diffuse trough general porins, thus its activity is only limited by efflux and not the outer membrane permeability. On the other hand, efflux works synergistically with the outer membrane barrier to limit the activity of erythromycin.

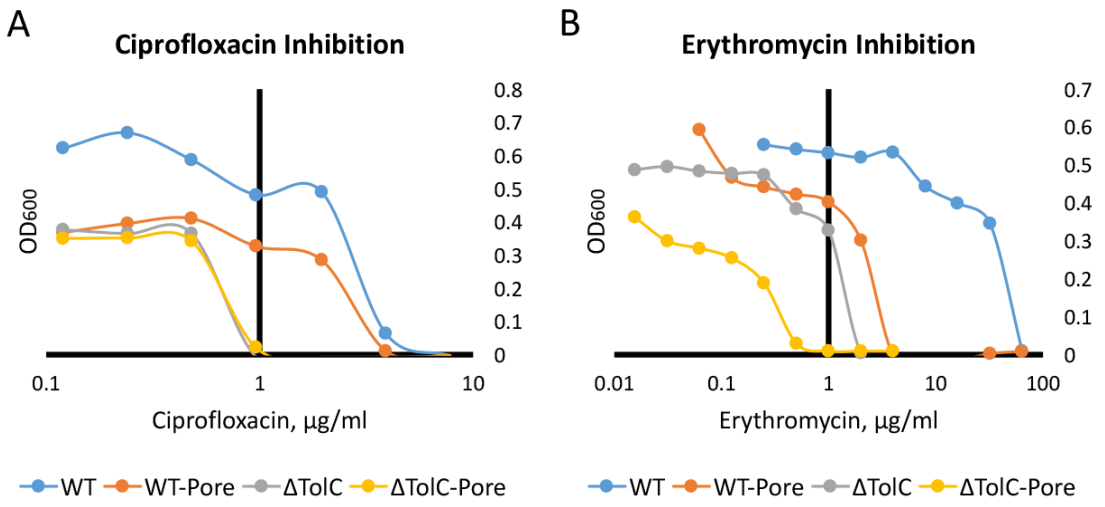

Figure 1.8 - Growth inhibition of antibiotics in *E. coli* pore strains.

Indicated cells were grown in the presence of different concentrations of ciprofloxacin (**A**) or erythromycin (**B**) for 18 hours in LB media at 37°C. Data is representative of 3 repetitions.

MIC in µg/ml	Ciprofloxacin	Erythromycin
WT	7.8	64
WT-Pore	3.9	4
ΔTolC	0.96	2
ΔTolC-Pore	0.96	0.5

Table 1.1 - Susceptibilities of pore strains to ciprofloxacin and erythromycin.

To test whether the increased sensitivity of the pore expressing strains correlates with a higher drug uptake, we measured accumulation of [14C]-erythromycin in our constructed *E. coli* strains. For this, we grew cells to early stationary phase with 0.1% arabinose to induce expression of the pore, washed them twice with buffer containing 0.4% glucose to energize the transporters, and incubated them with radiolabeled erythromycin at a specific activity of 25 mCi/mmol. From this mixture, we took aliquots at different time points and added them to filter disks that were attached to a vacuum manifold. The filters were subsequently dried and the radioactivity measured using a scintillation counter. The steady state accumulation of the antibiotic was estimated by using the intracellular concentration reached after 32 minutes of incubation. We noticed that the antibiotic was binding to the filter disks, thus the measured absolute values of intracellular antibiotic do not necessarily reflect the actual concentration inside the cell. However, comparing relative amounts of uptake still yields information about the differences of the strains (Fig. 1.9).

Comparing the accumulation of erythromycin in WT and WT-Pore, the hyperporination clearly increases the uptake of the drug as seen by a greater intracellular concentration of erythromycin (Fig. 1.9A and B). When looking at the steady state accumulation plotted against the extracellular erythromycin concentration (Fig. 1.9E), the WT strain follows a linear trend with a shallow slope at lower concentrations. Once the extracellular concentration is increased beyond 10 μM, we begin to see an increase in the slope and a hyperbolic relationship. A hyperbolic pattern indicates that at lower concentrations efflux transporters are able to keep the intracellular concentrations low. However, once we increase the extracellular

erythromycin concentration, high levels of the substrate overwhelm the transporters and efflux is becoming less efficient. Thus, the slope increases at higher concentrations of the drug. Overall uptake of erythromycin is the lowest in WT, which correlates well with the measured MICs of 64 μg/ml. The WT-Pore and ΔTolC showed comparable levels of erythromycin accumulation with a linear relationship, which is also reflected in a similar MIC value of 2-4 μg/ml. This suggests that hyperporination increases periplasmic concentrations of the drug beyond the capacities of the transporters, resulting in a similar accumulation of erythromycin in WT-Pore as in the efflux deficient strain. Hyperporinating the ΔTolC strain further increases the uptake, highlighting that there is significant efflux across the inner membrane (Fig. 1.9C and D). This is also in agreement with the overall lowest MIC of 0.5 μg/ml. In addition, the data also shows that the intracellular concentration was calculated to be higher than the extracellular concentration. This suggests that erythromycin is concentrated inside the cell likely due to binding to its target.

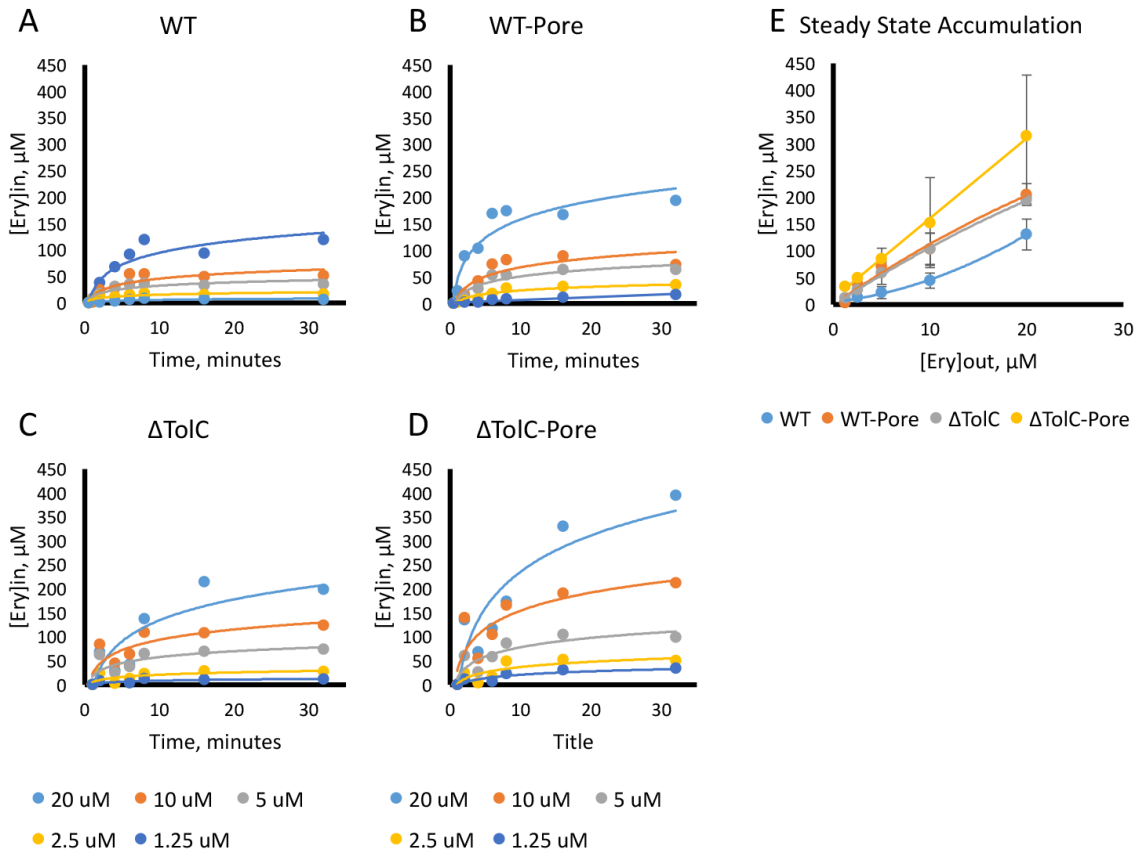

Figure 1.9 - Uptake of radiolabeled [14C]-Erythromycin in *E. coli* strains.

A-D: Time course of accumulation of the drug in WT, WT-Pore, ΔTolC, and ΔTolC-Pore respectively. Data shown is representative of 3 replicates. **E**: Steady state concentrations of intracellular erythromycin plotted against extracellular concentrations of the antibiotic. Steady states were estimated by the uptake after 32 minutes of incubation. Error bars are SD (n=3).

Overall, the growth inhibition results for erythromycin agree with the uptake experiments. The WT had the lowest uptake and correspondingly the highest MIC with 64 μg/ml. WT-Pore and ΔTolC both had comparable levels of uptake and also have similar MICs at 2-4 μg/ml. Growth inhibition and the uptake experiment showed that hyperporination of the TolC mutant potentiates the activity of erythromycin by an additional 4-fold and also further increased its uptake. These results show that the decrease in the MIC in hyperporinated cells directly correlates with increased uptake of the antibiotic. Thus, the pore potentiates large antibiotics by increasing their intracellular accumulation.

1.3.4 Hyperporination sensitizes *P. aeruginosa* to small and large antibiotics.

To study the effects of hyperporination on drug susceptibility in *P. aeruginosa*, we grew cells in the presence of azithromycin and carbenicillin and monitored the optical densities of the cultures. Azithromycin is a macrolide, similar to erythromycin, however with somewhat higher potency in *P. aeruginosa*. It is slightly larger with a molecular weight of about 750 Da and more polar, but kills with a similar, bacteriostatic mechanism of action. The experiment was carried out with PAO1, all efflux deficient mutants, and their respective pore variants. Since in *P. aeruginosa*, MexAB-OprM and MexXY-OprM are the most clinically relevant transporters, due to their broad specificities and high levels of expression, we expect to see a significant contribution of efflux in the PAO1 strain (89, 131). All efflux deficient strains are lacking these two efflux pumps, leading to significantly reduced efflux capacities even in PΔ3. Hence, when comparing the deep efflux deletion strains, we are able to see the contribution of

"minor" or "silent" transporters. In addition to the RND transporters and their respective MFP, PΔ4 and PΔ6 are also lacking the OMFs. Since these proteins are usually promiscuous, the difference between PΔ3 and PΔ4 highlights the contribution of all transporters that depend on the outer membrane factors OprM and OprJ as well as the transporter MexJK. Furthermore, MexJK has been reported to be at least partially reliant on OprM to facilitate efflux (95). Consequently, any changes in antibiotic susceptibility between PΔ4 and PΔ6 can be attributed to either the transporters MexEF and TriABC, or the outer membrane factor OprN.

Looking at the growth inhibition with azithromycin for non-hyperporinated strains (Figure 1.10A), we see the contribution of efflux towards resistance to this antibiotic. There is a 16-fold difference between in the MIC of azithromycin of PAO1 and PΔ3, indicating that azithromycin is recognized as a substrate by the major transporters. In addition, we measured a two-fold MIC difference between PΔ3 and the two deep efflux deficient strains PΔ4 and PΔ6, suggesting that some efflux pumps expressed at lower levels contribute to resistance of this macrolide. We also noticed reduced optical densities for PAO1 at higher, but not fully inhibiting concentrations of azithromycin. Possibly indicating that at these concentrations some transporters may already be exhausted in their capacities, allowing for a higher intracellular concentration of the drug. The exclusion size for the general porins in *P. aeruginosa* is estimated to be three fold lower than for *E. coli*, suggesting that overexpression of our mutant pore might have a more significant impact on susceptibility (30). Indeed, comparing the MIC of PAO1 and PAO1-Pore, we measured a 64-fold difference. This highlights that there is significant synergy between the outer membrane barrier and active efflux for

azithromycin (Fig. 1.10B and Table 1.2). Surprisingly, the contribution of the pore had a similar effect in PAO1 than it had in our efflux deficient strains. Hyperporination resulted in a similar 64 to 128-fold decrease in the MIC of all strains. Since the pore essentially increases the periplasmic concentration of the drug and the transporters translocate substrates from the periplasm, potentiation indicates that the high periplasmic concentration saturates the capacities of some transporters resulting in inefficient efflux. The fact that we see this potentiation even in the mutants, suggests that there is still significant efflux present. The deletion of efflux in conjunction with hyperporination shows a staggering 4,000-fold difference on susceptibility. Furthermore, the deletion of transporters and the expression of the pore individually potentiated the activity of azithromycin, which shows that there is significant synergy of the two in the efflux of this compound. Overall, macrolides in *P. aeruginosa* and *E. coli* showed a synergistic effect of the outer membrane and efflux.

Next, we tested the growth inhibiting effects of carbenicillin on the constructed *P. aeruginosa* strains (Fig. 1.10C and D). Carbenicillin is a beta-lactam with a molecular weight of about 380 Da and is also highly polar. Beta-lactams are considered bactericidal and inhibit transpeptidases that are required for the proper synthesis of peptidoglycan. In contrast to the previous antibiotics, the target of carbenicillin is in the periplasm, which could significantly affect the susceptibility of our pore strains to the drug. Since the mutant pore permeabilizes the outer membrane, the antibiotic would have direct access to its target without being limited by slow diffusion through general porins. Looking at our results, we measured a 16-fold difference in the MIC between the pore strains and their non-hyperporinated counterparts. This suggests that diffusion

through the pore is still somewhat of a limiting factor and does not give unrestricted access to the periplasm. The major efflux transporters of *P. aeruginosa* also contribute to resistance of this antibiotic. We measured a 32-fold decrease in the MIC of carbenicillin between PAO1 and PΔ3 (Fig. 1.10C and Table 1.2). We did not measure a difference between PΔ3 and PΔ4, and a 2-fold MIC reduction between PΔ4 and PΔ6. Surprisingly, when comparing efflux in the pore producing strains, we were still able to measure a 32-fold difference between PAO1-Pore and the efflux deficient pore strains (Fig. 1.10D and Table 1.2). If diffusion to the periplasm was unrestricted in pore strains, active efflux across the outer membrane should only have a minimal impact on susceptibility. This highlights that, although the pore drastically increases the outer membrane permeability, diffusion through the pore is still a limiting factor. In addition, our results also highlight that there is synergy between the outer membrane and efflux in limiting the activity of carbenicillin in *P. aeruginosa*.

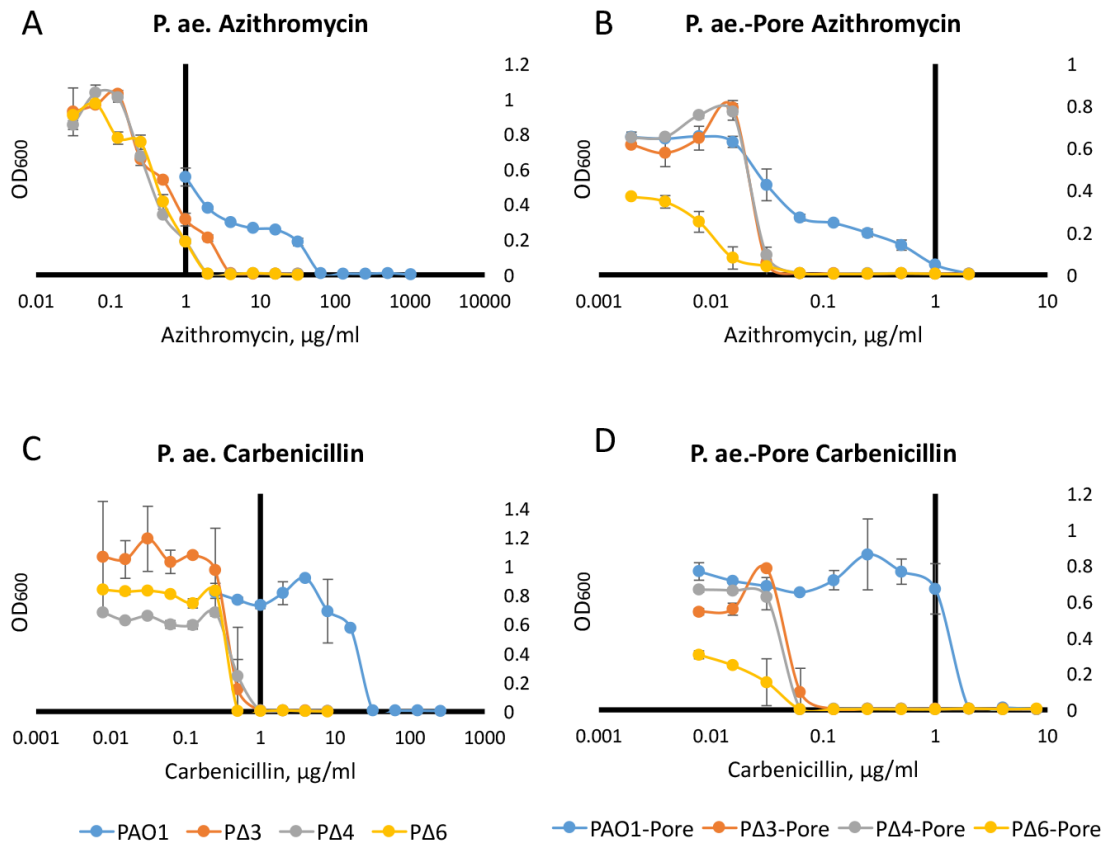

Figure 1.10 - Growth inhibiting effects of azithromycin and carbenicillin in *P. aeruginosa*.

Hyperporination in *P. aeruginosa* affects the activity of the two antibiotics in efflux proficient and deficient strains. Growth inhibition of azithromycin (**A** and **B**) and carbenicillin (**C** and **D**) with and without the pore as indicated. Indicated strains were induced with 0.1 mM IPTG and grown for 18 hours. After incubation, the optical densities were determined utilizing a microplate reader. Error bars are SD (n=2).

MICs in µg/ml	Azithromycin	Carbenicillin
PAO1	64	32
PΔ3	4	1
PΔ4	2	1
PΔ6	2	0.5
PAO1-Pore	1	2
PΔ3-Pore	0.031	0.063
PΔ4-Pore	0.031	0.063
PΔ6-Pore	0.016	0.063

Table 1.2 - Minimal inhibitory concentrations (MICs) of azithromycin and carbenicillin in hyperporinated or efflux deficient *P. aeruginosa* strains.

Overall, the pore increases susceptibilities in *P. aeruginosa* in much the same way it does in *E. coli*. Differences between the permeabilities of the cell envelopes of the two species are readily visible. Smaller antibiotics are not potentiated in *E. coli* by the pore, likely due to the large exclusion size of its general porins. In contrast, the pore significantly increases the susceptibilities of small antibiotics in *P. aeruginosa*, presumably because of a lack of general porins with large exclusion sizes in the bacterium. However, for large antibiotics that exceed the exclusion size of the porins of both organisms, hyperporination has a significant effect on susceptibility in both species.

1.3.5 Hyperporination increases the uptake of the fluorescent dye Hoechst 33342.

To measure the kinetic uptake of compounds in the pore strains, we decided to utilize environment-sensitive fluorescent probes. The approach of using radiolabeled antibiotics did not yield high enough resolution to accurately analyze accumulation and resulted in significant error in *P. aeruginosa*, presumably due to the differences of the

outer membrane and its tendency to form aggregates. Fluorescent dyes like Nile red, 1-N-phenylnaphthylamine (NPN), or Hoechst 33342 (HT) have been used in the past to assess the activity of efflux transporters and yield better time resolution (132-135). The method relies on the fact that the probes shift their emission spectra when they enter a hydrophobic environment, like binding the cell membrane or engaging in π-stacking interactions with DNA. For this experiment, we grew and washed cells in the same manner as for the radioactivity assay and, using a microplate reader with an injector system attached, added them to a 96-well plate that contained different concentrations of the fluorescent dye. Subsequently the fluorescence emission was read for 10 minutes every 20 seconds. The data output resembles that of a signal exponential function, thus we decided to fit the uptake kinetics to an equation in the form of:

$$\mathbf{F = A_1 + A_2\left(1 - e^{-k_2 * t}\right)} \quad (1)$$

Thus, the rate of uptake is given by:

$$\mathbf{F = A_1 + A_2 - A_2 e^{-k_2 * t}} \quad (2)$$

$$\mathbf{\frac{dF}{dt} = A_2 * k_2 e^{-k_{2*t}}} \quad (3)$$

Since at the initial rate of uptake t = 0, the rate can be described as:

$$\mathbf{initial\ rate = A_2 * k_2} \quad (4)$$

In addition, the amplitudes A_1 and A_2 can provide information about the total accumulation of fluorophore inside the cell.

Here we measured the uptake of Hoechst 33342 into *E.* coli and *P.* aeruginosa strains. Hoechst 33342 (HT) (Fig. 1.14D) is about 450 Da in size and is frequently used to stain DNA. It has an affinity to hydrophobic environments and binds to DNA as well as lipids. To relate the fluorescent units of the experiment to actual concentrations, we

measured binding of increasing concentrations of HT to either DNA or lipids alone. The calibrations were done assuming that 1 ml of cells at OD_{600} of 1.0 contain 17 μg of DNA and 27 μg of lipids (136, 137). We incubated HT with either DNA or lipids and measured the emission at 450 nm (excitation at 350 nm). The linear dependence of the fluorescent signal to the concentration of HT allowed us to calculate the emission coefficient of HT bound to either lipids or DNA.

When HT is incubated with cells, there is a very fast initial increase in the fluorescent signal (Fit. 1.11). For the purpose of our analysis, this was attributed to HT binding to lipids which are readily available on the outer membrane. In our fitting routine, this fast step is characterized by the first amplitude A_1 (Fig. 1.12B). Unfortunately, this step happens too fast for our equipment to measure the corresponding rate, since we are unable to accurately determine the exponent k_1. Following this fast step is a slower increase in fluorescence, which is interpreted as HT diffusing into the cell and binding to intracellular DNA. Consequently, the amplitude A_1 is converted to concentration using the lipid emission coefficient and A_2 using the DNA emission coefficient. Thus, the sum of both amplitudes describes the total accumulation of HT in the cell.

To fit large sets of uptake data to the equation above, scripts were written in Matlab (MathWorks) utilizing the fittype function in loops. This provided a fast way to extract the parameters A_1, A_2, and k_2 from uptake experiments with a wide range of fluorophore concentrations. Before fitting was performed, the datasets were inspected for outliers and the fluorescence signal was normalized to the initial emission of the fluorophore. Once the fitted parameters were determined, the initial rates and steady

states of fluorophore accumulation were calculated. The reported values are an average of at least three experiments. The uptake experiments reported here were carried out by Dr. Ganesh Krishnamoorthy, while this author was responsible for the data analysis. The *E. coli* results were further applied to a novel kinetic model of drug accumulation inside bacterial cells developed by Dr. Valentin Rybenkov and David Westfall (138). The *P. aeruginosa* data has been submitted as part of a separate manuscript.

For the HT uptake in *E. coli*, we found that the results are similar to what we previously measured with the radiolabeled [14C]-erythromycin, albeit with much better resolution. Looking at the time courses of HT uptake (Fig. 1.11), WT had the overall lowest fluorescent signal. When comparing the WT to ΔTolC, we notice a similar first initial increase in fluorescence but the subsequent uptake in the efflux deficient strain is much higher. This is reflected in the initial rates (Fig. 1.12A) and values of A1 (Fig. 1.12B) plotted against the extracellular HT concentration. The parameter A1 represents the amount of HT that initially binds to freely accessible lipids, which should be comparable between the WT and ΔTolC strains. At higher concentrations, the graph of both strains reaches a plateau, which is likely due to saturation of the available binding sites of the membrane. Looking at the initial rates of HT uptake for WT and ΔTolC (Fig. 1.12A), we see a similar sigmoidal curve for both strains. Here, a sigmoidal trend suggests that transporters initially limit the rate of uptake. Once the concentration of HT is increased to levels significantly above the Km of a given transporter, its efflux capacity is exhausted and it can no longer efficiently reduce the uptake(138). Thus, the initial rate of uptake increases faster. Increasing the concentrations further results in a plateau, suggesting that the initial rate reaches a maximum and that higher

concentrations of the fluorophore won't increase this rate any more. Active efflux provided by TolC dependent transporters significantly lower the rates of uptake at all concentrations tested, suggesting that we are not exceeding the K_m for at least some of the transporters. The fact that we still see sigmoidal behavior in ΔTolC highlights that this strain is not completely deficient in efflux. When comparing the WT to WT-Pore, we saw a similarly small rate of uptake at very low extracellular concentrations of HT. However, the pore significantly increases the uptake at higher concentrations. At very high concentrations, the rate of uptake of the WT-Pore strain is similar to ΔTolC-Pore, suggesting that TolC dependent transporters are overwhelmed and can no longer provide efficient efflux. We noticed a similar trend for the initial binding of lipid in the pore strains. This binding is increased in strains expressing our mutant pore, which suggests that the pore initially provides more access to membrane binding sites. This could likely include binding to the inner membrane and explain the differences in the sigmoidal shapes of the WT-Pore and the ΔTolC-Pore strains. TolC dependent transporters can capture the dye from the inner membrane and expel them from the cell, which could explain the lower initial concentration of HT. The fact that ΔTolC-Pore still exhibits sigmoidal behavior suggests that it still has significant efflux, suggesting that other non-TolC dependent transporters exist and are able to utilize HT as a substrate. Unfortunately, we are unable to reliably estimate the second amplitude A_2, because the time courses of the uptake experiments did not saturate for all concentrations. Thus, we are unable to estimate the total steady state accumulation of HT inside each strain.

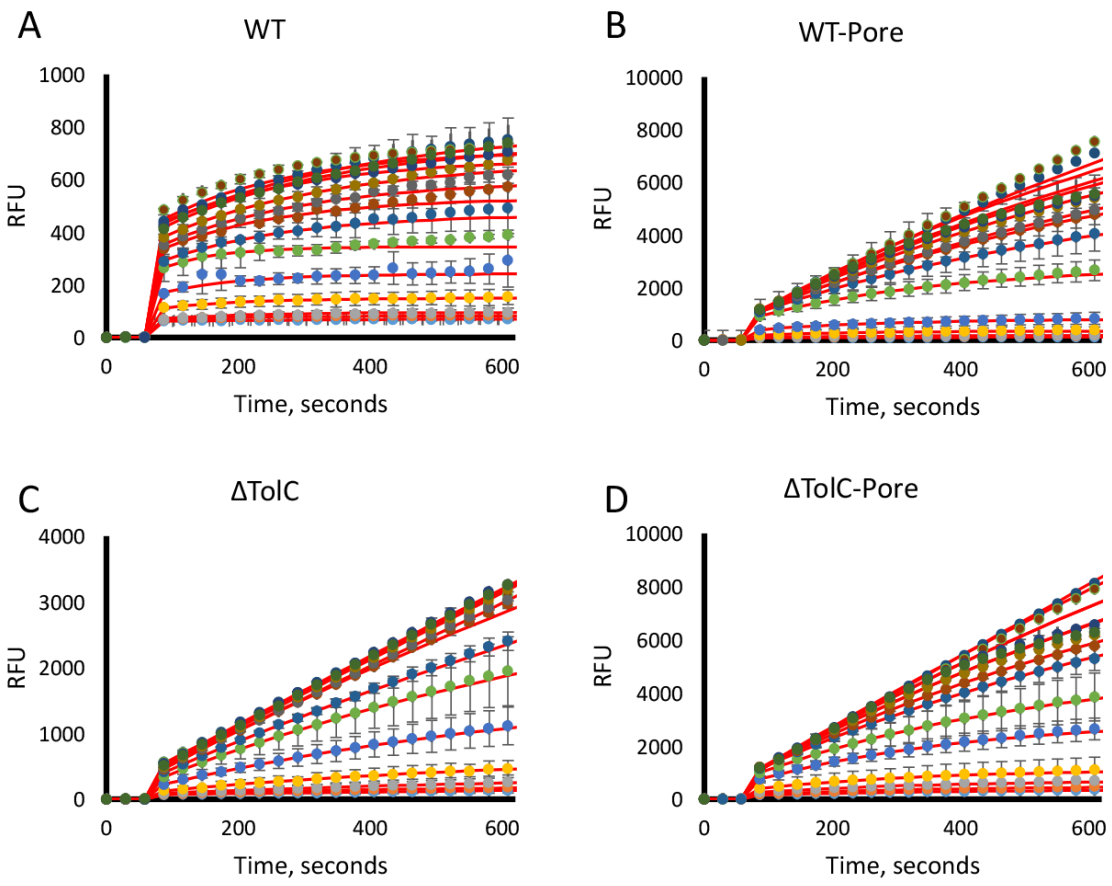

Figure 1.11 - Time courses of HT uptake in *E. coli* strains.

HT uptake in WT (**A**), WT-Pore (**B**), ΔTolC (**C**), and ΔTolC-Pore (**D**) at increasing concentrations of HT (0.5-16 μM). Data was fit to an exponential equation and initial rates and accumulation of HT was calculated. Lines in red indicate fitted lines. Error bars are SD (n=2 for WT and ΔTolC, n=4 for WT-Pore and ΔTolC-Pore).

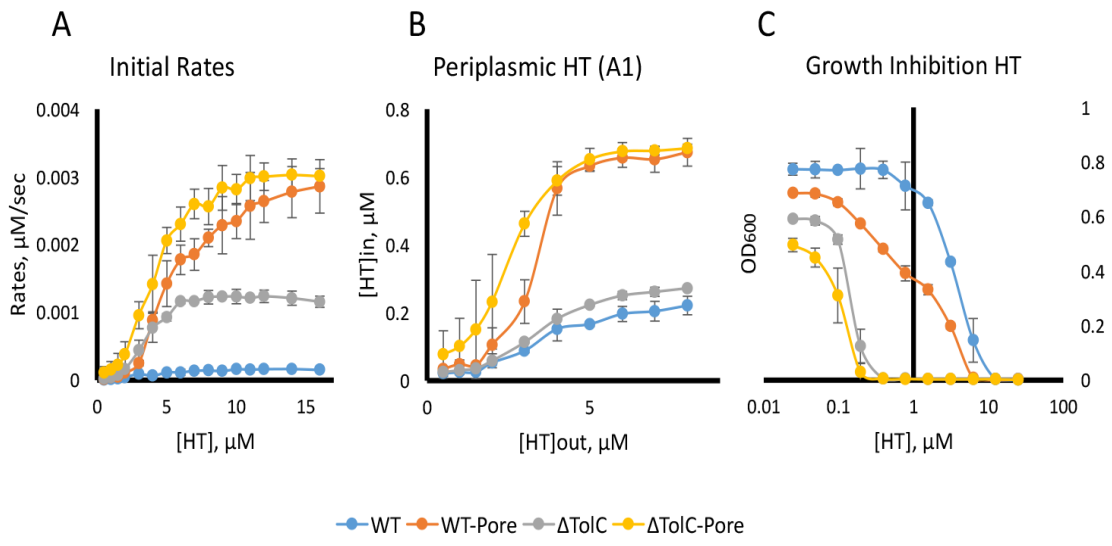

Figure 1.12 - Fitted parameters and growth inhibition of HT.

A: Initial rates of HT uptake in all four *E. coli* strains. **B:** Initial binding of HT to lipids, as indicated by the first amplitude. **C:** Inhibition curves of HT. Error bars are SD (n=2 for WT and ΔTolC, n=4 for WT-Pore and ΔTolC-Pore).

Since HT binds to DNA, it is toxic to the cell and exhibits antimicrobial behavior. To test whether the uptake correlates with MICs for HT, we measured the susceptibility of our strains to the dye (Fig. 1.12C). Surprisingly, although the pore increased the rate of HT uptake significantly, it almost has no effect on the MIC of the fluorophore. We only measured a two-fold reduction of the MIC when the pore is expressed. In contrast, efflux had a significant impact on the MIC, resulting in a 32-fold difference between WT and ΔTolC. This result shows that our results from the uptake experiment do not correlate with the measured MICs and the fluorescent signal is not directly related to binding of HT to its target.

When looking at the time courses of uptake in *P. aeruginosa*, we notice some similarities with *E. coli* (Fig. 1.13 and Fig. 1.14). In both bacteria, the pore significantly increases the accumulation of HT inside the cell. When comparing the steady state accumulation between the strains expressing the pore and not expressing the pore (Fig. 1.15B and C), we see that the overall uptake of HT is higher in pore strains. This is especially true at higher extracellular HT concentrations, where efflux capacities are exhausted. Looking at the overall uptake in non-pore expressing strains (Fig. 1.15B), we noticed a big difference between PAO1/PΔ3 and PΔ4/PΔ6. This could either point towards minor, lower expressed transporters having a bigger effect of uptake of HT or, more likely, that the absence of OMFs in PΔ4 and PΔ6 decreases efflux. OMFs in *P. aeruginosa* are promiscuous and can be used by several transporters, thus deleting them might also inactivate other efflux pumps (94). Surprisingly, the overall lowest accumulation of HT was measured in PΔ3 and not PAO1.

Looking at the uptake in hyperporinated strains (Fig. 1.14C), the contribution of the major efflux transporters on accumulation of HT is readily visible. In contrast to the non-pore strains, PAO1-Pore showed the lowest total uptake at all concentrations tested. Furthermore, we can clearly see that increasing the extracellular concentration of HT beyond 6 μM overwhelms the major transporters in *P. aeruginosa*, allowing for higher levels of accumulation. This sigmoidal behavior can also be seen in PΔ3. However, the transporters already saturate at about 3 μM, highlighting the difference in efflux capacities between the two strains. The difference between PΔ3-Pore and the deeper efflux deletion mutants suggests a contribution of minor transporters on HT uptake.

When looking at the initial rates (Fig. 1.14A), we also noticed that the pore significantly increases the rates of HT uptake. Surprisingly, PAO1 showed a higher rate of uptake than the efflux deficient mutants in non-pore strains but not in pore expressing strains.

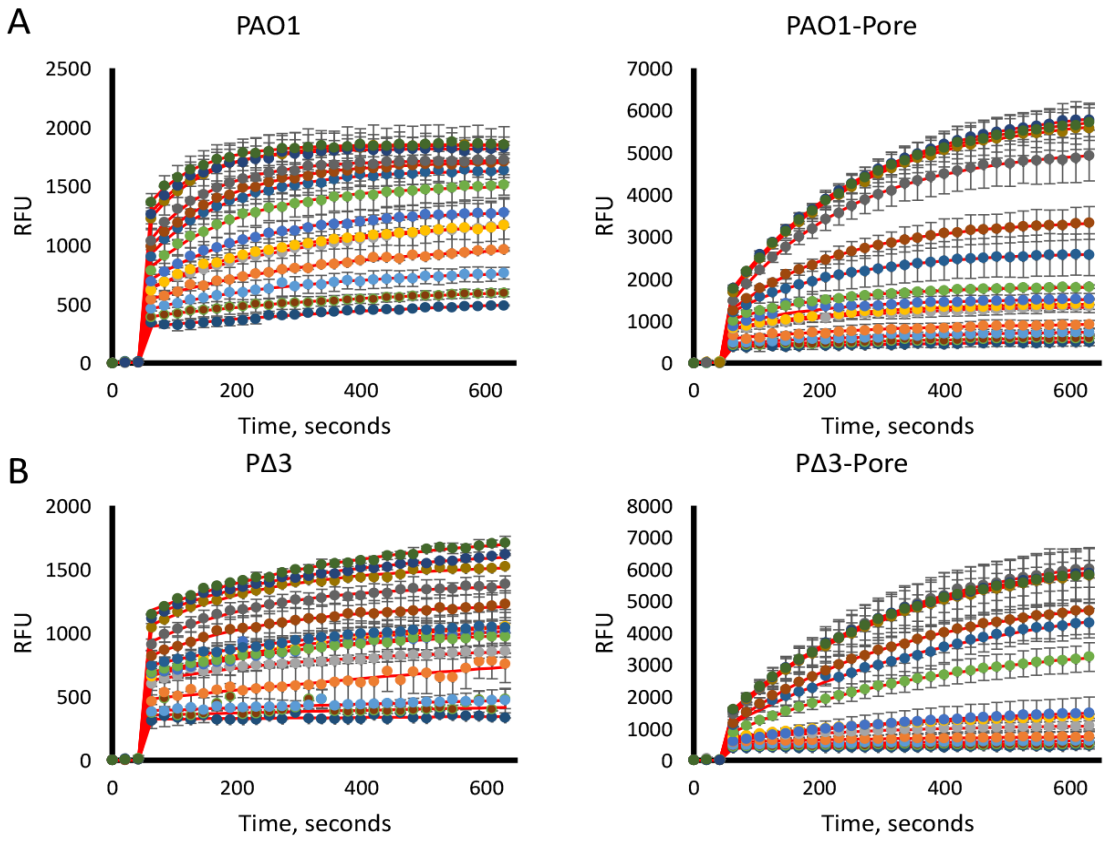

Figure 1.13 - HT uptake in PAO1 and PΔ3.

Time courses of uptake in the indicated *P. aeruginosa* strains with and without the pore. HT concentrations used were from 0.5 to 16 µM. Lines in red indicated fitted lines. Error bars are SD (n≥2).

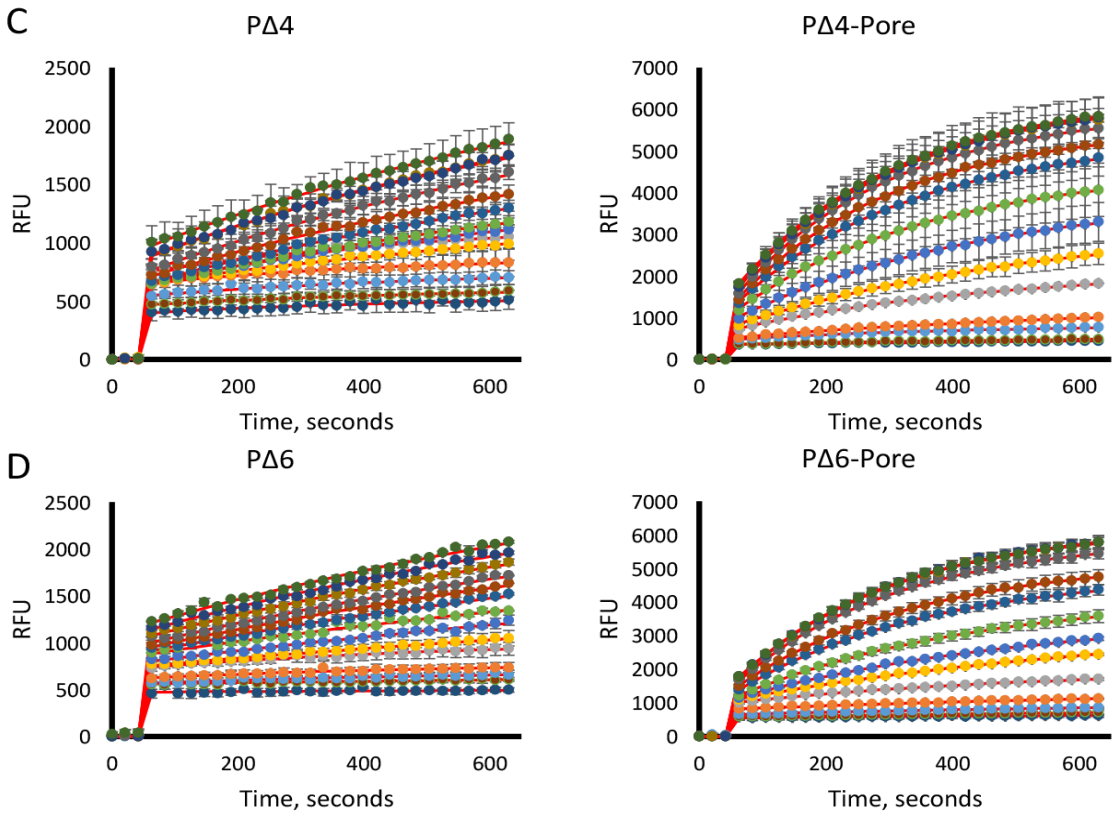

Figure 1.14 - HT uptake in PΔ4 and PΔ6.

Time courses of uptake in the indicated *P. aeruginosa* strains with and without the pore. HT concentrations used were from 0.5 to 16 μM. Lines in red indicated fitted lines. Error bars are SD (n≥2).

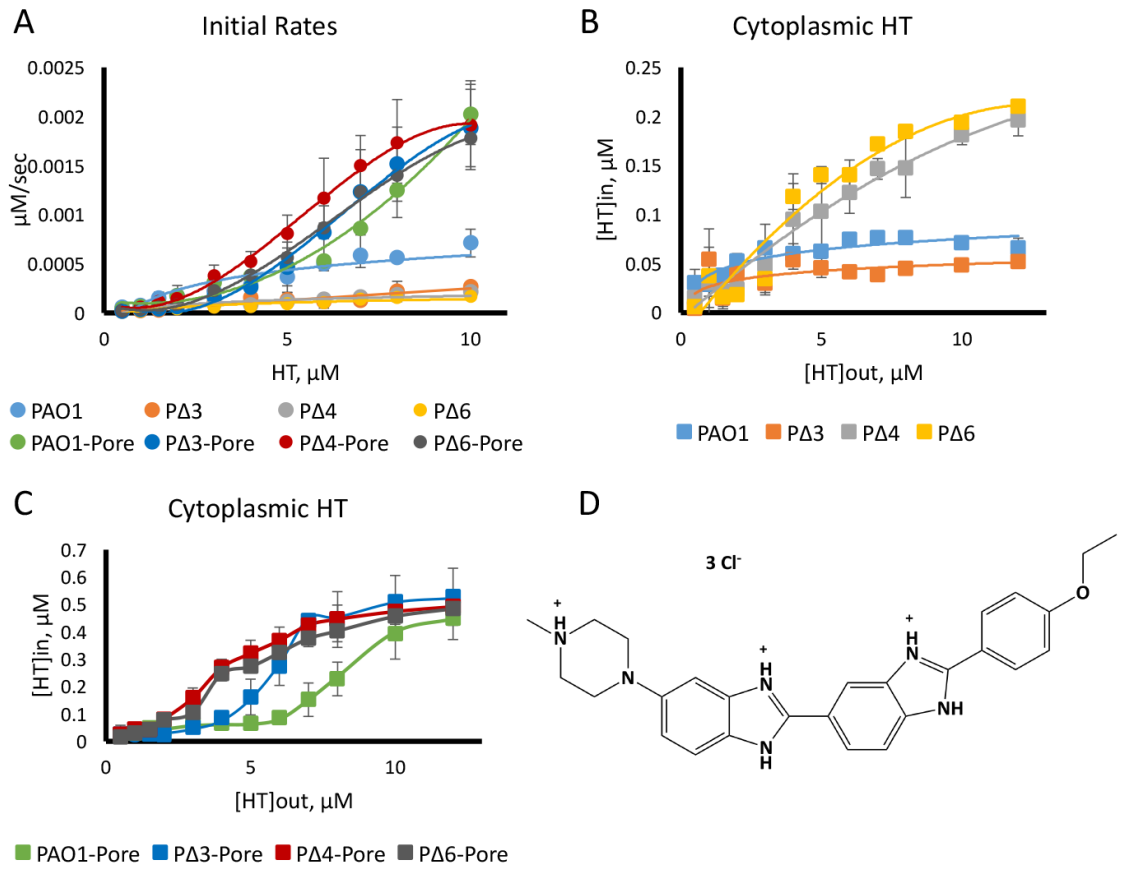

Figure 1.15 - Fitted parameters of HT uptake in *P. aeruginosa*.

A: Initial rates of uptake of all *P. aeruginosa* strains. **B and C:** Total accumulation of HT in *P. aeruginosa* strains with (**C**) and without (**B**) the pore. **D)** Structure of Hoechst 33342 (HT). Error bars are SD (n≥2).

MIC, μg/ml	Pore	
	-	+
PAO1	64	64
PΔ3	16	2
PΔ4	4	1
PΔ6	2	0.5

Table 1.3 - Susceptibilities of *P. aeruginosa* strains to HT.

Like in *E. coli*, the MICs of HT do not always correlate with the overall accumulation of the fluorophore (Fig. 1.15D). For example, the measured MIC in PAO1 was 64 μg/ml with and without the pore. This suggests that the major transporters can compensate for the increase in outer membrane permeability. However, the pore clearly increased the overall accumulation of HT. Furthermore, PΔ3 showed a lower uptake than PAO1 but its MIC is below that of PAO1 by 4-fold. Again, this suggests that HT might have a different target inside the cell. However, the rest of the MICs generally agree with the trends we see in the uptake experiments. The pore decreases the MICs of all the efflux deficient strains by 4 to 8-fold, and it also increases the overall HT accumulation in those strains. In addition, there is also a 4 to 8-fold difference between PΔ3 and PΔ4/PΔ6, suggesting a contribution of minor transporters in resistance. This is also in agreement with our uptake experiments, which show higher accumulation of HT in the deeper efflux deficient strains.

1.4 Discussion

Infections caused by multidrug resistant bacteria are becoming increasingly more difficult to treat, which could lead to a time when conventional antibacterial therapy will be insufficient to cure these diseases. This has never been as true as it is

now with the discovery of resistance to last line of defense antibiotics, like the recent finding of colistin resistance in a US hospital (2). Gram-negative bacteria pose a unique challenge in the fight against drug resistance due to the synergy of active efflux and low outer membrane permeability (5). Slow diffusion across the outer membrane limits the concentrations of antibiotics in the periplasm, so that the substrate concentrations of efflux transporters are kept low. This allows them to operate efficiently, providing robust intrinsic resistance. The study of this synergism requires a detailed analysis of the individual contributions of efflux and the outer membrane barrier.

RND transporters have been studied extensively and their activity can readily be determined by simple chromosomal deletions and the measurement of drug susceptibilities. On the contrary, removal of the contribution of the outer membrane barrier on drug resistance has been extremely difficult. Current methods to permeabilize the outer membrane, like the use of polymyxins, significantly change the properties of the outer membrane and disproportionately favor the uptake of hydrophobic compounds (102, 103). This makes them inadequate for the study of the outer membrane permeability barrier.

In this study, we introduce a novel approach at permeabilizing the outer membrane without changing its physical properties by the expression of a genetically engineered pore protein. This approach does not affect cell viability (Fig. 1.6F) and increases the uptake of compounds inside the cell (Fig. 1.9, 1.12, and 1.15). Furthermore, the pore sensitizes cells to large antibiotics that are generally thought to be unable to cross the outer membrane (Fig. 1.3).

Controlling the outer membrane permeability has significant advantages for the development of new antibiotics. Gram-negative bacteria are notorious for their low hit rate during drug screening (7), which limits the amount of possible lead compounds. Utilizing this hyperporination approach during the screening process would significantly increase the number of hits resulting in an increase in the number of lead compounds and the discovery of new antibiotics. Furthermore, structural properties that allow antibiotics to penetrate the cell envelope are largely unknown. Some antibiotics, like the aminoglycosides, are able to promote their own uptake by a mechanism that is proposed to be similar to that of polymyxins (139). However, it is still difficult to predict the penetration of other compounds through the outer membrane barrier. The potentiation of a compound by hyperporination reveals the contribution of the low permeability outer membrane and whether diffusion through it limits its activity. This could potentially lead to the discovery of the so called “rules of permeation”, an as of yet unknown list of structural characteristics that facilitate faster diffusion through the barrier. Overall, hyperporination has significant implications for the development of new drugs and the study of the outer membrane permeability barrier.

Chapter 2. Differential contribution of active efflux and the outer membrane barrier on drug susceptibility

2.1 Abstract

The increased frequency of multidrug resistant isolates of infectious pathogens necessitates improvements to the way we discover antibiotics. Current efforts in the field have only produced one novel class of antibiotics in the last 50 years (140). One of the major bottlenecks is the screening process in gram-negative bacteria due to their high levels of intrinsic resistance provided by a low permeability outer membrane and active efflux (5). Here, we are utilizing a combination of efflux deficient and hyperporinated strains to study the differential contribution of active efflux and outer membrane permeability on antimicrobial susceptibility. Our results suggest that most antibiotics belong to one of four groups depending on their potentiation by the deletion of efflux or hyperporination. This study also highlights the differences of the cell envelope of *P. aeruginosa* and *E. coli* and that so-called "rules of permeation" will likely be different depending on the bacterial species.

2.2 Introduction

Infections caused by multidrug resistant bacteria are becoming increasingly more frequent and are projected to even surpass cancer as one of the leading causes of death (1). As seen in a recent report by the US Center for Disease Control, the most critical threats are drug resistant gram-negative bacteria (6). Gram-negative bacteria possess a high level of intrinsic resistance due to their low permeability outer membrane and an arsenal of efflux pumps that significantly decrease the intracellular accumulation of antibiotics. The low outer membrane permeability coupled with active efflux causes problems not only in the treatment of patients with infections, but also in the process of drug discovery. The hit rate during drug screening is estimated to be 1,000-fold lower for *P. aeruginosa* when compared to gram-positive bacteria and is one of the major bottlenecks in the discovery of new antibiotics against gram-negatives (7). Improving the antibiotic pipeline is of great importance to ensure the continued efficacy of our arsenal of drugs. Currently, the frequency of emergence of drug resistance is much higher than the amount of time it takes to discover and approve new antibiotics. This will ultimately result in a post-antibiotic era where some infections can no longer be efficiently treated (141). Hence, new innovations in the drug discovery pipeline are desperately needed.

To study the permeability of the gram-negative cell envelope, it is necessary to separate the contributions of the outer membrane and active efflux on drug activity. It is important to identify which chemical features allow antibiotics to easily diffuse through the outer membrane or to circumvent efflux. Here, we are describing the use of efflux proficient and deficient *E. coli* and *P. aeruginosa* strains that have a chromosomally

encoded open pore in order to study the contribution of active efflux and outer membrane permeability on drug activity. The pore is a genetically modified porin from *E. coli* that was altered by removing 4 extracellular loops and its cork domain, resulting in an internal diameter of about 2.4 nm that can facilitate diffusion of large molecules (106, 122, 123). Expression of the pore is inducer-dependent and does not result in significant changes to the physiology of the bacteria (106). Furthermore, uptake experiments utilizing radiolabeled [14C]-erythromycin showed that the pore increases the accumulation of this large antibiotics (106).

Using these strains, we tested the contributions of the outer membrane and active efflux to resistance of a range of antimicrobials belonging to different classes of drugs. Our findings suggest that antibiotics can be clustered into four distinct groups, which are divided based on their potentiation by hyperporination, deletion of efflux, or both. Furthermore, these groups differ between *E. coli* and *P. aeruginosa* due to differences in their respective outer membrane permeability and arsenal of RND transporters. Grouping antibiotics this way may lead to the discovery of specific chemical features that facilitate uptake into the cell. In addition, our studies showed that measuring MICs in hyperporinated strains reveals true substrate specificities of efflux transporters and that the outer membrane barrier can significantly mask the contributions of these pumps. We present here a first approach to separate the synergistic effects of the outer membrane from active efflux on antimicrobial activity in gram-negative bacteria. The antimicrobial susceptibility tests described here were carried out by Dr. Ganesh Krishnamoorthy and the author of this dissertation.

2.3 Results

2.3.1 Interpretation of antimicrobial susceptibilities in the context of hyperporination.

Measuring antimicrobial susceptibility is typically done by MIC experiments. The minimal inhibitory concentration (MIC) is the concentration of a compound that inhibits visible growth of the bacteria. The traditional way of determining the MIC is by two-fold broth dilution in a 96-well plate of the compound and subsequent inoculation of the bacteria into each well. The plates are incubated at 37°C for 16-20 hours depending on the organism and the MIC is determined visually (113). The MIC does not give any indication of whether the compound is bactericidal or bacteriostatic and cannot be used to determine the activity of the compound *in vivo*, as there are many pharmacokinetic and pharmacodynamic parameters that need to be considered (113). Hyperporination of some antibiotics has a significant impact on the MIC and interpretation of such results needs to be evaluated with the context of permeability and active efflux due to the existence of synergy between the two. The following interpretations are made based on our novel kinetic model of drug uptake which was submitted and is currently under review(138).

In order for cell growth to be inhibited by a compound, it needs to accumulate to a certain concentration threshold inside the bacteria to efficiently bind its target. This intracellular concentration threshold is largely determined by the K_D of the compound and its target. Consequently, the MIC is determined by the extracellular concentration of the drug that allows the compound to sufficiently accumulate inside the cell past this threshold. Accumulation is largely hindered by diffusion across the outer membrane and

the opposing flux of efflux transporters. These two forces act in synergy, meaning that the low outer membrane permeability significantly limits the flux across the membrane barrier. Thus, the effective periplasmic concentrations of the antimicrobial that RND transporters encounter at any given time is much lower than what is present outside the cell. As we will see in the results, this lower periplasmic concentration allows transporters to provide effective efflux. This synergy provides effective means to protect the cell from the compound. However, since we are able to measure MICs for the vast majority of the antimicrobials, increasing the extracellular concentrations of the drug eventually leads to higher periplasmic accumulation due to higher rates of passive diffusion across the barrier. If the drug concentration in the periplasm is higher than the K_m of the transporter and its activity approaches V_{max}, the transporter is overwhelmed and efflux is inefficient. At that point, increasing the extracellular concentration of the compound has a bigger impact on the intracellular accumulation.

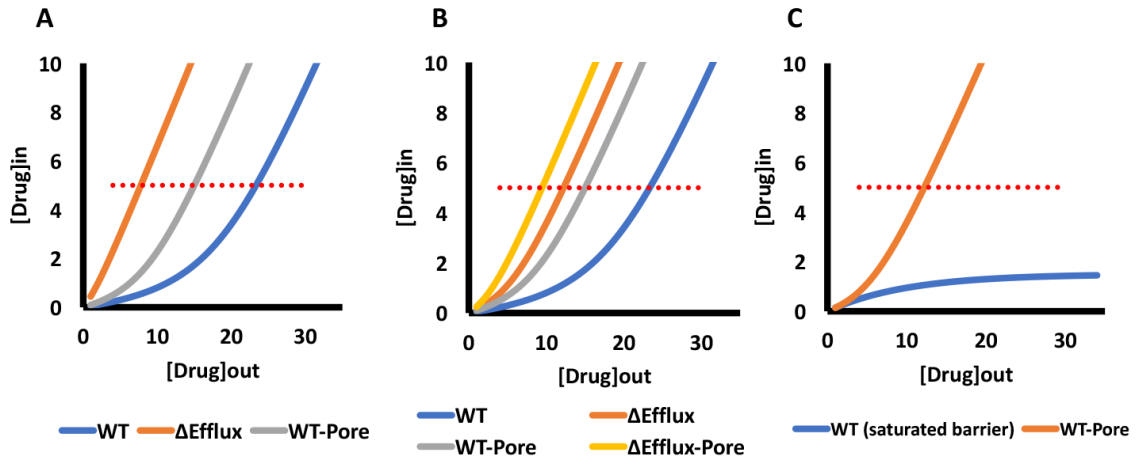

Figure 2.1 - Correlation between drug accumulation and active efflux in the context of hyperporination.

Simplified model of the accumulation of antimicrobials and its dependence on the synergy between the outer membrane and active efflux. The dotted, red line signifies the intracellular concentration threshold required for inhibition of bacterial growth. The y- and the x-axis show the intracellular and extracellular drug accumulation respectively. **A:** Theoretical accumulation of efflux proficient (WT), ΔEfflux, and WT-Pore cells. Accumulation in ΔEfflux cells is largely determined by passive diffusion. The WT curve shows slow initial uptake due to efficient efflux. Once the periplasmic concentration is high enough, the transporter is overwhelmed and drug accumulation increases. Hyperporination of the WT (WT-Pore) allows for increased flux across the outer membrane, resulting in a higher periplasmic concentration of the drug. The transporters are overwhelmed at a lower extracellular concentration. **B:** This figure is in agreement with most of our fluorescent uptake studies. The ΔEfflux mutant is not completely efflux deficient and hyperporination still potentiates compounds in this strain. **C:** If binding sites on the outer membrane are saturated before the drug can overwhelm efflux, the intracellular concentration of the compound will plateau and

never reach the concentration threshold required to inhibit the growth of the bacterium. In these cases, hyperporination will reveal potential susceptibilities of the cell to the drug.

When the cells are hyperporinated, the flux of compounds increases across the outer membrane barrier and, consequently, their concentration in the periplasm. Thus, lower extracellular concentrations are sufficient to saturate and overwhelm the transporter, resulting in a decrease of the MIC (Fig. 2.1A). To further complicate this, there are several efflux transporters, each with their own K_m, that transport their substrates across the inner and outer membrane. In *E. coli*, most efflux across the outer membrane is depleted by deleting the universal OMF TolC (55). Hence any observed efflux in the ΔTolC mutant is likely due to transporters that translocate their substrates across the inner membrane. *P. aeruginosa* has several RND transporters encoded on its chromosome, many of which with their own OMF, which makes it significantly more difficult to deplete efflux across the outer membrane alone. The transporters also differ in their substrate specificities. If more than one transporter is contributing to efflux of a compound, increasing the extracellular concentration should overwhelm the transporters sequentially according to their respective K_m of the substrate. Furthermore, our observations from kinetic uptake experiments utilizing fluorescent dyes showed that our efflux deficient mutants still possess efflux capacities. We detected a low initial accumulation that, after a certain extracellular concentration (about 3 μM of HT in *P. aeruginosa*), became more rapid. Thus, our results most closely resemble a drug

accumulation model that can be seen in figure 2.1B, which shows the presence of efflux in all four strains. Another possibility is that the drug will saturate the available binding sites on the outer membrane before it can accumulate to high enough levels to overwhelm the efflux transporter. In this case, efflux will always operate efficiently and render the cell completely resistant (Fig. 2.1C). Due to the limited nature of MIC measurements, we will not be able to determine whether there is still residual efflux in our efflux deficient and hyperporinated strains. However, we will be able to delineate the contributions of the outer membrane and active efflux at growth inhibiting, intracellular concentrations.

2.3.2 Effects of efflux and outer membrane permeability on drug susceptibilities of *E. coli*.

We tested the antimicrobial susceptibilities of BW25113 (WT), BW25113 with insertion of *fhuAΔC/Δ4L* (WT-Pore), the BW25113 TolC mutant GD102 (ΔTolC), and GD102 with *fhuAΔC/Δ4L* (ΔTolC-Pore) using antibiotics from a wide range of classes. To rule out a negative impact of the arabinose promoter of the fitness of the pore strains, we inserted this promoter together with the multiple-cloning site of the plasmid pTJ1 into our non-pore expressing variants. Expression of the pore was induced with 0.1% arabinose, which we previously showed to results in about 150 copies of the pore per cell (106).

Drug	MIC (µg/ml)				Fold MIC change				Properties	
	WT		ΔTolC		OM barrier		Efflux			
	(-) Pore	(+) Pore	(-) Pore	(+) Pore	WT/ Pore	ΔTolC/ Pore	WT/ ΔTolC	WT-P ΔTolC-P	Mass	logD
Amikacin	2	2	2	2	1	1	1	1	585.6	-15.1
Gentamicin	4	2	4	4	2	1	1	0.5	477.6	-11.79
Streptomycin	2	2	4	2	1	2	0.5	1	581.57	-12.16
Coumermycin	64	16	64	8	4	8	1	2	1110.08	0.7
Rifampicin	4	0.25	4	0.25	16	16	1	1	822.94	2.76
Vancomycin	128	1	256	1	128	256	0.5	1	1449.25	-4.86
Carbenicillin	16	2	4	1	8	4	4	2	378.4	-5.91
Ampicillin	64	4	16	1	16	16	4	4	349.405	-2.26
Levofloxacin	0.032	0.016	0.004	0.004	2	1	8	4	361.37	-0.28
Nalidixic acid	8	8	1	1	1	1	8	8	232.24	-0.25
Lincomycin	512	512	64	64	1	1	8	8	406.54	-0.99
Chloramphenicol	2	2	0.5	0.5	1	1	4	4	323.13	0.69
Triclosan	0.031	0.031	0.004	0.004	1	2	8	8	289.54	4.8
Tetracycline	0.5	0.25	0.125	0.125	2	1	4	2	467.52	-1.63
Ciprofloxacin	0.016	0.004	0.002	0.002	4	1	8	2	331.34	-0.81
Proflavine	32	32	8	8	1	1	4	4	209.25	0.94
Novobiocin	128	32	0.5	0.125	4	4	256	256	612.62	1.36
SDS	>10000	625	19.5	19.5	>16	1	128	32	288.38	2.04
Cloxacillin	512	32	1	1	16	1	512	32	435.88	-0.98
Erythromycin	64	4	2	0.125	16	16	32	32	733.93	1.57
Azithromvcin	2	0.5	0.5	0.03	4	16	4	16	748.98	-1.23
Virginiamycin	512	256	8	0.5	2	16	64	512	525.59	2.38

Table 2.1 - Antibiotic susceptibilities of *E. coli* strains to different classes of antibiotics.

The susceptibilities were determined by MIC measurements using the traditional two-fold broth dilution method into 96-well plates. Cultures were first grown to OD_{600} of 0.3, induced, and further grown to an OD_{600} of 1.0. Cells were inoculated into the plates at an inoculum size of $5*10^5$, as is commonly done (113), and incubated for 16 hours at 37°C. Arabinose was present in all wells throughout the incubation time to ensure proper expression of the pore. The MIC was determined visually or, alternatively, the absorbance at OD_{600} was read using a micro-plate reader. Contributions of active efflux and outer membrane permeability were determined by calculating the fold change of the MIC due to the loss of efflux or the introduction of the mutant pore. The results can be seen in table 2.1.

Based on our results, we can divide the antibiotics into four groups depending on their potentiation by efflux, hyperporination, or both. Group I antibiotics are neither affected by hyperporination, nor by deletion of efflux, and are exclusively made up of aminoglycosides. Aminoglycosides bind the 30S subunit of the ribosome and inhibit protein synthesis, and need to permeate both membranes to reach their target. These antibiotics are highly polar as seen by their very low logD values compared to all other antibiotics tested (Fig. 2.2). The logD is a measure of polarity and is calculated by the decadic logarithm of the concentrations of ionic and non-ionic species of a compound in octanol divided by their concentrations in water. Hence, a low logD means that the particular compound mainly partitions into the aqueous phase. Aminoglycosides typically contain several amino groups that carry a positive charge at physiological pH and are thought to permeate the cell envelope by a “self-promoted” uptake mechanism (139). The positively charged aminoglycosides displace divalent ions at the outer leaflet

of the outer membrane and disrupt the organization of lipopolysaccharides (LPS) (139). This causes the membrane to permeabilize and allows for increased uptake of the drug. We noticed no significant potentiation of the activity of the aminoglycosides when we expressed the pore, which suggests that this "self-promoted" uptake is not a limiting factor for these drugs to enter the cell. Additionally, there is no significant difference between WT and our TolC deletion mutant, suggesting that there are no aminoglycoside proficient transporters that translocate substrates across the outer membrane in *E. coli*.

The second group consists of antibiotics that are affected by hyperporination but not efflux. Most members of this group are large antibiotics like coumermycin and rifampin (Table 2.1 and Fig 2.2). Their size is well above the cut off of the major porins in *E. coli* OmpF/C, and hyperporination allows them access to the cell. Efflux transporters are not proficient in transporting these compounds, likely because they cannot penetrate the cell envelope and transporters have not evolved to use them as substrates. Interestingly, β-lactams are also part of this group and are somewhat of an exception. These antibiotics are below the exclusion size of the general porins and were shown to diffuse through OmpF (142). However, the fact that hyperporination potentiates the activity of this class of antibiotics suggests that this diffusion is still a limiting factor for these antimicrobials. β-lactams target the cell wall synthesis in the periplasm and their accumulation in hyperporinated strains is likely greatly increased. Efflux also somewhat effects their activity, however the outer membrane permeability seems to be the major determinant of their MIC.

The third group is the largest one of the drugs tested, and is potentiated by deletion of efflux but not by hyperporination. This group consists of chloramphenicol,

tetracycline, proflavine, triclosan, and fluoroquinolones. With the exception of triclosan and tetracycline, their logD values are around zero, suggesting that they are amphiphilic in nature (Fig. 2.2). Furthermore, they are all below the exclusion size of OmpF/C. Thus, these antibiotics likely freely diffuse either through general porins or the outer membrane. Our data suggests that this diffusion is fast, since hyperporination has no impact on these antibiotics. Deletion of TolC dependent efflux results in a modest 4 to 8-fold change of the MIC on average. The exception to this is novobiocin, which showed a staggering 256-fold change in susceptibility with the deletion of TolC. Novobiocin is an aminocoumarin and targets DNA gyrase. Interestingly, the other aminocoumarin tested, coumermycin, is a group II antibiotic and, thus, only affected by hyperporination and not efflux. The molecular weight of novobiocin is significantly lower than coumermycin, allowing it to permeate the cell envelope through general porins. This is, presumably, why efflux transporters are proficient in the efflux of novobiocin but not coumermycin.

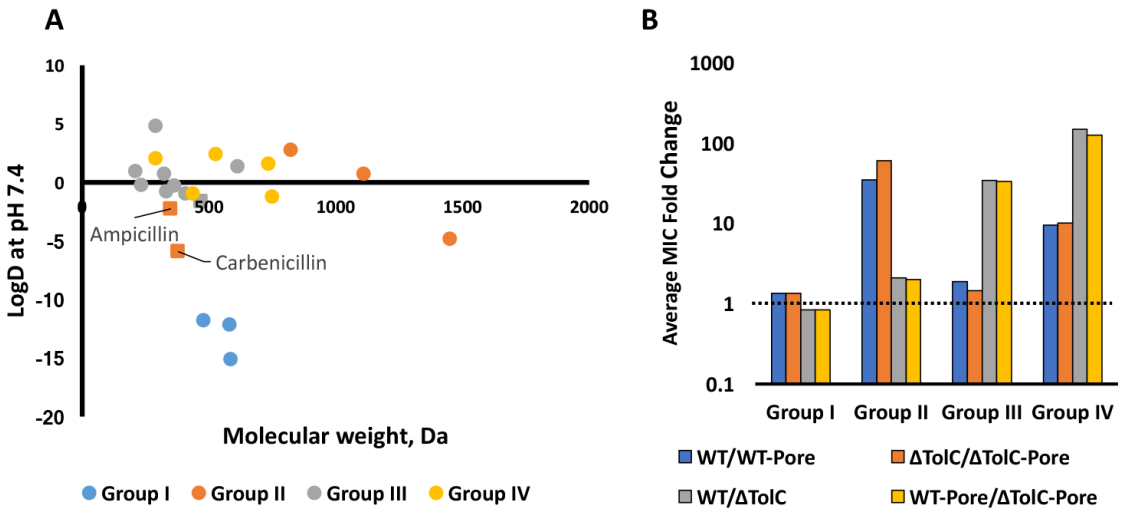

Figure 2.2 - Features of antibiotics divided into four groups in *E. coli*.

A: Correlation between logD and the respective molecular weight of antibiotics belonging to the four groups. Outliers are marked by a square shape with their corresponding name. **B:** Average MIC fold changes of the indicated strains of antibiotics in their respective group. The dotted, black line represents no fold change.

Group IV antibiotics are potentiated by hyperporination and efflux. For these antibiotics, efflux acts in synergy with the outer membrane to significantly limit their accumulation inside the cell. Members of this group include macrolides, as well as the smaller antibiotics virginiamycin and the β-lactam cloxacillin. Macrolides are large antibiotics that cannot freely diffuse through general porins. However, other than group II antibiotics, efflux transporters are able to use them as substrates. Surprisingly, hyperporination of the TolC deficient strain further decreased their MIC, suggesting that there is significant efflux across the inner membrane of these antibiotics. Interestingly, cloxacillin, a member of the β-lactam family, is also part of this group. Other than ampicillin and carbenicillin, this β-lactam is a very good substrate of efflux pumps, as seen by a 512-fold decrease of the MIC once TolC is deleted. Since its target is in the periplasm, cloxacillin is not potentiated by hyperporination in the ΔTolC strain. The detergent SDS is also in this group also falls into this group and its activity is significantly affected by outer membrane permeability and efflux. Similar to cloxacillin, SDS is not affected by the mutant pore in the ΔTolC strain, suggesting that it is not a substrate of transporters that translocate substrates across the inner membrane. Surprisingly, there is a significant difference when comparing the contribution of efflux in cells with an intact outer membrane and hyperporinated cells. In cells without the pore, this contribution varies from 32 to 512-fold, but in cells expressing the mutant pore the fold change is much lower and constant between 16 and 32-fold. This highlights that the outer membrane barrier masks substrate specificities and efflux capacities of transporters, and removal of this barrier reveals the actual contribution of efflux on the activity of antimicrobials.

2.3.3 Antibiotic susceptibilities in hyperporinated and efflux deficient *P. aeruginosa* variants.

Next, we tested a similar range of antibiotics on drug susceptibility in the *P. aeruginosa* strains described in chapter 1 with the exception of PΔ3, which was replaced with a close relative PΔ3S (Δ*mexAB-oprM* Δ*mexCD-oprJ* Δ*mexJKL*) and its pore expressing variant. Similar to PΔ3, this strain is deficient in three efflux transporters. We chose this strain because it lacks the OMFs OprM and OprJ, making it more similar to PΔ4 and PΔ6. This should allow for a better comparison of the contributions of minor efflux transporters. Insertion of the pore in this strain was confirmed by PCR and functionality tested via vancomycin spot assays. The cell envelope of *P. aeruginosa* is significantly different from *E. coli* and its permeability is reduced largely due to the absence of general porins with large exclusion sizes (5, 30, 32). Thus, we are expecting differences in the potentiation of MICs by hyperporination compared to *E. coli*. Additionally, *P. aeruginosa* has a much larger arsenal of RND transporters, making it significantly more difficult to reduce the efflux across the outer membrane. Any differences we see in efflux deficient strains when we introduce the mutant pore are likely due to contributions of minor transporters. The results of the antimicrobial susceptibility testing can be seen in table 2.2.

Drug	MIC (μg/ml)							
	PAO1		PΔ3		PΔ4		PΔ6	
	-	Pore	-	Pore	-	Pore	-	Pore
Amikacin	2	2	1	1	2	1	2	2
Tobramycin	2	1	1	1	1	1	1	1
Coumermycin	32	4	32	1	32	0.5	32	1
Rifampin	16	0.5	16	0.5	16	0.5	16	0.5
Vancomycin	1024	128	2048	128	256	128	512	64
Levofloxacin	0.125	0.063	0.031	0.004	0.008	0.004	0.008	0.002
Ciprofloxacin	0.063	0.031	0.016	0.002	0.004	0.001	0.002	0.0005
Nalidixic acid	64	32	8	1	4	1	4	1
Chloramphenicol	8	2	1	0.5	0.5	0.25	0.5	0.125
Triclosan	1024	1024	64	16	32	4	16	4
SDS	>10000	10000	5000	78.125	5000	78.13	312.5	39.1
Novobiocin	512	64	32	4	8	4	8	0.125
Azithromycin	128	4	8	0.06	2	0.03	2	0.0156
Erythromycin	128	2	16	0.5	8	0.125	8	0.0625
Tetracycline	4	0.5	1	0.125	0.5	0.125	0.25	0.0625
Ampicillin	256	16	32	2	32	0.5	16	0.25
Cloxacillin	>2048	512	128	8	128	8	128	4
Carbenicillin	32	2	1	0.25	0.5	0.125	1	0.125

Table 2.2 - Susceptibilities of *P. aeruginosa* strains to different antibiotics.

Again, we divided the antibiotics up into four groups by whether they are potentiated by hyperporination, deletion of efflux, or both. Similar to *E. coli*, aminoglycosides represent group I, due to their "self-promoted" uptake mechanism and their ability to circumvent efflux. MexXY-OprM is the only transporter that was reported to provide resistance to aminoglycosides, however we do not see potentiation of these antibiotics in the OprM deficient PΔ3S or in the MexXY deletion mutants PΔ4 and PΔ6 (143, 144). Like for *E. coli*, the "self-promoted" uptake mechanism seems to be faster than diffusion through the large mutant pore, hence hyperporination has no effect on the activity of these antibiotics. This group of antibiotics is highly effective at crossing the gram-negative cell envelope and bypassing the intrinsic resistance mechanisms. Aminoglycoside resistance is mainly mediated by aminoglycoside-modifying enzymes that typically act by transferring acetyl groups onto the antibiotic thus, inactivating it (145).

Drug	MIC, µg/ml				MIC fold changes					Mass	LogD pH 7.4
	PAO1		PΔ6		Outer Membrane		Efflux				
	-	Pore	-	Pore	PAO1/ Pore	PΔ6/ PΔ6-Pore	PAO1 / PΔ6	PAO1-Pore/ PΔ6-Pore			
Amikacin	2	2	2	2	1	1	1	1		585.6	-15.1
Tobramycin	2	1	1	1	2	1	2	1		467.51	-9.54
Coumermycin	32	4	32	1	8	32	1	4		1110.08	0.7
Rifampin	16	0.5	16	0.5	32	32	1	1		822.94	2.76
Vancomycin	1024	128	512	64	8	8	2	2		1449.25	-4.86
Levofloxacin	0.125	0.063	0.00 8	0.002	2	4	16	32		361.37	-0.28
Ciprofloxacin	0.063	0.031	0.00 ?	0.0005	2	4	32	62		331.34	-0.81
Nalidixic acid	64	32	4	1	2	4	16	32		232.24	-0.25
Chloramphenicol	8	2	0.5	0.125	4	4	16	16		323.13	0.69
Triclosan	1024	1024	16	4	1	4	64	256		289.54	4.8
SDS	20000	10000	5	39.1	2	8	64	256		288.38	2.04
Novobiocin	512	64	8	0.125	8	64	64	512		612.62	1.36
Azithromycin	128	4	2	0.0156	32	128	64	256		748.98	-1.23
Erythromycin	128	2	8	0.0625	64	128	16	32		733.93	1.57
Tetracycline	4	0.5	0.25	0.0625	8	4	16	8		467.52	-1.63
Ampicillin	256	16	16	0.25	16	64	16	64		349.405	-2.26
Cloxacillin	4096	512	128	4	8	32	32	128		435.88	-0.98
Carbenicillin	32	2	1	0.125	16	8	32	16		378.4	-5.91

Table 2.3 - Contributions of efflux and outer membrane permeability to the MIC of selected antibiotics in *P. aeruginosa*.

Group II antibiotics are all fairly large molecules with molecular weights exceeding 800 Da. These antibiotics are unable to cross the outer membrane, which limits their activity in gram-negative bacteria. Similar to *E. coli*, efflux transporters are unable to use them as substrates, possibly due to the fact that efflux transporters have not evolved to translocate these large compounds. The only exception to this may be coumermycin, which shows a 4-fold decrease in the MIC when comparing PAO1-Pore and PΔ6-Pore (Table 2.3). This change in the MIC is not seen with an intact outer membrane, suggesting that the major limiting factor is still the uptake of this antibiotic. Structurally, it is very similar to novobiocin, which is an excellent substrate for efflux transporters. This could explain why some transporters might be able to translocate coumermycin.

Group III antibiotics are potentiated by efflux are significantly potentiated by the depletion of efflux, but less by hyperporination. These antibiotics are relatively small with 200-400 Da (Table 2.3 and Fig. 2.3). Their size should preclude them from free diffusion through porins in *P. aeruginosa* due to their estimated exclusion size of 200 Da, thus it is likely that they diffuse through the outer membrane (32). Alternatively, a small fraction of OprF porins are suggested to form larger channels that could facilitate the diffusion of group III antibiotics (146). The group consists of fluoroquinolones, chloramphenicols, SDS, and triclosan and generally have a logD value of around zero. Two group III members from *E. coli* are absent in the group III of *P. aeruginosa*. Tetracycline and novobiocin are both group III antibiotics for *E. coli*. They are between 450 and 600 Da which allows them to diffuse through OmpF in *E. coli*, but are too large for diffusion through *P. aeruginosa* porins.

Group IV consists of antibiotics that are potentiated by depletion of efflux and permeabilization of the outer membrane. In contrast to *E. coli*, this is the largest group of the antibiotics tested and also includes the β-lactams ampicillin and carbenicillin, both of which belong to group II in *E. coli*. These two drugs are good substrates of *P. aeruginosa* efflux transporters, but not for TolC dependent transporters in *E. coli*. In addition to β-lactams, macrolides, novobiocin, and tetracycline belong to group IV in *P. aeruginosa*. They appear to have logD values that are further away from zero when compared to group III, making them less amphiphilic, and their molecular mass is higher on average.

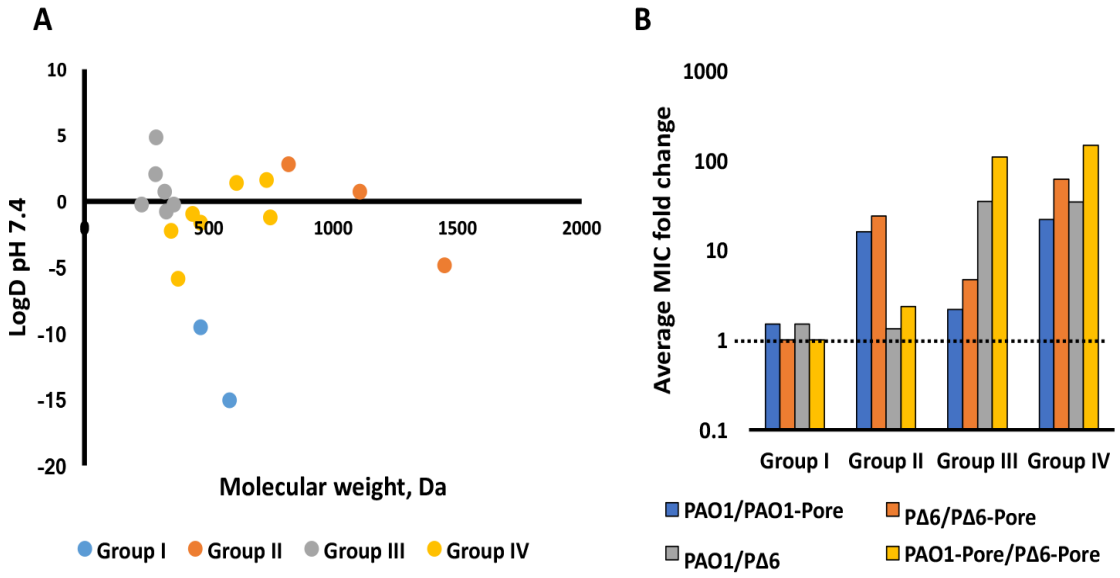

Figure 2.3 - Properties of antibiotics belonging to the four groups in *P. aeruginosa*.

A: Correlation between LogD at pH 7.4 and molecular weight for the four groups in *P. aeruginosa*. **B:** Average MIC fold changes of deletion of efflux or hyperporination. The dotted, black line signifies no fold change.

In *P. aeruginosa*, we still measured significant contributions of efflux in the hyperporinated strains as seen by a 4 to 8-fold greater change in the MIC for triclosan, SDS, novobiocin, azithromycin, and cloxacillin due to removal of efflux. This is in contrast to *E. coli*, where the contribution of efflux is either equal to or lower in hyperporinated strains. This suggests that efflux still significantly contributes to resistance in *P. aeruginosa* even when the outer membrane permeability is increased. Furthermore, the lower fold changes for cells with an intact outer membrane highlight that the residual efflux works in synergy with the outer membrane. When looking at the contributions of minor efflux transporters on the activity of the tested antibiotics, we noticed that for many cases, like ciprofloxacin, azithromycin, erythromycin, and tetracycline the stepwise deletion of transporters also resulted in a stepwise reduction of the MIC (Table 2.4). The difference between PΔ3S and PΔ4 is the presence of MexXY in PΔ3S. This transporter is a major contributor for clinical resistance in *P. aeruginosa* isolates and has a broad substrate specificity (89). This results in a relatively large MIC fold change between PΔ3S and PΔ4 for vancomycin (Table 2.4). MexXY is generally thought to utilize the outer membrane factor OprM, which is absent in PΔ3S (144). However, some research groups reported that it can utilize other outer membrane factors like OpmH that are present in PΔ3S (147). In hyperporinated cells, we did not observe this large fold change, suggesting that MexXY is overwhelmed in PΔ3S due to high concentrations of substrates in the periplasm and provides inefficient efflux. Another large increase in susceptibility is seen for SDS of 16-fold when comparing PΔ4 and PΔ6. This is likely due to deletion of TriABC, which was previously reported to provide resistance to the detergent (148, 149).

Drug	MIC fold chages				
	PΔ3/ PΔ4	PΔ4/ PΔ6	PΔ3-Pore/ PΔ4-Pore	PΔ4-Pore/ PΔ6-Pore	
Amikacin	0.5	1	1	0.5	Group I
Tobramycin	1	1	1	1	
Coumermycin	1	1	2	0.5	
Rifampin	1	1	1	1	Group II
Vancomycin	8	0.5	1	2	
Levofloxacin	4	1	1	2	
Ciprofloxacin	4	2	2	2	
Nalidixic acid	2	1	1	1	Group III
Chloramphenicol	2	1	2	2	
Triclosan	2	2	4	1	
SDS	1	16	1	2	
Novobiocin	4	1	1	2	
Azithromycin	4	1	2	2	
Erythromycin	2	1	4	2	
Tetracycline	2	2	1	2	Group IV
Ampicillin	1	2	4	2	
Cloxacillin	1	1	1	2	
Carbenicillin	2	0.5	2	1	

Table 2.4 - Contribution of minor transporters to resistance against selected antibiotics.

Overall, the four groups remained largely the same for *P. aeruginosa* and *E. coli*. The antibiotics that behaved different were β-lactams, which were good substrates of transporters in *P. aeruginosa* but not *E. coli*, novobiocin, and tetracycline. The last two were likely too large to free diffuse through the general porins in *P. aeruginosa* and were significantly potentiated by the expression of the pore. Efflux capacities also seem to be higher in *P. aeruginosa*, likely due to its bigger arsenal of RND transporters. Interestingly, *P. aeruginosa* is more resistant to many antibiotics, like macrolides and fluoroquinolones, but when efflux is deleted and the outer membrane permeability is increased it is oftentimes more susceptible than *E. coli* ΔTolC-Pore. This shows that overall intrinsic resistance is much higher in this bacterium than in *E. coli*.

2.3.4 Effects of structural differences of antibiotics on their potentiation by efflux or hyperporination.

The strains that we created represent ideal tools to study the contribution of the outer membrane and active efflux on antibiotic activities in *E. coli* and *P. aeruginosa*. The ideal outcome of a study like this would be a set of physicochemical properties that define the permeation of compounds through the cell envelope. These "rules of permeation" could be added to Lipinski's rule of five to significantly improve current drug design efforts (5, 140). Here, we are describing a preliminary screening of a library of structurally diverse β-lactams, cephalosporins, sulfonamides, and fluoroquinolones on their activity in our *E. coli* and *P. aeruginosa* strains. The data presented here are the results of the susceptibility testing. Tables of all results can be found in appendix B for *E. coli* and appendix C for *P. aeruginosa*. At the time of writing, further analysis of

physicochemical correlations by potentiation of the outer membrane or deletion of efflux is currently done in collaboration with Dr. Jerry M. Parks from the Oak Ridge National Laboratory and Dr. John K. Walker from the Saint Louis University School of Medicine.

Overall, we tested 18 fluoroquinolones (FQs), 23 sulfonamides (sulfas), and 44 β-lactams (PEN), of which 28 were cephalosporins (CEF) and plotted their activities with respect to potentiation in pore expressing strains and efflux deficient strains of *E. coli* (Fig. 2.4) and *P. aeruginosa* (Fig. 2.5). The sulfonamides showed the lowest activity against both species, and were only marginally potentiated by inactivation of efflux and hyperporination. When compared to PAO1, PΔ6-Pore MICs were reduced by an average of only 5-fold. Most of the sulfonamides were not potentiated at all and other by 4-fold. The exceptions were sulfameter, sulfamethoxypyridazine, sulfamonomethoxine, and sulfamethoxazole, which were potentiated 16-fold in PΔ6-Pore compared to PAO1. Of those, deletion of efflux seemed to have the biggest impact on activity, since most sulfonamides are small antibiotics and should be able to diffuse through porins of *P. aeruginosa*. Similarly, the activity of this class of antibiotics was very low in *E. coli*, with an average potentiation of about 2.75-fold when comparing the WT to ΔTolC-Pore.

Cephalosporins were modestly potentiated by the mutant pore and the deletion of efflux. With the exception of ceftriaxone and cefmenoxime, the average fold change was about 10 between PAO1 and PΔ6-Pore. Ceftriaxone was potentiated by 256-fold and cefmenoxime a staggering 1024-fold when comparing those strains. On average, the potentiation of cephalosporins in *P. aeruginosa* was similar for hyperporination and

deletion of efflux, both of which showed an average potentiation of about 5-fold. Cephalosporins had the highest average molecular weight of the four groups of about 450 Da. In *E. coli*, the most potentiated cephalosporin was cefoperazone with a 256-fold difference between WT and ΔTolC-Pore, and the average overall potentiation was about 10-fold for the other members of that family. Hyperporination had the biggest contribution to cephalosporin activity in *E. coli* with an average potentiation of about 5-fold.

Hyperporination and the deletion of efflux had a much greater impact for the other β-lactams. About half of these penicillins were excellent efflux substrates in *P. aeruginosa* with MIC fold changes greater of at least 16, while the other half were not good substrates of efflux transporters. Some of the penicillins, like methicillin and nafcillin, showed a staggering 4000 to 8000-fold reduction in the MIC when comparing PAO1 and PΔ6-Pore. This change is mainly due to deletion of efflux, however hyperporination also potentiated these antibiotics by 8 and 16-fold respectively. The group of penicillins that was not potentiated by the deletion of efflux also only showed modest potentiation when strains were hyperporinated. Since most of them still had very high MICs, i.e. higher than 125 μM, they either have low affinity to the penicillin-binding proteins in *P. aeruginosa* or the bacterium possesses other means of resistance to these antibiotics. The penicillins were also highly potentiated by the deletion of efflux in *E. coli*, with an average fold change of 283 between WT and ΔTolC. Interestingly, about half the penicillins were good substrates of TolC dependent efflux transporters, and the other half was only modestly or not at all potentiated by the deletion of efflux. However, the two groups seemed to be different in *E. coli* and *P.*

aeruginosa, highlighting the differences in substrate specificities of the transporters in the two species.

With the exception of nadifloxacin and moxifloxacin, fluoroquinolones were much more potentiated by the deletion of efflux than hyperporination in *P. aeruginosa*. The two exceptions have higher molecular weights compared to the rest of the fluoroquinolones, which likely results in limited diffusion across the cell envelope of *P. aeruginosa*. The average potentiation due to efflux was 35-fold, with difloxacin being the only fluoroquinolone with a modest 4-fold potentiation. Deletion of efflux also potentiated *E. coli* strains more than hyperporination. The average fold change due to deletion of efflux in *E. coli* was 26, with many fluoroquinolones only potentiated by 4-fold. Hyperporination only decreased the MIC of fluoroquinolones about 5-fold in *P. aeruginosa* and about 3-fold in *E. coli*. Thus, these antibiotics are not limited by the diffusion across the outer membrane but by the presence of active efflux transporters.

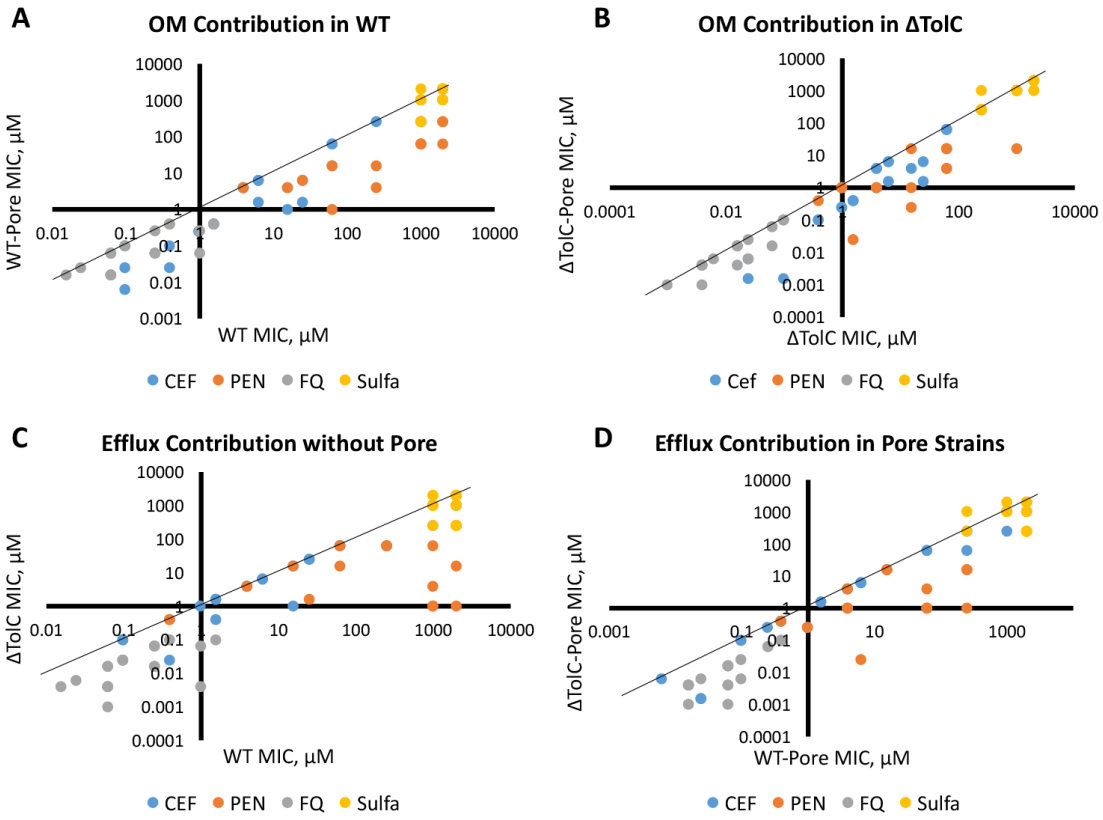

Figure 2.4 - Antibiotic susceptibilities of members of four families in *E. coli*.

A and **B:** Contributions of the outer membrane to susceptibilities of antibiotics from the four indicated groups. Pore strains are plotted on the y-axis and the parent strain on the x-axis. The black line indicates no fold change. **C** and **D:** similar to A and B but showing the contribution of efflux.

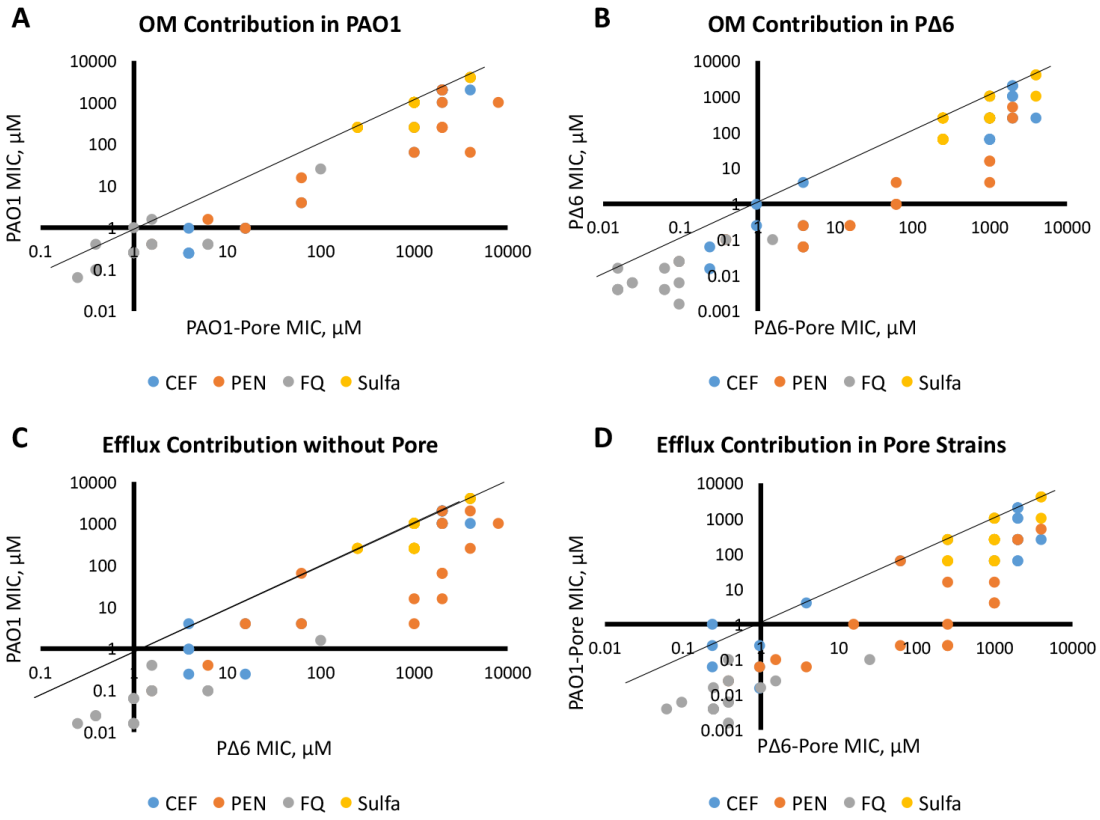

Figure 2.5 - Susceptibilities of diverse members of four families of antibiotics in *P. aeruginosa*.

A and **B:** MICs of antibiotics in pore strains plotted against their respective parental strain, highlighting the contribution of outer membrane permeability to resistance against the indicated families of drugs. **C** and **D:** Similar as A and B but indicating the contribution of efflux instead. The black lines indicate no fold change.

Overall, active efflux and the outer membrane permeability affected the susceptibilities of both *E. coli* and *P. aeruginosa*. *P. aeruginosa* was overall more resistant to the tested antibiotics, but also showed a higher potentiation when efflux is deleted and the mutant pore is expressed. This highlights the differences of the cell envelope of the two species and the greater levels of intrinsic resistance of *P. aeruginosa* compared to *E. coli*. Further analysis of this data will hopefully reveal correlations between physicochemical properties of antibiotics and their potentiation in hyperporinated or efflux deficient strains.

2.4 Discussion

Infections caused by multidrug resistant gram-negative bacteria represent a huge challenge for the clinician, and are expected to become more frequent in the coming years (1). These bacteria are especially difficult to treat due to their high intrinsic resistance mediated by active drug efflux and a low permeability across the outer membrane. This intrinsic resistance directly translates to much lower hit rates during drug screening, significantly diminishing the rate of drug discovery for these bacteria (5). New innovations in the drug development process are desperately needed in order to ensure that we possess a potent arsenal of antibiotics. One approach is to define physicochemical properties of antibiotics that could predict their propensity to cross the gram-negative cell envelope (140). These "rules of permeation" could be added to Lipinski's rules of five to dramatically improve the development of antibiotics (5).

The strains described in chapter one of this dissertation provide the means to separate the contribution of the outer membrane and active efflux to resistance of *E. coli*

and *P. aeruginosa*. They represent a significantly better way to study the outer membrane permeability barrier then currently available methods like the use of polymyxins. These tools allow us to specifically screen for chemical features that allow better penetration of the outer membrane or circumvent efflux, and can help in the development of rules of permeation. Here, we described a first attempt at classifying antibiotics into four distinct groups based on their activity in hyperporinated or efflux deficient strains. Members of the proposed groups of antibiotics differ slightly between *E. coli* and *P. aeruginosa*, highlighting the differences in their respective outer membrane and arsenal of efflux transporters. Group I antibiotics are not potentiated by compromising the outer membrane barrier or by deleting efflux. These antibiotics likely follow a "self-promoted" uptake mechanism and carry positive charges. Hence, resistance to these antibiotics will mainly come from enzymatic inactivation or modification. Group II antibiotics are drugs that are affected by the outer membrane permeability but not by efflux. These are large antibiotics, greater than 800 Da, that are typically unable to penetrate through the outer membrane. Efflux transporters may not have evolved to utilize them as substrates due to their limited exposure to these compounds. The exception are some β-lactams in *E. coli*, which are much smaller than 800 Da but still poor substrates of efflux transporters. Antibiotics of the group III are generally small, with an average molecular weight of about 350 Da, and are good efflux substrates. This group is potentiated by the deletion of efflux but not by hyperporination. Since hyperporination does not potentiate efflux proficient cells, there is little synergy between efflux and the outer membrane permeability for these antibiotics, which results in semi-efficient efflux. Group IV antibiotics are affected by

both hyperporination and the deletion of efflux. Thus, there is significant synergy between efflux transporters and the low permeability outer membrane barrier. These antibiotics are larger than group III antibiotics, but smaller than drugs from group II. Their average molecular weight is around 500 Da and they seem to be slightly less amphiphilic than group III antibiotics.

We also showed a first approach at screening of libraries of structurally diverse members of three antibiotic families. Although detailed analysis of physicochemical properties is not yet completed, we see a clear difference in the contribution of hyperporination and active efflux between *E. coli* and *P. aeruginosa*. This suggests that if there are such "rules of permeation", they will likely differ between different gram-negative bacteria. Differences in the properties of the outer membrane and in the arsenal of efflux transporters necessitates to carry out similar screenings in other gram-negative species like *Acinetobacter* and *Burholderia* among others. Nevertheless, our approach to utilize a genetically modified outer membrane porin provides valuable insight into the contribution of outer membrane and active efflux to antibiotic resistance.

Chapter 3. Kinetic control of quorum sensing in *Pseudomonas aeruginosa* by multidrug efflux pumps.

3.1 Abstract

Pseudomonas aeruginosa **is an important human pathogen, the physiology and virulence of which are under control of quorum sensing signals. These signals often have dual physiological roles, functioning as toxins to other cells and as oxidative-stress protectors of their producer cells. Hence, their internal and external concentrations should be tightly controlled to maintain the steady-states. In this study, we analyzed the efficiencies and substrate specificities of two multidrug efflux transporters MexEF-OprN and MexG/HI-OpmD implicated in transport of quorum sensing signals in *P. aeruginosa.* Our results show that the two transporters, when overproduced, can provide clinical levels of resistance to diverse fluoroquinolones and protect *P. aeruginosa* against exogenous toxic phenazines. The two transporters however, differ significantly in their efficiencies, with MexG/HI-OpmD saturated by much lower concentrations of substrates. Unlike MexEF-OprN, mutational inactivation of MexG/HI-OpmD leads not only to a reduction of the levels of the important virulence factor pyocyanin, but also makes *P. aeruginosa* cells hypersusceptible to phenazines. In addition, we demonstrate that MexG binds pyocyanin, physically associates with MexHI and represses the activity of the transporter, pointing onto a negative regulatory role. We conclude that differences in kinetic properties of transporters are critical to maintain proper intra- and extra- cellular concentrations of phenazines and other**

signaling molecules, and that the kinetic properties of MexG/HI-OpmD are responsible for the steady-state in the synthesis and secretion of phenazines.

3.2 Introduction

Pseudomonas aeruginosa is a gram-negative, opportunistic human pathogen that is most commonly associated with nosocomial diseases and infections in cystic fibrosis patients (8). The increased frequency of multidrug resistant isolates of this bacterium is of particular concern. The World Health Organization recently published their priority list of antibiotic resistant bacteria and placed *P. aeruginosa* into the highest priority group (150). The pathogen achieves its high level of drug resistance mainly through the interplay of low outer membrane permeability and active drug efflux across the cell envelope (4, 5). In gram-negative bacteria, the most prominent efflux transporters involved in resistance are RND type transporters, largely because of their ability to translocate substrates across the outer membrane and their broad range of substrates (4, 58). These transporters associate as tripartite complexes consisting of the inner membrane RND transporter, a membrane fusion protein (MFP), and an outer membrane channel (OMF). *P. aeruginosa* has at least twelve RND transporters encoded on its chromosome, which differ from each other in their level of expression and substrate specificity (151, 152).

The most clinically relevant of these are MexAB-OprM (40), MexCD-OprJ (41), MexEF-OprN (42, 43), and MexXY (43). The role these transporters play in resistance is well documented and their broad substrate specificity highlights some redundancy between them. What is less understood is their role in cell physiology and virulence and why different transporters are overproduced and selected under different environmental conditions. It has been shown that MexAB-OprM translocates 3-oxo-acyl-homoserine lactones and, thus, exerts some control over the quorum sensing network of *P.*

aeruginosa (80). HHQ (4-hydroxy-2-heptylquinoline), a direct precursor for the quorum sensing regulator PQS (*Pseudomonas* Quinolone Signal), was found to be a substrate of MexEF-OprN (81). In fact, overexpression of this RND transporter was shown to decrease the production of PQS, and several PQS regulated virulence factors like pyocyanin and rhamnolipids (81, 153, 154). In addition, MexHI-OpmD was also shown to be involved in virulence of *P. aeruginosa* (83, 88*)*. A mutation in either *mexI* or *opmD*, the RND transporter or the OMF respectively, resulted in the loss of virulence and a reduction of quorum sensing signaling molecules (83). These phenotypes were suggested to result from MexHI-OpmD transport a PQS precursor (83). Another study found that a deletion of MexHI-OpmD results in different colony morphology when compared to WT colonies, and that the transporter exports the endogenously produced phenazine 5-methylphenazine-1-carboxylate (5-Me-PCA) (84).

MexHI-OpmD is a somewhat unusual RND transporter because of the fourth protein MexG encoded by the first gene in the operon. Sequence analysis indicates that MexG is an inner membrane protein with four transmembrane α-helices, a longer, and a shorter periplasmic loop. Other transporters containing additional genes in the operons, like MdtABC of *E. coli* (155) or TriABC from *P. aeruginosa* (156)*,* contain either an additional RND or MFP subunit, whereas MexG does not share any homology to those components. It is also distinctly different from small peptides like AcrZ of *E. coli*, which changes the substrate specificity of the transporter (157). Previous studies found that MexG is not required for the antibiotic efflux activity of MexHI-OpmD (93), and that MexG binds to PQS (158). However, the function of MexG and whether or not it is a component of the complex is still unknown.

All RND transporters function in the context of the two-membrane cell envelope and are believed to translocate their substrates through the specific outer membrane channel and across the outer membrane. The outer membrane of *P. aeruginosa* is notorious for its low permeability as it lacks general porins, such as E. *coli* OmpF and OmpC. The synergistic interactions with the low permeability barrier of the outer membrane masks the activities of efflux pumps and complicates the assessment of their kinetic properties and substrate specificities (138, 159). We previously developed a hyperporination approach that enables influx of various compounds across the Gram-negative outer membranes and separates contributions of active efflux and the outer membrane barrier in intracellular accumulation of compounds and in antibacterial activities (160, 161). We also found that hyperporinated *P. aeruginosa* strains are hypersusceptbile to quorum sensing signals, deficient in secretion of pyocyanin and prone to cell aggregation (161).

Pyocyanin is one of the most important virulence factors in *P. aeruginosa* and is required to establish full virulence of the pathogen (162, 163). It leads to oxidative stress by the formation of reactive oxygen species and reduces ATP levels through the oxidation of NADH and NADPH in host cells (163, 164). The phenazine has significant antimicrobial and antifungal activity, and was also shown to be important for mammalian lung infections (165-167). However, *P. aeruginosa* is intrinsically resistant to its antibiotic activity. Furthermore, pyocyanin was shown to assist in the adaptation to anaerobic conditions by acting as an electron mediator between NADH and oxygen(168). The virulence factor also serves as a signaling molecule and was, in fact, found to upregulate expression of MexG/HI-OpmD (127). The genes required for

pyocyanin synthesis are located directly downstream of the *mexGHI-opmD* operon, suggesting a possible interaction between the transporter and the virulence factor. Thus, the intracellular and extracellular levels of this compound have to be carefully regulated to ensure that it can act as a signaling molecule and electron mediator without becoming toxic to the cell.

Here, we analyzed substrate specificities and efflux capacities of MexG/HI-OpmD and MexEF-OprN, the two pumps implicated in efflux of quorum sensing signals. We also characterized the function and the role of MexG/HI-OpmD in physiology of *P. aeruginosa*. Our results show that MexG interacts with MexHI-OpmD complex and negatively affects the efflux activity of MexHI-OpmD. Unexpectedly, the overexpression of MexG/HI-OpmD provides strong resistance to fluoroquinolones, at levels comparable to those provided by MexEF-OprN. Furthermore, MexHI-OpmD is more efficient then MexEF-OprN in protection of *P. aeruginosa* against toxic phenazines, as seen not only in strains overexpressing the pumps but also in mutants lacking MexGHI-OpmD. The transporter allows for the extracellular accumulation of pyocyanin, while providing resistance from its toxic effects. The outer membrane barrier acts in synergy with RND transporters and significantly masks the efflux efficiencies of the transporters towards substrates. Our results suggest that, in contrast to MexEF-OprN, the ability of MexG/HI-OpmD to provide resistance to fluoroquinolones is dependent on the presence of the barrier. However, increasing the outer membrane permeability does not significantly affect its ability to translocate phenazines, highlighting its specificity towards this class of substrates. We conclude that the endogenous activity of MexG/HI-OpmD establishes the steady-state concentration of

phenazines inside and outside of cells and its ability to provide resistance to fluoroquinolones is strongly affected by the permeability properties of the outer membrane and activities of efflux pumps with overlapping substrate specificities.

3.3 Results

3.3.1 The small inner membrane protein MexG associates with MexHI-OpmD.

MexHI-OpmD is a unique transporter in that its operon contains a fourth gene encoding MexG, a protein of unknown function. To test whether MexG physically associates with MexHI we created a construct expressing MexG with an N-terminal FLAG tag, MexH, and MexI with a C-terminal His tag. The plasmid was introduced into PΔ3 cells lacking *mexAB*, *mexCD*, and *mexXY* transporters. Cells producing the tagged MexGHI were split into two aliquots and the short 12 Å crosslinker dithiobis(succinimidylpropionate) (DSP) was added to one of them, before the purification of MexI using His•Bind resin. After purification, the MexI-containing fractions were analyzed by immunoblotting with anti-His and anti-FLAG antibody to detect MexI and MexG, correspondingly. No MexG was detected by immunoblotting in MexI fractions purified from cells untreated with the cross-linker. In contrast, we could clearly detect MexG in elution fractions purified from the cross-linked cells, even after extensive washes with imidazole. Reduction of the cross-linker yielded a 15 kDa band reacting with anti-FLAG antibody and corresponding by size to MexG (Fig. 3.1A). We repeated the experiment with a plasmid expressing MexG with N-terminal FLAG tag and MexH with a C-terminal His tag, however we were unable to detect any crosslinking of MexG and MexH (Fig. 3.1A). This result suggests that there is a

physical interaction between MexG and MexHI-OpmD, and that MexI or the MexHI complex are required for this interaction.

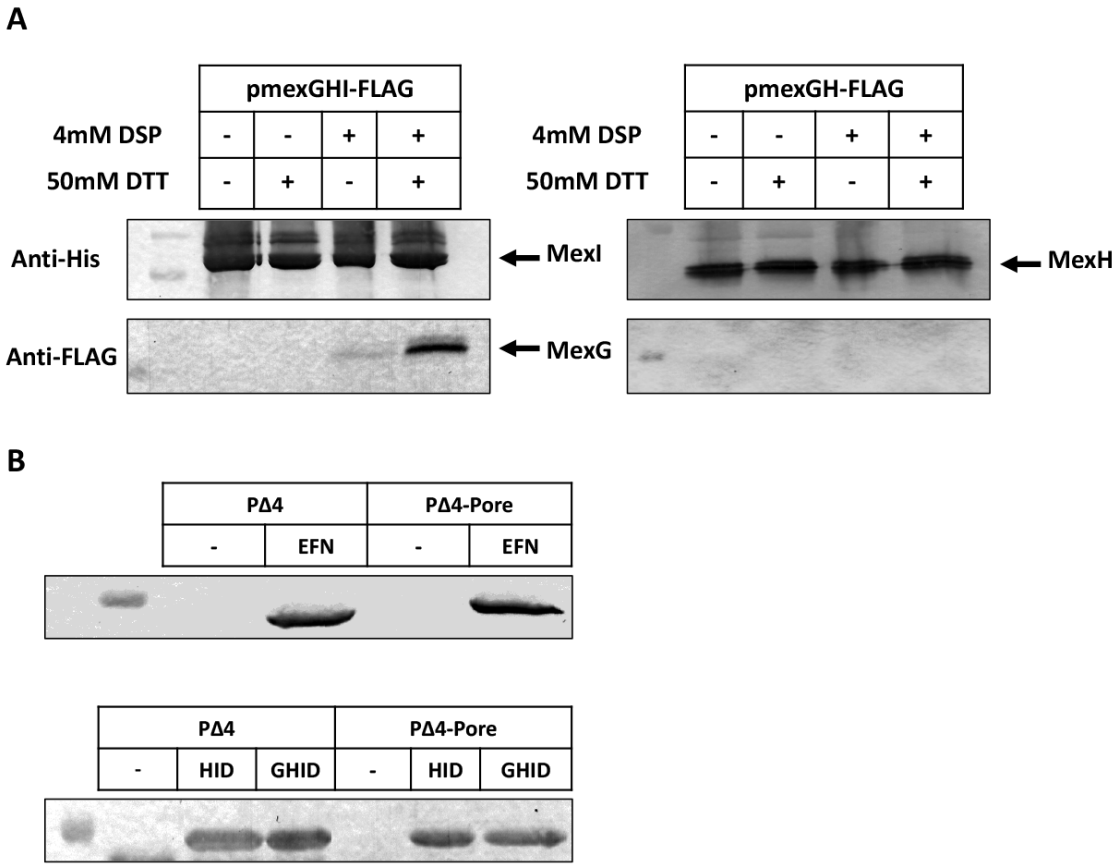

Figure 3.1 - MexG crosslinks to MexHI in *P. aeruginosa* whole cells.

A: Immunoblotting of $MexI^{His}$ (left) and $MexH^{His}$ (right) elution fractions purified from PΔ3 cells harboring pMexGHI-FLAG and pMexGH-Flag respectively. Cells were treated with crosslinker prior to lysis as indicated. The lower panel shows the release of FLAG-tagged MexG from crosslinked samples when elution fractions are treated with a reducing agent (DTT), due to the presence of a disulfide bond in the crosslinker. DSP, Dithiobis(succinimidylpropionate); DTT, Dithiothreitol. Top panels show the development with anti-His and the lower panels with anti-FLAG primary antibodies. **B:** Immunoblot of membrane fractions from cells harboring the corresponding plasmids showing the expression of efflux transporter constructs. The respective outer membrane

channels (OMF) are tagged with a C-terminal His tag and visualized with anti-His monoclonal antibody.

3.3.2. MexHI-OpmD confers resistance to structurally diverse fluoroquinolones at comparable levels to MexEF-OprN.

The overexpression of MexHI-OpmD in antibiotic susceptible strains of *P. aeruginosa* was previously found to provide resistance to some antimicrobials including fluoroquinolones, ethidium bromide, and some dyes such as acriflavine and rhodamine 6G (93). To compare the efficiency and substrate specificity of MexHI-OpmD to MexEF-OprN, which is frequently overproduced in clinical isolates and provides clinical levels of resistance, we created three constructs that constitutively express either MexGHI-OpmD, MexHI-OpmD, or MexEF-OprN using the *Escherichia-Pseudomonas* shuttle vector pBSPII (169). We confirmed similar expression levels of these constructs in an efflux deficient mutant PΔ4 deficient in *mexAB-oprM*, *mexCD-oprJ*, *mexJKL*, and *mexXY* (Figure 3.1B) and tested susceptibilities against several antibiotics (Table 1). In agreement with previous results, all three constructs provided resistance against the fluoroquinolones ciprofloxacin and levofloxacin, ethidium bromide and acriflavine but only the overexpression of MexEF-OprN drastically increased the MICs of chloramphenicol, tetracycline, triclosan, and trimethoprim. Hence, all three pumps are overproduced and functional. Interestingly, we were unable to find an antibiotic that is a substrate of MexGHI-OpmD but not MexEF-OprN. Thus, in agreement with previous studies (42, 93), MexEF-OprN has a broader substrate specificity than MexGHI-OpmD.

Drugs	MICs (µg/ml)							
	PΔ4				PΔ4-Pore			
	-	MexEF -OprN	MexHI -OpmD	MexGHI -OpmD	-	MexEF -OprN	MexHI -OpmD	MexGHI -OpmD
CIP	0.007	0.41	0.41	0.21	0.002	0.052	0.026	0.013
LEV	0.007	0.45	0.9	0.45	0.002	0.056	0.014	0.014
EtBr	128	2048	2048	2048	8	16	32	32
ACR	32	>1024	>1024	>1024	4	8	16	16
TET	0.25	1	0.25	0.25	0.031	0.063	0.031	0.031
CF	0.5	>128	0.5	0.5	0.25	2	0.25	0.25
TRI	128	>256	64	64	16	128	16	16
TRM	1	>256	1	1	1	32	1	1

Table 3.1 - Antibiotic selectivity profiles of cells producing MexEF-OprN and MexG/HI-OpmD.

CIP, ciprofloxacin; LEV, levofloxacin; EtBr, ethidium bromide; ACR, acriflavine; TET, tetracycline; CF, chloramphenicol; TRI, triclosan; TRM, trimethoprim.

Fluoroquinolones	MICs, µM				Fold Changes		
	PΔ4	PΔ4 MexEF-OprN	PΔ4 MexHI-OpmD	PΔ4 MexGHI-OpmD	MexEF-OprN	MexHI-OpmD	MexGHI-OpmD
Ciprofloxacin	0.02	1.25	1.25	0.625	64	64	32
Enrofloxacin	0.039	5	5	1.25	128	128	32
Levofloxacin	0.02	1.25	2.5	1.25	64	128	64
Gatifloxacin	0.039	2.5	2.5	1.25	64	64	32
Moxifloxacin	0.039	5	2.5	0.313	128	64	8
Prulifloxacin	0.01	0.313	0.313	0.156	32	32	16
Sparfloxacin	0.039	2.5	5	2.5	64	128	64
Difloxacin	0.039	5	2.5	0.625	128	64	16
Lomefloxacin	0.078	5	5	2.5	64	64	32
Ofloxacin	0.078	5	5	2.5	64	64	32
Pazufloxacin	0.039	2.5	1.25	0.625	64	32	16
Norfloxacin	0.039	2.5	1.25	1.25	64	32	32
Pefloxacin	0.078	5	5	2.5	64	64	32
Sarafloxacin	0.02	1.25	0.625	0.313	64	32	16
Nadifloxacin	0.078	5	5	2.5	64	64	32

Table 3.2 - Susceptibilities of PΔ4 cells overexpressing different RND transporters to fluoroquinolones.

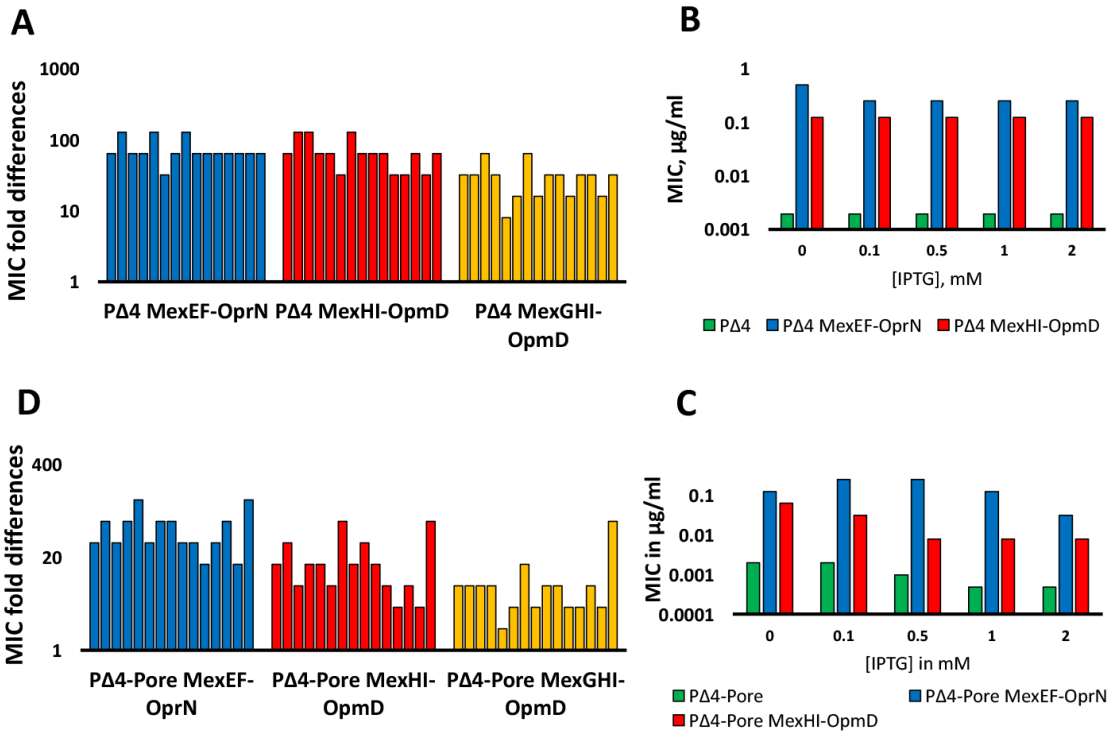

Figure 3.2 - Susceptibilities of cells expressing MexHI-OpmD, MexGHI-OpmD, and MexEF-OprN to fluoroquinolones.

A, D: PΔ4 (**A**) or PΔ4-Pore (**D**) cells harboring either pMexHI-OpmD, pMexGHI-OpmD, or pMexEF-OprN are tested against a library of structurally diverse fluoroquinolones. MICs of fluoroquinolones are expressed as fold changes compared to PΔ4 cells with empty vector. Fluoroquinolones for each column from left to right: Ciprofloxacin, Enrofloxacin, Levofloxacin, Gatifloxacin, Moxifloxacin, Prulifloxacin, Sparfloxacin, Difloxacin, Lomefloxacin, Ofloxacin, Pazufloxacin, Norfloxacin, Pefloxacin, Sarafloxacin, and Nadifloxacin. **B, C:** Effect of IPTG inducer concentration on MICs of ciprofloxacin in PΔ4 (**B**) and PΔ4-Pore (**C**) cells expressing indicated transporters.

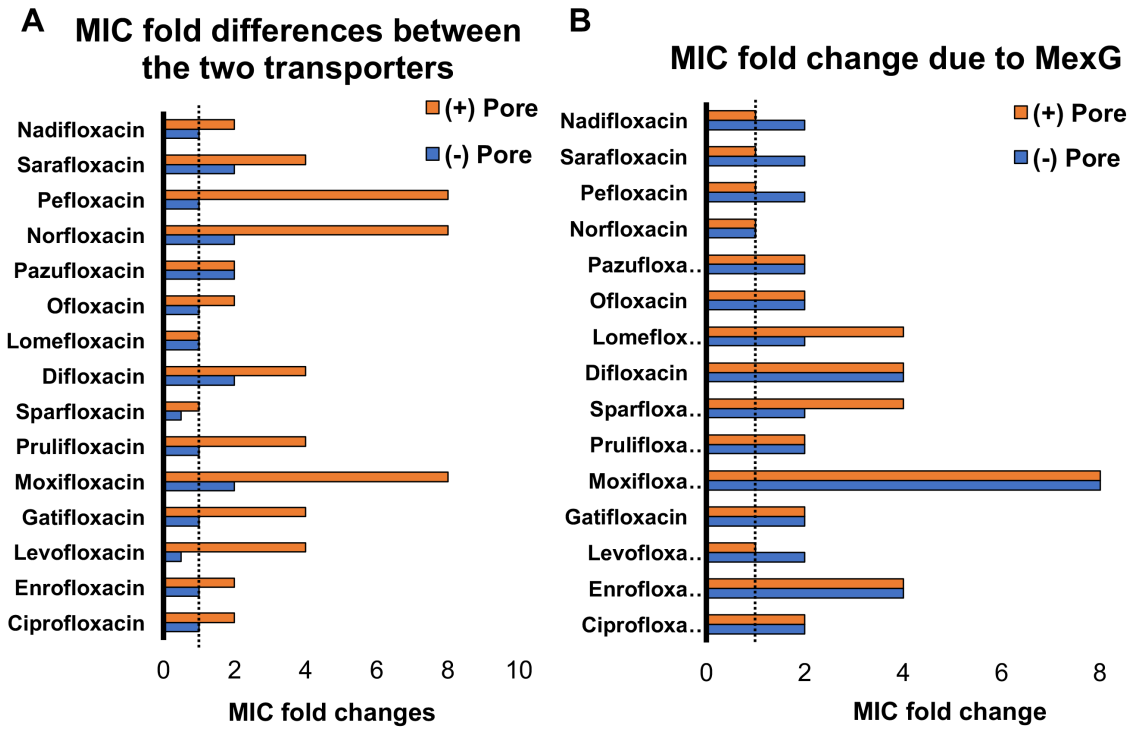

Figure 3.3 - MIC fold differences between the transporters and due to co-expression of MexG with MexHI-OpmD.

A: Fold changes of the MIC between MexEF-OprN and MexHI-OpmD as calculated by MIC(MexEF-OprN)/MIC(MexHI-OpmD) with and without the pore. **B:** Fold changes of the MIC as a result of co-expression of MexG with MexHI-OpmD as calculated by MIC(MexHI-OpmD)/MIC(MexGHI-OpmD). The dotted line represents no change.

Since fluoroquinolones are common substrates between these pumps, we next analyzed MICs of a library of 15 fluoroquinolones in PΔ4 cells carrying the three efflux pump constructs. Examples of some of these quinolones can be seen in Figure 3.4. In PΔ4, both MexEF-OprN and MexHI-OpmD transporters provided strong resistance to all the drugs tested, indicating that overexpression of either one of them could lead to clinical levels of fluoroquinolone resistance (Fig. 3.2A). Surprisingly, for the majority of tested fluoroquinolones there was no difference in MICs in cells producing either one of these two pumps. In a few cases, the MICs differed only by two-fold (Table 2 and Fig. 3.3A). Furthermore, for most fluoroquinolones the fold MIC change in PΔ4(empty vector)/PΔ4(pump) was 64-128 with a few exceptions of 32-fold change in MICs. Thus, despite the different substrate specificities, MexEF-OprN and MexHI-OpmD do not recognize differences in structures of fluoroquinolones.

As was previously reported(93), MexG was not required for the functionality of MexHI-OpmD. In fact, we observed a slight reduction of the activity of MexHI-OpmD when MexG is co-expressed (Table 2 and Fig. 3.3). However, this difference was not the same across all compounds. For example, most of the compounds tested showed 2 to 4-fold decrease in MIC, whereas the presence of MexG potentiated the activity of moxifloxacin by 8-fold, decreasing the MIC from 2.5 μM in PΔ4(pMexHI-OpmD) to an MIC of 0.3 μM in PΔ4(pMexGHI-OpmD).

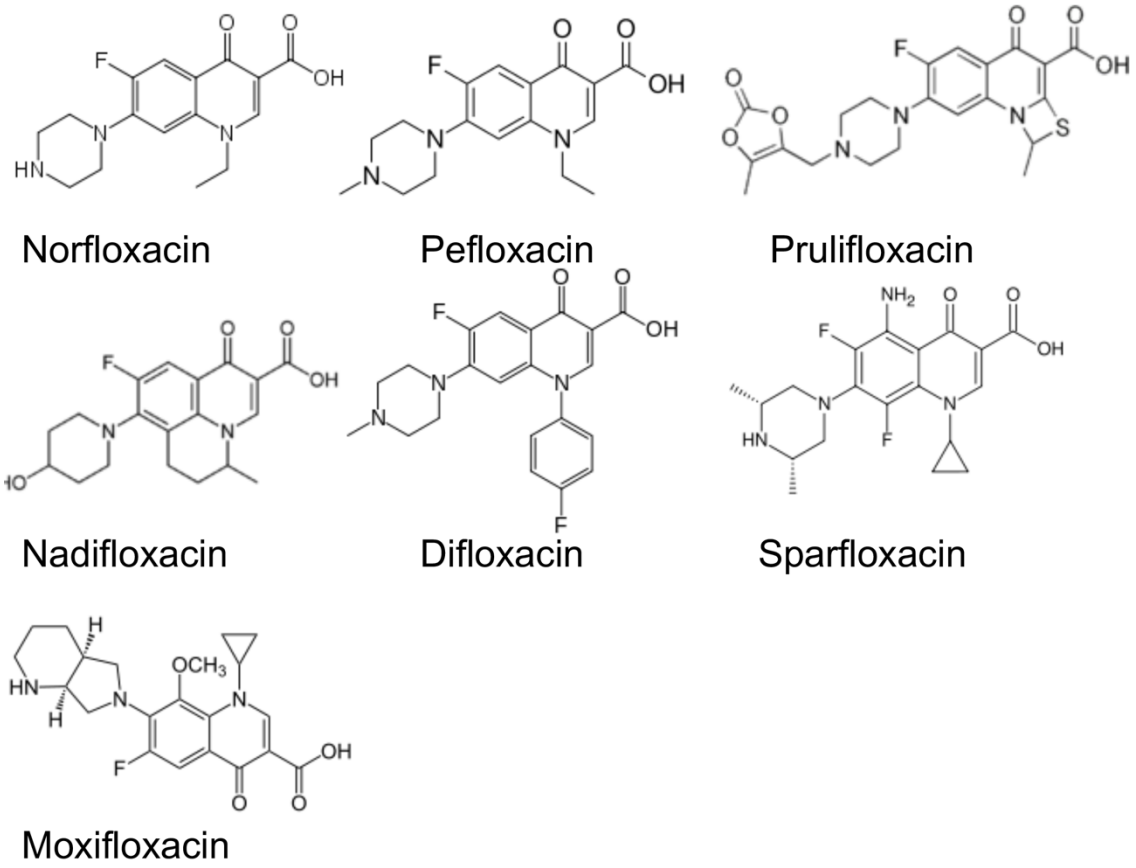

Figure 3.4 - Examples of structural diversity of the tested fluoroquinolones.

Examples of structural differences between the fluoroquinolones tested. Moxifloxacin showed the largest (8-fold) reduction in the MIC due to co-expression of MexG.

To determine whether the expression of MexG negatively affects the expression of MexHI-OpmD components, we isolated and analyzed by immunoblotting the membrane fractions from PΔ4 cells carrying the respective constructs. Figure 3.1B shows the expression of the His-tagged outer membrane channels of all three plasmids. We did not detect significantly different levels of expression between the MexHI-OpmD and MexGHI-OpmD constructs. This suggests that the reduction of activity for certain substrates when MexG is co-expressed is not due to differences in protein expression. Thus, the presence of MexG negatively affects the fluoroquinolone efflux by MexHI-OpmD to varying degrees depending on the compound.

3.3.3. Hyperporination of the outer membrane differentially affects antibacterial activities of fluoroquinolones in cells overproducing MexEF-OprN and MexHI-OpmD.

We next analyzed the change in MICs of fluoroquinolones in the hyperporinated PΔ4-Pore overproducing efflux pumps, thus removing the contribution of the outer membrane barrier on antibacterial activities. We first titrated IPTG, the inducer of the pore, to select its optimal concentration (Fig. 3.2 B and C). As expected, a decrease in MICs of ciprofloxacin with increasing concentration of inducer was seen in PΔ4-Pore strains, but not in PΔ4 strains. We measured a 4-fold decrease in the MIC of ciprofloxacin in PΔ4-Pore(pBSPII) in the presence of 2 mM IPTG. Similarly, we also observed a decrease in the MIC by 4-fold and 8-fold in the induced PΔ4-Pore(pMexEF-OprN) or PΔ4-Pore(MexHI-OpmD), respectively. We then tested the remaining fluoroquinolones in PΔ4-Pore strains induced by 2 mM IPTG (Table 3 and Fig. 3.2D).

In agreement with previous studies (161), hyperporinated cells were much more susceptible to the antibiotics as seen by a decrease of the MIC up to 64-fold when comparing PΔ4 and PΔ4-Pore(pBSPII). Hyperporination also increased susceptibilities of strains overexpressing the efflux pump constructs, albeit to a different extent. Surprisingly, the hyperporination seemed to affect the activity of MexHI-OpmD/MexGHI-OpmD much stronger than MexEF-OprN. For most of the fluoroquinolones, the overexpression of MexEF-OprN in PΔ4-Pore generated the same 64 to 128-fold increase in MICs, efficiently overcoming the increased influx of antibiotics due to hyperporination. For pazufloxacin and sarafloxacin the change in MICs was only 16-fold, suggesting that the outer membrane barrier has a significant contribution in the activities of these antibiotics and MexEF-OprN is effective against them only when the outer membrane is intact. On the other hand, MexHI-OpmD could provide the same 64-fold MIC change only for nadifloxacin in hyperporinated cells, whereas for all other antibiotics the fold MIC changes were significantly lower with most in the 4 to 16-fold range. As a result, for such antibiotics as moxifloxacin, norfloxacin, or pefloxacin the difference in susceptibility between MexHI-OpmD and MexEF-OprN in hyperporinated PΔ4-Pore was up to 8-fold (Fig. 3.3A). This result suggests that MexEF-OprN is much more effective than MexHI-OpmD in efflux of fluoroquinolones and that the low permeability barrier of the outer membrane enables high levels of fluoroquinolone resistance provided by overexpression of MexHI-OpmD. In agreement, hyperporination also diminished the ability of MexGHI-OpmD to protect against fluoroquinolones as seen from only a 4 to 8-fold change in MICs for most of the compounds. Surprisingly, the efflux of nadifloxacin remained unaffected by

hyperporination and MexG, further supporting the conclusion that the negative effect of MexG depends on specific substrates of MexHI-OpmD.

	MICs, µM				Fold Changes		
Fluoroquinolones	PΔ4-Pore	PΔ4-Pore MexEF-OprN	PΔ4-Pore MexHI-OpmD	PΔ4-Pore MexGHI-OpmD	MexEF-OprN	MexHI-OpmD	MexGHI-OpmD
Ciprofloxacin	0.005	0.16	0.08	0.04	32	16	8
Enrofloxacin	0.005	0.31	0.16	0.04	64	32	8
Levofloxacin	0.005	0.16	0.04	0.04	32	8	8
Gatifloxacin	0.002	0.16	0.04	0.02	64	16	8
Moxifloxacin	0.002	0.31	0.04	0.01	128	16	2
Prulifloxacin	0.002	0.08	0.02	0.01	32	8	4
Sparfloxacin	0.001	0.08	0.08	0.02	64	64	16
Difloxacin	0.002	0.16	0.04	0.01	64	16	4
Lomefloxacin	0.010	0.31	0.31	0.08	32	32	8
Ofloxacin	0.010	0.31	0.16	0.08	32	16	8
Pazufloxacin	0.010	0.16	0.08	0.04	16	8	4
Norfloxacin	0.020	0.63	0.08	0.08	32	4	4
Pefloxacin	0.020	1.25	0.16	0.16	64	8	8
Sarafloxacin	0.005	0.08	0.02	0.02	16	4	4
Nadifloxacin	0.001	0.16	0.08	0.08	128	64	64

Table 3.3 - Antibiotic resistance profile of PΔ4-Pore cells producing indicated RND pumps.

3.3.4 MexEF-OprN and MexHI-OpmD have different efficiencies in efflux of a fluorescent probe.

To establish that the changes in MICs observed in hyperporinated cells are due to the differences in efflux activities of the overproduced pumps, we utilized a real-time fluorescence uptake assay. For this purpose, we used a fluorescent probe Hoechst 33342 (HT) to carry out the uptake experiment. Like fluoroquinolones, HT is an inhibitor of DNA topoisomerases (170). But HT is also a fluorescent probe, the emission of which is significantly enhanced when it binds to lipids or DNA, allowing us to monitor its uptake into cells (44). The uptake data were fitted to an exponential equation to extract initial rates of uptake (Fig. 3.5). We observed a clear difference in the initial rates of HT uptake with and without the transporters present, indicating that HT is a substrate of both MexEF-OprN and MexHI-OpmD efflux pumps. Overexpression of MexEF-OprN dramatically, up to 10-fold, decreased the rates of uptake of HT both in the absence and presence of the pore, suggesting that HT is an excellent substrate of this efflux pump. Thus, in agreement with MIC measurements, hyperporination does not affect the activity of this pump. The overexpression of MexHI-OpmD also decreased the rates of HT uptake, but only in cells with an intact outer membrane. In PΔ4(pMexHI-OpmD) cells, the rate of HT uptake decreased by about 2-fold, indicating that HT is also a substrate of MexHI-OpmD, but it is expelled from the cells much slower than by MexEF-OprN. The co-expression of MexG with MexHI-OpmD further reduced its activity, supporting the conclusion that MexG negatively affects the activity of the efflux pump. Furthermore, neither MexHI-OpmD nor MexGHI-OpmD overexpression was able to reduce the rate of HT uptake in hyperporinated cells, indicating that unlike

for MexEF-OprN, the integrity of the outer membrane is critical for activity of MexG/HI-OpmD.

Taken together with MIC measurements, these results suggest that MexHI-OpmD is a weak efflux pump that heavily relies on the outer membrane barrier for its activity against fluoroquinolones and HT. Alternatively, MexHI-OpmD is presented with an elevated concentration of an endogenously produced substrate in hyperporinated cells that outcompetes the antibiotics, resulting in increased susceptibility.

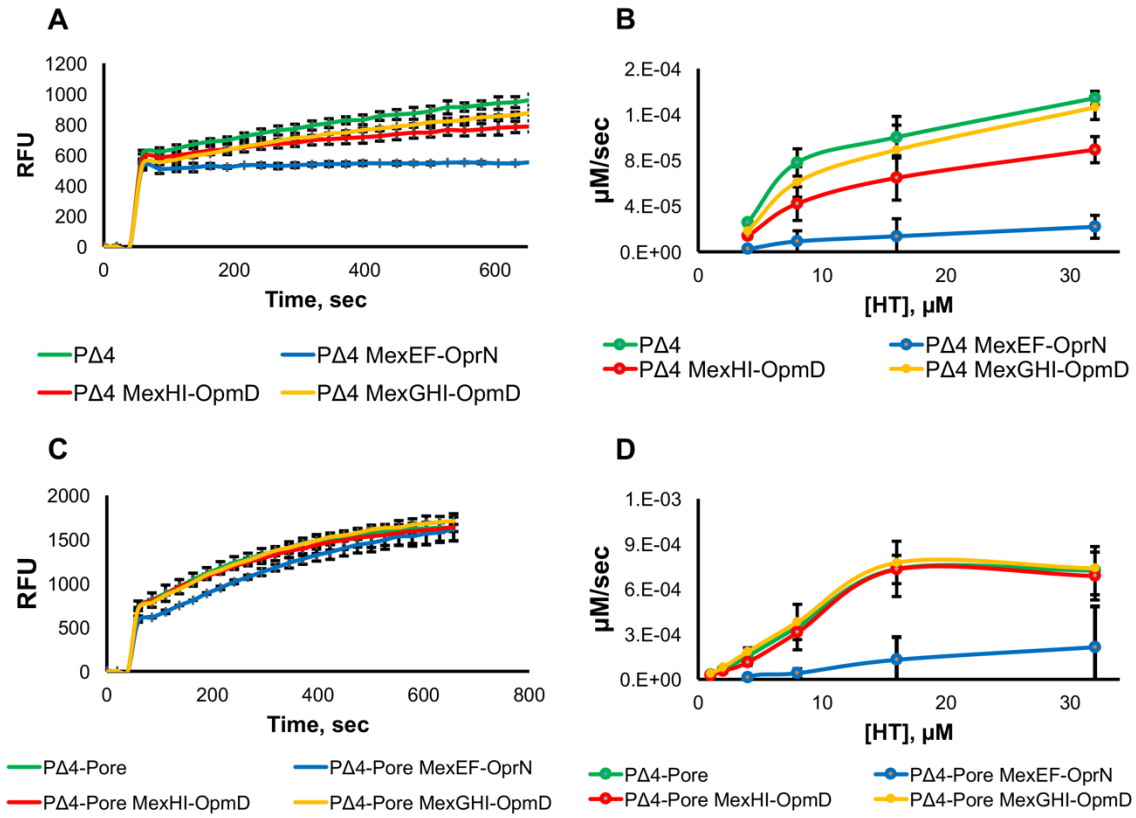

Figure 3.5 - Kinetic uptake measurements comparing MexEF-OprN to MexG/HI-OpmD.

A, C: A real-time course of intracellular accumulation of 32 µM HT in PΔ4 (**A**) and PΔ-Pore (**C**) expressing indicated efflux pump constructs. Kinetic curves were fitted to an exponential equation and initial rates were calculated. **B:** The plot of initial rates of HT accumulation in the indicated cells as a function of extracellular HT concentration. **D:** Graph of the initial rates of HT accumulation in pore expressing cells plotted against the extracellular HT concentration. All kinetic measurements were done in triplicate. Error bars are SD (n=3).

3.3.5 Deletion of MexGHI-OpmD leads to a decrease in the extracellular levels of pyocyanin.

We next investigated a possibility that endogenous substrates outcompete fluoroquinolones in the hyperporinated cells overproducing MexG/HI-OpmD. For this purpose, we constructed a series strains lacking *mexGHI-opmD*. In addition to the wild type PAO1 strain, the *mexGHI-opmD* operon was deleted from PΔ3, PΔ4 and PΔ6 (same as PΔ4 but with additional deletions of *mexEF-oprN* and *triABC*). For simplicity reasons, the Δ*mexGHI-opmD* variants will be referred to as PAO1ΔG, PΔ3ΔG, PΔ4ΔG, and PΔ6ΔG respectively. We used this approach of a stepwise deletion due to the known significant overlap in substrate specificities of RND transporters in *P. aeruginosa* and the progressive loss of the secretion of pyocyanin due to changes in quorum sensing signaling (161).

The constructed mutants did not show an extended lag phase (Fig. 3.6A and B) that was previously reported (83). Similarly, we were unable to see a decrease in the production of PQS (data not shown), but we did notice that the Δ*mexGHI-opmD* mutants produced significantly less pyocyanin even in already pyocyanin-deficient efflux mutants (Fig. 3.6C). We measured the amounts of this phenazine in supernatants of bacterial cultures and found a noticeable, more than 2-fold, decrease in the amounts of pyocyanin in the cultures of all Δ*mexGHI-opmD* strains when compared to their respective parental strains (Fig. 3.6C).

To confirm that MexGHI-OpmD is linked to the synthesis and excretion of pyocyanin, we measured amounts of this pigment in the cultures of the PAO1 strains overproducing different components of the transporter (Fig. 3.6D). When compared to

the wild type, PAO1 overexpressing MexGHI-OpmD or MexHI-OpmD produced twice the amount of pyocyanin. Expression of MexG alone did not change the amounts of pyocyanin in the culture medium, but expression of MexGHI without the outer membrane channel OpmD resulted in a 50% increase. This suggests that MexHI might be able to associate with another outer membrane channel to achieve at least partial activity. MexG does not appear to be required for this functionality of the transporter. In agreement with previous results, overexpression of MexEF-OprN resulted in decreased production of pyocyanin (153). Thus, the amount of secreted pyocyanin positively correlates with the expression of MexG/HI-OpmD in *P. aeruginosa* cells and this correlation is independent of the presence or absence of other RND pumps.

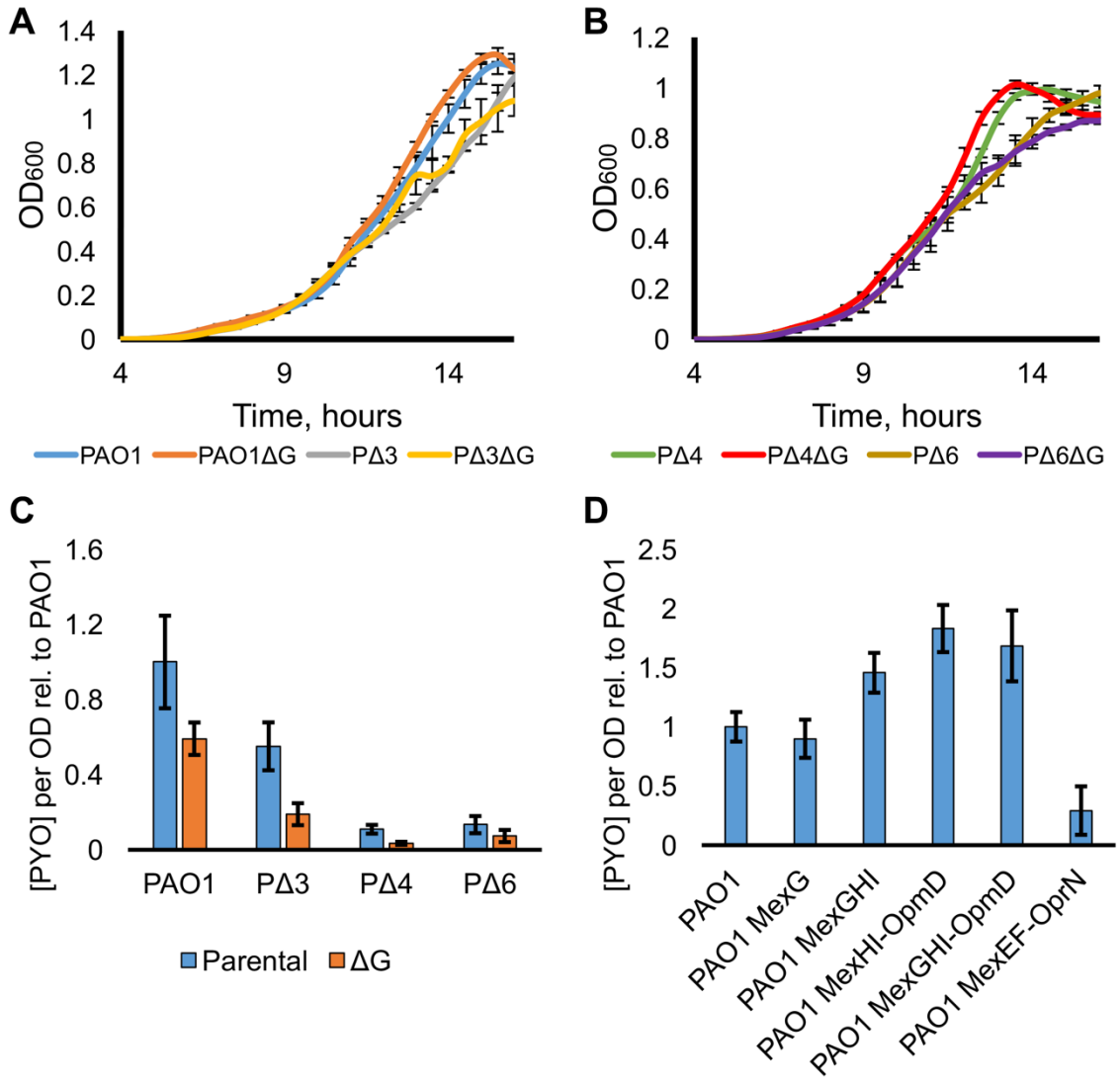

Figure 3.6 - Deletion of *mexGHI-opmD* results in a decrease of pyocyanin production.

A and **B:** Growth curves of the indicated strains. **C:** Extracellular concentrations of pyocyanin in PAO1, PΔ3, PΔ4, and PΔ6 parental strains (blue) and their derivatives macking *mexGHI-opmD* (ΔG) mutants (orange). **D:** Extracellular concentrations of pyocyanin in cultures of PAO1 strains overexpressing MexEF-OprN or different combinations of MexG/HI-OpmD components. All measurements were done on cultures grown to stationary phase and in triplicate. Error bars are SD (n=3).

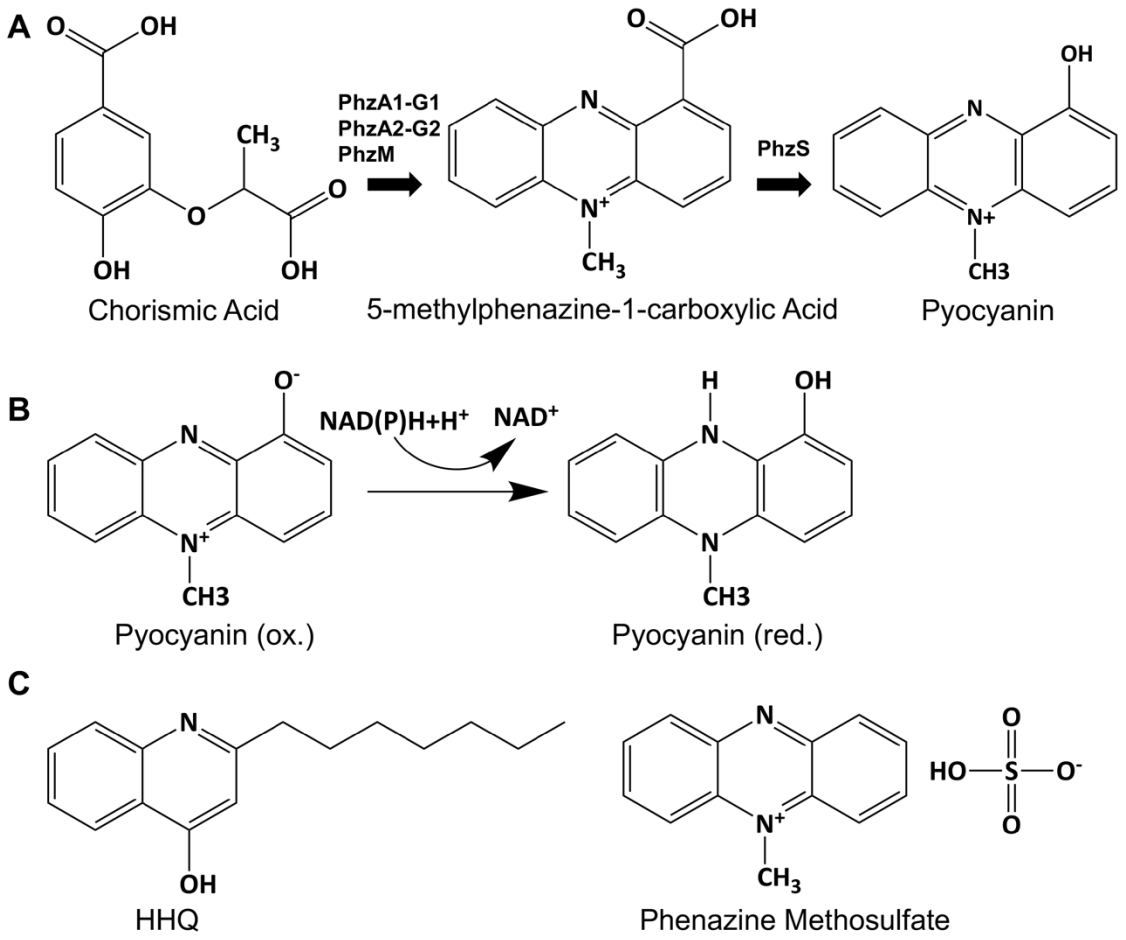

Figure 3.7 - Structures of phenazines and quorum signals.

A: Synthesis pathway of pyocyanin, showing the intermediate 5-methyl-1-carboxylic Acid (5-Me-PCA). **B:** Pyocyanin exerts its toxic effects by reducing NADH and NADPH, thus reducing the intracellular levels of ATP. At the same time, this allows it to serve as an electron shuttle during oxygen poor conditions. **C:** Structures of HHQ and phenazines methosulfate (PMS). HHQ is suggested to be exported by MexEF-OprN.

3.3.6 MexGHI-OpmD provides a self-protection of *P. aeruginosa* to phenazines.

Pyocyanin is a powerful toxin that inhibits the electron transport chain and several other pathways (162, 168). Figure 3.7B shows the oxidized and reduced forms of this compound. To test whether pyocyanin is a substrate of MexG/HI-OpmD we performed growth spot inhibition assays with PAO1 and all efflux deficient mutants (Fig. 3.8A). All strains that contained a chromosomal copy of *mexGHI-opmD* were fully resistant to pyocyanin. On the other hand, the efflux deficient mutants that lacked *mexGHI-opmD* were all hypersusceptible, as seen from large zones of inhibition. This is the first time that a *P. aeruginosa* strain was found to be susceptible to pyocyanin. PAO1ΔG was still resistant to pyocyanin at the concentrations tested, indicating that the constitutively expressed MexAB-OprM can provide some level of resistance to phenazines. However, the pyocyanin hypersusceptibility of all efflux-deficient strains suggests that MexG/HI-OpmD is expressed in these strains and provides immunity against this toxin.

We inserted the pore into PΔ4ΔG and PΔ6ΔG strains and measured the MICs of pyocyanin (Table 4). Deletion of MexGHI-OpmD from PΔ4 resulted in a 4-fold decrease of the MIC of pyocyanin. Interestingly, this strain is 4 times more resistant to chloramphenicol and ciprofloxacin, which suggests that another transporter, based on the resistance profile likely MexEF-OprN, is overexpressed. Thus, MexEF-OprN is still able to provide some level of resistance to phenazines in PΔ4ΔG. The MIC of pyocyanin decreased by a staggering 64-fold when MexGHI-OpmD was deleted in PΔ6 and no further decrease was observed with hyperporination, suggesting that PΔ6ΔG is depleted of phenazine efflux. The strain PΔ5S, same as PΔ4 but with deletion of

mexEF-OprN, was still completely resistant to pyocyanin, indicating that MexGHI-OpmD is sufficient to provide efflux of this virulence factor. Furthermore, PΔ4ΔG-Pore showed the same MIC of pyocyanin as PΔ6ΔG, suggesting that the phenazine efflux in PΔ4ΔG is weak and highly dependent on the presence of the outer membrane barrier. On the other hand, hyperporination of PΔ4 only decreased the MIC of pyocyanin by 4-fold, indicating that MexGHI-OpmD can compensate for the loss of the barrier and still provide resistance to phenazines. Taken together, these results show that MexGHI-OpmD is highly efficient in the efflux of pyocyanin, whereas deleting MexEF-OprN has no effect on the MIC of phenazines.

As could be expected based on the above results and previous studies (84), deletion of *mexGHI-opmD* resulted in a drastic increase in susceptibility to PMS, a close analog of 5-Me-PCA, which is an endogenous highly reactive precursor of pyocyanin (Fig. 3.8B). Unlike with pyocyanin, the zone of inhibition for PAO1ΔG was roughly 2-fold larger than for PAO1, indicating that PMS is more toxic and the MexG/HI-OpmD-dependent self-protection is seen even in the presence of MexAB-OprM. Furthermore, the deletion of MexGHI-OpmD in PΔ4 resulted in a large 16-fold decrease of the MIC, whereas the deletion of MexEF-OprN had no impact in the MIC. Similar to pyocyanin, PΔ6 was still fully resistant to PMS and the deletion of MexGHI-OpmD in that strain resulted in the same MIC as for PΔ4ΔG, further confirming that these strains are depleted of phenazine efflux.

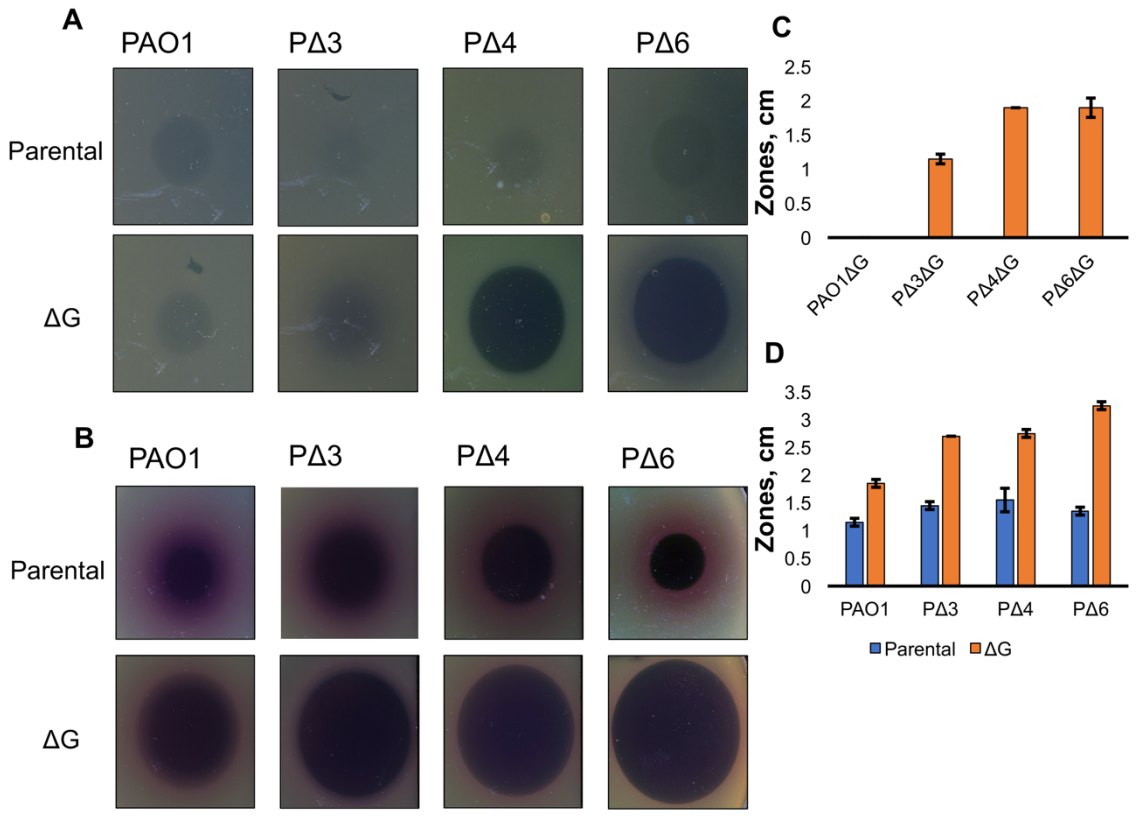

Figure 3.8 - MexGHI-OpmD provides resistance to pyocyanin and PMS.

A, B: Spot assays with pyocyanin (**A**) and PMS (**B**) showing zones of inhibition in strains with and without *mexGHI-opmD*. **C, D**: Quantification of zones of inhibition of pyocyanin (**C**) and PMS (**D**) in indicated strains. Error bars are SD (n=2).

To test whether phenazines are responsible for the decreased activity of MexHI-OpmD against fluoroquinolones in hyperporinated strains, we set up checkerboard assays to analyze possible interactions between ciprofloxacin and pyocyanin with PΔ4-Pore cells containing different plasmids (Fig. 3.9). For each strain, we calculated an average fractional inhibitory concentration (FIC) index. The FIC is the fraction of the MIC in combination with a second drug and the MIC by itself. The FIC index is the sum of the two FIC from each drug and is commonly used to describe interactions of two antimicrobials (171, 172). Generally, a FIC index of ≤0.5 represents synergy, a FIC index of 1 represents an additive/inconclusive effect, and an FICI of ≥2 is defined as antagonism between the two antimicrobials (173, 174). We found the FIC index of ~2.3 for the control PΔ4-Pore with empty vector, whereas the FIC indexes measured for PΔ4-Pore cells expressing MexEF-OprN, MexHI-OpmD, and MexGHI-OpmD were 1.6, 1.1, and 1.0 respectively. Thus, there are no significant interactions between pyocyanin and ciprofloxacin in the hyperporinated strains overproducing efflux pumps but an antagonistic interaction is possible in the absence of these efflux pumps. The higher FIC indexes for MexEF-OprN and the empty vector strain could, presumably, be due to complementation effects of exogenous pyocyanin. These strains produce very low levels of pyocyanin, which also serves to maintain redox homeostasis in *P. aeruginosa*. It is likely that low, non-inhibitory concentrations of pyocyanin could stimulate cell growth in these strains (168). These results also show that in the strains overproducing MexG/HI-OpmD, ciprofloxacin and pyocyanin do not interact with each other and the antibacterial activities are simply additive. Thus, the reduction of the activity of MexHI-OpmD against fluoroquinolones in hyperporinated strains highlights

the low efficiency of the transporter for these substrates and that the efflux is highly dependent on the presence of the outer membrane barrier. This is in contrast to phenazine efflux of MexGHI-OpmD and shows that the outer membrane can significantly mask the efflux efficiencies of RND transporters.

	Pyocyanin		PMS		Chloramphenicol		Ciprofloxacin	
MIC, µM	**(-) Pore**	**(+) Pore**	**(-) Pore**	**(+) Pore**	**(-) Pore**	**(+) Pore**	**(-) Pore**	**(+) Pore**
PΔ4	1000	250	500	62.5	3.09	1.55	0.003	0.0007
PΔ4ΔG	250	31.25	31.25	31.25	12.38	1.55	0.012	0.0007
PΔ5S	>1000	250	500	25	3.09	1.55	0.003	0.0007
PΔ6	>1000	125	500	125	1.55	1.55	0.003	0.0007
PΔ6ΔG	31.25	31.25	31.25	15.625	1.55	1.55	0.0007	0.0004
PΔ6ΔG MexEF-OprN	>500	-	500	-	>396	-	0.38	-
PΔ6ΔG MexHI-OpmD	>500	-	2000	-	1.55	-	0.38	-
PΔ6ΔG MexGHI-OpmD	>500	-	1000	-	1.55	-	0.19	-

Table 3.4 - MICs of phenazines in efflux deficient mutants.

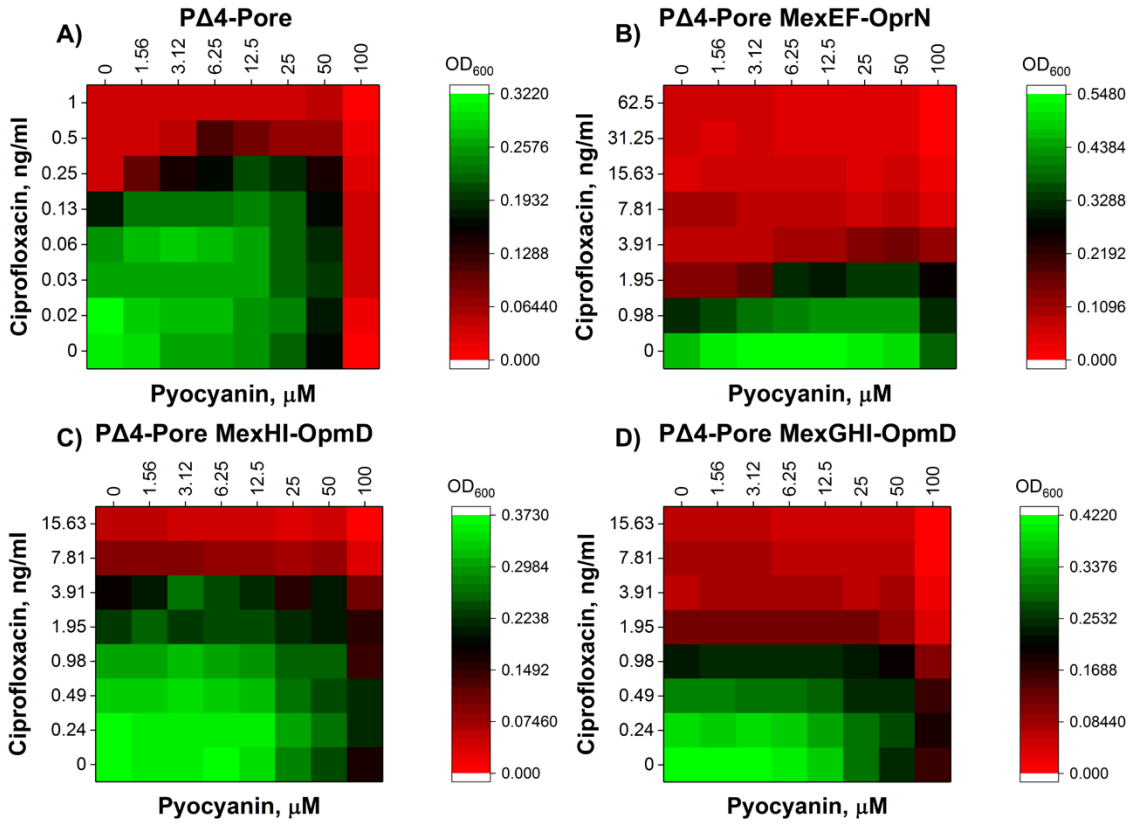

Figure 3.9 - Checkerboard assay with pyocyanin and ciprofloxacin.

Growth of the indicated strains at different combinations of pyocyanin and ciprofloxacin concentrations. The optical densities of cultures are indicated with green (high) to red (low).

3.3.7 MexG binds to pyocyanin *in vitro* suggesting a functional relationship with MexHI-OpmD.

In all assays described above, the presence of MexG had a negative effect on the activity of MexHI-OpmD. We next analyzed whether MexG will bind to pyocyanin. To test this, we purified MexG using metal affinity chromatography and analyzed binding to pyocyanin by fluorescence spectroscopy. MexG contains five tryptophan residues that are predicted to be in the transmembrane helices. As tryptophan residues were excited, the emission of MexG fluorescence peaked at around 330 nm. In contrast, pyocyanin has a very low fluorescence at the same excitation and emission wavelengths (Fig. 3.10A). However, addition of increasing concentrations of pyocyanin to MexG significantly quenches the fluorescence of MexG and causes a slight red shift in the emission spectra (Fig. 3.10B), suggesting that pyocyanin binds MexG and causes a change in the environments of the tryptophan residues. We calculated a K_D of pyocyanin to MexG to be about 0.6 μM (Fig. 3.11A). This suggests that the binding is quite strong, with the K_D similar to what was previously reported for MexG and PQS (158). The solvent used for pyocyanin did not alter the fluorescence of MexG in the amounts used during each experiment (Fig. 3.10C).

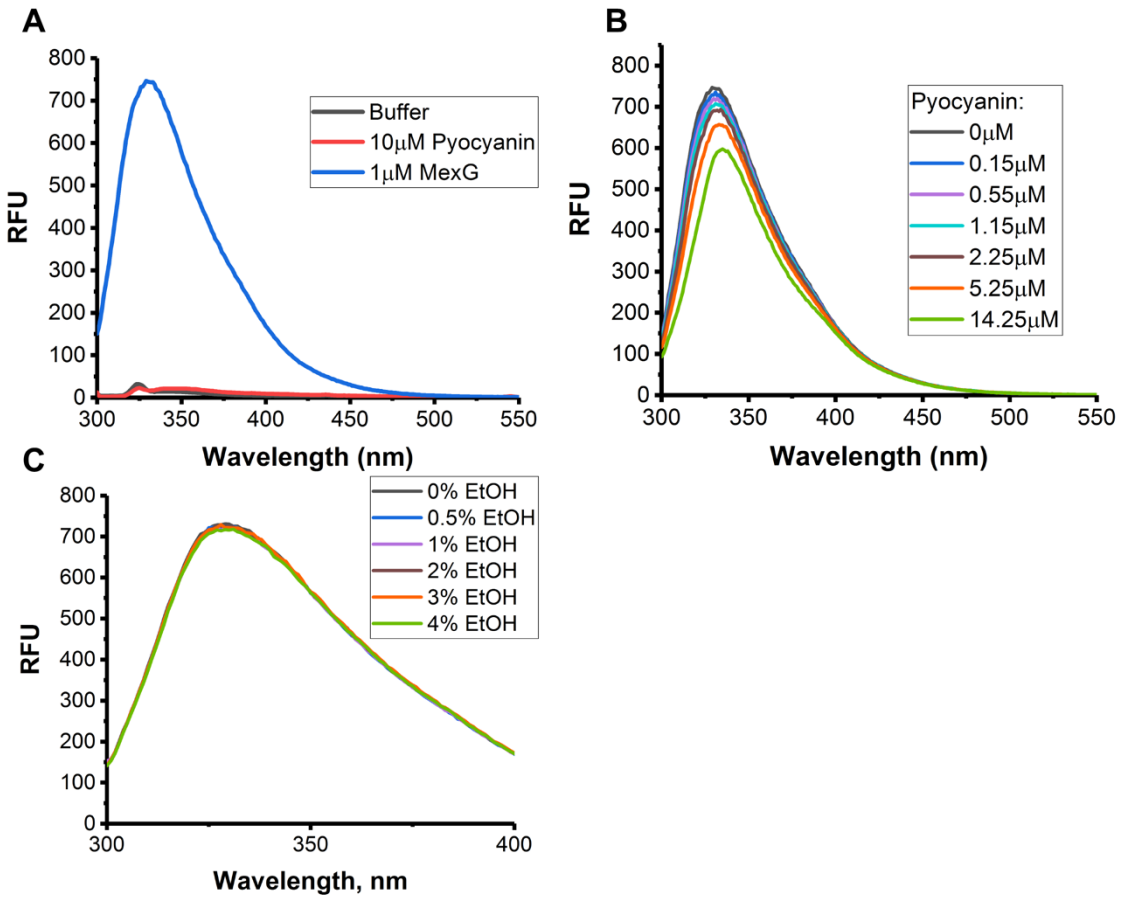

Figure 3.10 - Emission Spectra of MexG and Pyocyanin.

A: Fluorescence emission spectra of MexG (1 μM) and pyocyanin (10 μM) excited at 290 nm. **B:** Titration of indicated concentrations of pyocyanin into a sample of 1 μM MexG. Addition of pyocyanin quenches MexG fluorescence indicating a physical interaction. **C:** Effects of ethanol (solvent for pyocyanin) on fluorescence of MexG. Amounts of ethanol shown are exceeding the ones used during the experiment.

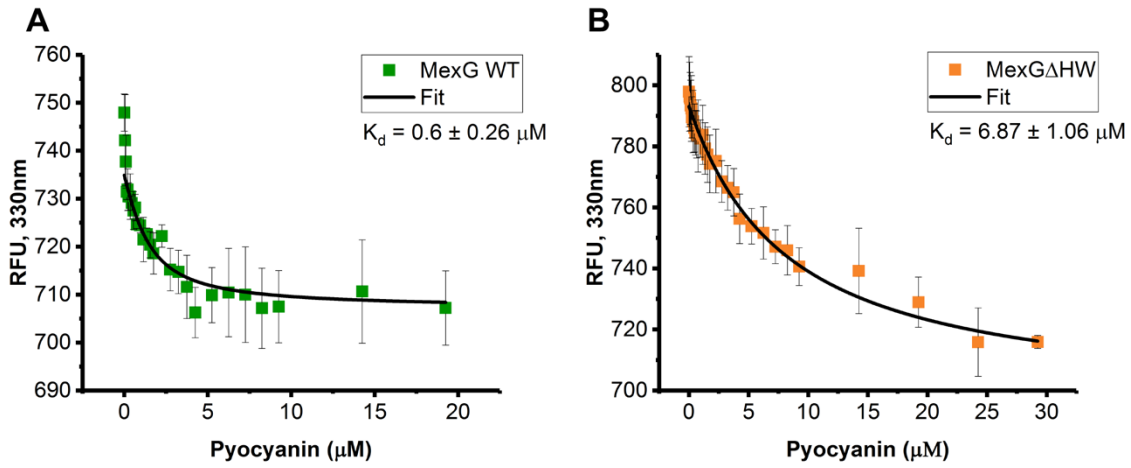

Figure 3.11 - Pyocyanin binding to MexG.

Fluorescence emission at 330 nm (excitation at 290 nm) of the wild type MexG (**A**) and MexGΔHW (**B**) incubated with increasing concentration of pyocyanin was measured and normalized as described in Methods and is plotted as a function pyocyanin concentration. Fitted line shown in black. Error bars are SD (n=3).

To determine whether pyocyanin binding is specific, we constructed the MexG mutant MexGΔHW, which contains two substitutions His95Ala and Trp98Ala at the C-terminal end of the transmembrane domain 3. The mutant was purified in the same manner as MexG WT. We repeated the fluorescence binding experiment with this mutant and found that the affinity of MexGΔHW to pyocyanin decreased by at least 10-fold when compared to MexG WT to a K_D of about 7 μM (Fig. 3.11B). The lower binding affinity for MexGΔHW shows that pyocyanin binds specifically to MexG, which suggests that there is a functional relationship between the protein and the MexHI-OpmD transporter.

3.4 Discussion

P. aeruginosa is a highly resistant human pathogen that is infamous for its colonization of lungs in cystic fibrosis patients. The high intrinsic resistance stems from its 12 chromosomally encoded RND efflux transporters and its outer membrane, which presents a significant permeability barrier for most antibiotics. Though RND transporters are most commonly associated with an antibiotic resistance phenotype, they also play important roles in the physiology of *P. aeruginosa*. The natural substrates of these transporters are often still unknown and more research is needed to elucidate the roles they play in establishing homeostasis of signaling molecules and virulence factors.

In this study, we investigated the properties and functions of MexG/HI-OpmD efflux pump and compared them to MexEF-OprN. Our results suggest that the two pumps differ significantly not only in substrate specificity but also in their efflux efficiencies. When influx of compounds is slowed down by the low permeability barrier

of the outer membrane, overexpression of MexG/HI-OpmD provides resistance to a broad range of fluoroquinolones and endogenous phenazines at the same levels as MexEF-OprN. Surprisingly, despite differences in their structures, all fluoroquinolones appeared to be excellent substrates of both transporters, as seen from 64 to 128-fold changes in MICs for all tested fluoroquinolones. However, this lack of selectivity faded when we removed the contribution of the outer membrane to resistance by hyperporination, which leads to an increase of the substrate in the periplasm. This highlights the differences of the efficiencies of transporters toward the efflux of fluoroquinolones when the outer membrane permeability is compromised. As described above, the overproduction of MexEF-OprN increases the MICs of all FQ by 32 to 128-fold even in hyperporinated cells (Fig. 3.2D). However, some substrate specificity could be deduced from the fold MIC change in MexEF-OprN overproducers with and without the Pore. Norfloxacin, prulifloxacin and perfloxacin are excellent substrates of MexEF-OprN and their activities are only weakly (4-fold) affected by hyperporination (Table 3). Thus, even in the hyperporinated cells, MexEF-OprN is far from saturation with these fluoroquinolones. In contrast, MexEF-OprN is significantly more effective against nadifloxacin, sparfloxacin and difloxacin only if the influx of these drugs is very slow, as seen by the differences in MICs between hyperporinated and non-hyperporinated cells (Table 2 and 3).

The effect of hyperporination was even stronger in cells overproducing MexHI-OpmD. The increased influx across the outer membrane significantly reduced the efficiency of this pump against all fluoroquinolones by 16 to 64-fold. Among the least affected, 16-fold change in MIC (-pore/+pore), are norfloxacin, ciprofloxacin,

pazufloxacin, lomofloxacin and prulifloxacin. With FQs that are strongly affected by hyperporination, in addition to nadifloxacin, sparfloxacin and difloxacin for which MexEF-OprN is not as effective, MexHI-OpmD lost its efficiency also against moxifloxacin, gatifloxcin and levofloxacin (64-fold MIC change). Thus, MexHI-OpmD is not only less efficient in efflux of FQs than MexEF-OprN, but also less specific to fluoroquinolones. On the other hand, MexG/HI-OpmD is more efficient in the efflux of phenazines, which demonstrates that these two transporters have distinctly different native substrates. Interestingly, for other non-FQ substrates of MexEF-OprN and MexHI-OpmD, hyperporination dramatically reduced the efficiency of both pumps (Table 1), suggesting that they are effective against these drugs only because of the low permeability barrier of the outer membrane.

Previously, MexHI-OpmD was found to transport the pyocyanin precursor 5-Me-PCA (84). Here we demonstrated that MexHI-OpmD also transports pyocyanin. Aendekerk et al. have shown that a disruption in *mexI* or *opmD* affects the virulence of PA14 cells (83), which agrees with our finding that deletion of *mexGHI-OpmD* leads to a decrease in pyocyanin production in all strains tested. Since this deletion also made the strains more susceptible to pyocyanin, it is likely that the decrease of its synthesis is due to a reduced tolerance to this toxin and that its intracellular concentration must be strictly controlled. This is in agreement with our finding that overexpression of MexHI-OpmD leads to an increased level of pyocyanin synthesis in PAO1. While there is some functional overlap with other RND efflux pumps, our results show that MexHI-OpmD is likely the primary transporter for phenazines. These findings also establish a direct link between MexHI-OpmD and virulence in *P. aeruginosa*.

The role of MexEF-OprN in efflux of phenazines is more complex and seems to be similar to FQ efflux of MexGHI-OpmD. The susceptibility to pyocyanin and PMS is the same in PΔ4 and PΔ6 strains, suggesting that MexEF-OprN is not expressed in these cells and does not contribute to protection against endogenously produced phenazines. On the other hand, MexEF-OprN seems to be overexpressed in PΔ4ΔG but we still measured a 4-fold decrease in the MIC of pyocyanin between PΔ4 and PΔ4ΔG. In addition, hyperporination of PΔ4ΔG completely depleted the efflux capacities of the strain with respect to phenazines, indicating that the efflux provided by MexEF-OprN of these compounds is weak (Table 4). This is even more apparent for PMS, were the deletion of MexGHI-OpmD could not be complemented by the elevated expression of another efflux transporter (Table 4). Taken together, our studies show that true efficiencies of transporters towards certain substrates can be masked significantly by the presence of the outer membrane and that they can only be revealed by removing its contribution to resistance. It appears that the primary substrates of MexEF-OprN are quinolones, like its proposed quorum sensing substrate HHQ (81), whereas the primary substrates of MexG/HI-OpmD seem to be phenazines.

The small membrane protein MexG appears to play a role as a negative regulator of the efflux activity of MexHI-OpmD. We showed here that it physically associates with the transporter *in vivo*, establishing that at least a fraction of this pump exists as a four-component complex MexGHI-OpmD. Antibiotic susceptibility testing showed a decrease in activity of the transporter in respect to some substrates when MexG is co-expressed (Fig. 3.3B). This decrease seems to vary depending on the substrate tested. Norfloxacin, ethidium bromide, and acriflavine did not show any

changes in activity, whereas moxifloxacin showed the biggest reduction of the MIC of 8-fold. Some substrates might more closely resemble the native binding partner of MexG and can activate the small membrane protein. This could point to a regulatory function of MexG with respect to the activity of MexHI-OpmD. Our fluorescence assays showed that MexG binds pyocyanin and that this binding is specific with a K_D of about 0.6 μM. It is possible that MexG could act as a sensor of phenazines and other signaling molecules in the inner membrane and modulate the activity of MexHI-OpmD by dissociating from the complex in the ligand-bound state (Fig. 3.12).

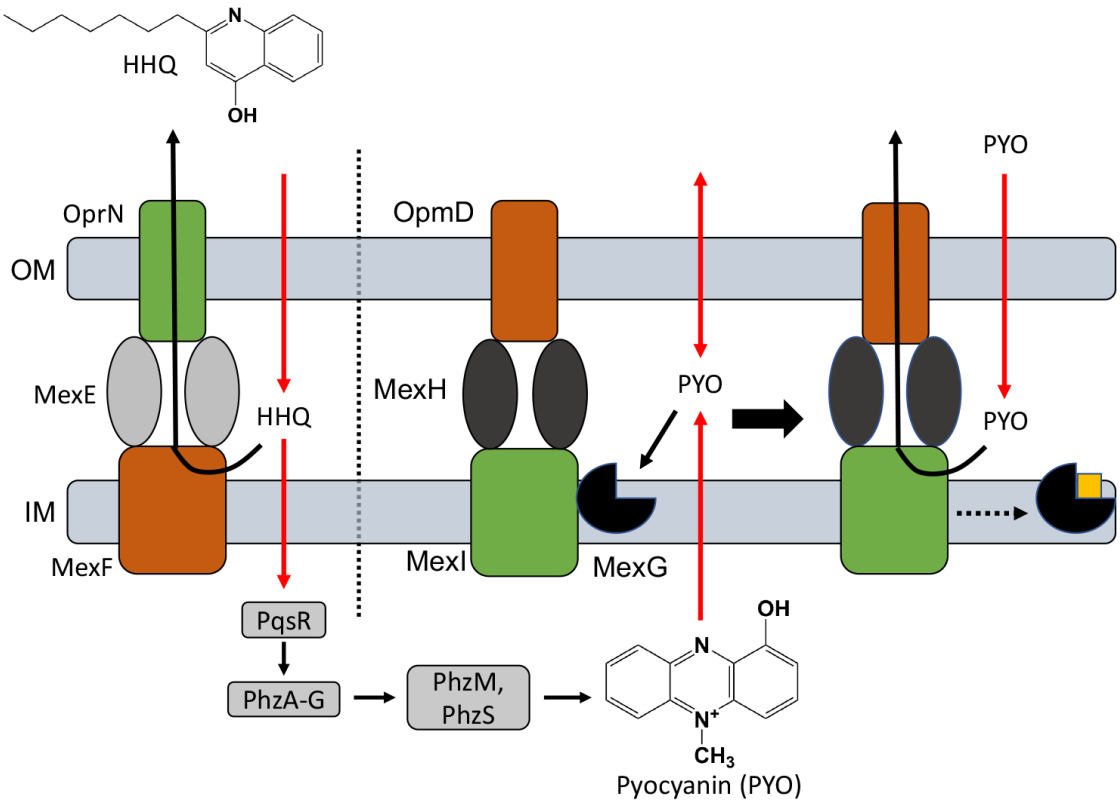

Figure 3.12 - Proposed model of the functional role of MexG.

Pyocyanin has a dual role for the cell as it acts as an electron shuttle for *P. aeruginosa* during oxygen poor conditions and a virulence factor. Thus, the intracellular concentrations need to be regulated. When periplasmic concentrations of pyocyanin are low, MexG is bound to MexHI-OpmD and the transporter displays a low efflux activity. When the concentrations of pyocyanin increase it binds to MexG, which results in dissosication of the small inner membrane protein from the transporter. This increases the activity of MexHI-OpmD and allows it to provide protection from the virulence factor.

References

1. Antimicrobial Resistance : Tackling a crisis for the health and wealth of nations. In: Resistance RoA, editor. 2014. p. 1-16.

2. Mediavilla JR, Patrawalla A, Chen L, Chavda KD, Mathema B, Vinnard C, Dever LL, Kreiswirth BN. Colistin- and Carbapenem-Resistant Escherichia coli Harboring mcr-1 and blaNDM-5, Causing a Complicated Urinary Tract Infection in a Patient from the United States. mBio. 2016;7(4):e01191-16. doi: 10.1128/mBio.01191-16.

3. Antimicrobial resistance. In: Organization WH, editor. 2014. p. 383-94.

4. A Blair JM, Webber MA, Baylay AJ, Ogbolu DO, V Piddock LJ. Molecular mechanisms of antibiotic resistance. Nature Publishing Group. 2014;13. doi: 10.1038/nrmicro3380.

5. Zgurskaya HI, Löpez CA, Gnanakaran S. Permeability Barrier of Gram-Negative Cell Envelopes and Approaches To Bypass It. ACS infectious diseases. 2015;1(11):512-22. doi: 10.1021/acsinfecdis.5b00097.

6. Global priority list of antibiotic-resistant bacteria to guide research, discovery, and development of new antibiotics. In: Organization WH, editor. 2017.

7. Silver LL. Challenges of antibacterial discovery. Clin Microbiol Rev. 2011;24(1):71-109. Epub 2011/01/15. doi: 10.1128/cmr.00030-10. PubMed PMID: 21233508; PMCID: PMC3021209.

8. Mulcahy LR, Isabella VM, Lewis K. Pseudomonas aeruginosa Biofilms in Disease. Microb Ecol. 2013;68(1):1-12. Epub 10/08. doi: 10.1007/s00248-013-0297-x.

9. Hogardt M, Heesemann J. Microevolution of Pseudomonas aeruginosa to a chronic pathogen of the cystic fibrosis lung. Curr Top Microbiol Immunol. 2013;358:91-118. Epub 02/09. doi: 10.1007/82_2011_199 10.1007/82_2011_199.

10. Oliphant CM, Green GM. Quinolones: a comprehensive review. American family physician. 2002;65(3):455-64. Epub 2002/02/23. PubMed PMID: 11858629.

11. Hooper DC. New Uses for New and Old Quinolones and the Challenge of Resistance. Clinical Infectious Diseases. 2000;30(2):243-54. doi: 10.1086/313677.

12. Obritsch MD, Fish DN, MacLaren R, Jung R. Nosocomial infections due to multidrug-resistant Pseudomonas aeruginosa: epidemiology and treatment options. Pharmacotherapy. 2005;25(10):1353-64. Epub 2005/09/28. doi: 10.1592/phco.2005.25.10.1353. PubMed PMID: 16185180.

13. Alhede MM, Bjarnsholt T, Givskov M, Alhede MM. Pseudomonas aeruginosa Biofilms: Mechanisms of Immune Evasion. Adv Appl Microbiol. 2014;86:1-40. Epub 01/01. doi: 10.1016/b978-0-12-800262-9.00001-9 10.1016/B978-0-12-800262-9.00001-9.

14. Breidenstein EB, de la Fuente-Nunez C, Hancock RE. Pseudomonas aeruginosa: all roads lead to resistance. Trends Microbiol. 2011;19(8):419-26. Epub 2011/06/15. doi: 10.1016/j.tim.2011.04.005. PubMed PMID: 21664819.

15. Paterson DL. The Epidemiological Profile of Infections with Multidrug-Resistant Pseudomonas aeruginosa and Acinetobacter Species. Clinical Infectious Diseases. 2006;43(Supplement_2):S43-S8. doi: 10.1086/504476.

16. Aloush V, Navon-Venezia S, Seigman-Igra Y, Cabili S, Carmeli Y. Multidrug-resistant Pseudomonas aeruginosa: risk factors and clinical impact. Antimicrob Agents Chemother. 2006;50(1):43-8. Epub 2005/12/27. doi: 10.1128/aac.50.1.43-48.2006. PubMed PMID: 16377665; PMCID: PMC1346794.

17. Zavascki AP, Carvalhaes CG, Picão RC, Gales AC. Multidrug-resistant Pseudomonas aeruginosa and Acinetobacter baumannii: resistance mechanisms and implications for therapy. Expert Review of Anti-infective Therapy. 2010;8(1):71-93. doi: 10.1586/eri.09.108.

18. Welbourn CR, Young Y. Endotoxin, septic shock and acute lung injury: neutrophils, macrophages and inflammatory mediators. The British journal of surgery. 1992;79(10):998-1003. Epub 1992/10/01. PubMed PMID: 1422741.

19. Ernst RK, Yi EC, Guo L, Lim KB, Burns JL, Hackett M, Miller SI. Specific lipopolysaccharide found in cystic fibrosis airway Pseudomonas aeruginosa. Science. 1999;286(5444):1561-5. Epub 1999/11/24. PubMed PMID: 10567263.

20. Hancock RE, Mutharia LM, Chan L, Darveau RP, Speert DP, Pier GB. Pseudomonas aeruginosa isolates from patients with cystic fibrosis: a class of serum-sensitive, nontypable strains deficient in lipopolysaccharide O side chains. Infect Immun. 1983;42(1):170-7. Epub 1983/10/01. PubMed PMID: 6413410; PMCID: PMC264539.

21. Kulshin VA, Zähringer U, Lindner B, Frasch CE, Tsai CM, Dmitriev BA, Rietschel ET. Structural characterization of the lipid A component of pathogenic Neisseria meningitidis. Journal of Bacteriology. 1992;174(6):1793-800. PubMed PMID: PMC205780.

22. Liu PV, Matsumoto H, Kusama H, Bergan T. Survey of Heat-Stable, Major Somatic Antigens of Pseudomonas aeruginosa†. International Journal of Systematic and Evolutionary Microbiology. 1983;33(2):256-64. doi: doi:10.1099/00207713-33-2-256.

23. Liu PV, Wang S. Three new major somatic antigens of Pseudomonas aeruginosa. Journal of clinical microbiology. 1990;28(5):922-5. Epub 1990/05/01. PubMed PMID: 2112563; PMCID: PMC267837.

24. Beckmann F, Moll H, Jager KE, Zahringer U. Preliminary communication 7-O-carbamoyl-L-glycero-D-manno-heptose: a new core constituent in the lipopolysaccharide of Pseudomonas aeruginosa. Carbohydrate research. 1995;267(2):C3-7. Epub 1995/02/17. PubMed PMID: 7895224.

25. Galanos C, Luderitz O, Rietschel ET, Westphal O, Brade H, Brade L, Freudenberg M, Schade U, Imoto M, Yoshimura H, et al. Synthetic and natural Escherichia coli free lipid A express identical endotoxic activities. European journal of biochemistry. 1985;148(1):1-5. Epub 1985/04/01. PubMed PMID: 2579812.

26. Knirel YA, Bystrova OV, Kocharova NA, Zahringer U, Pier GB. Conserved and variable structural features in the lipopolysaccharide of Pseudomonas aeruginosa. J Endotoxin Res. 2006;12(6):324-36. Epub 2007/01/27. doi: 10.1179/096805106x118906. PubMed PMID: 17254386.

27. Walsh AG, Matewish MJ, Burrows LL, Monteiro MA, Perry MB, Lam JS. Lipopolysaccharide core phosphates are required for viability and intrinsic drug resistance in Pseudomonas aeruginosa. Mol Microbiol. 2000;35(4):718-27. Epub 2000/02/26. PubMed PMID: 10692150.

28. Kooistra O, Bedoux G, Brecker L, Lindner B, Sanchez Carballo P, Haras D, Zahringer U. Structure of a highly phosphorylated lipopolysaccharide core in the Delta algC mutants derived from Pseudomonas aeruginosa wild-type strains PAO1 (serogroup O5) and PAC1R (serogroup O3). Carbohydrate research. 2003;338(23):2667-77. Epub 2003/12/13. PubMed PMID: 14670725.

29. Metzger LE, Lee JK, Finer-Moore JS, Raetz CRH, Stroud RM. LpxI structures reveal how a lipid A precursor is synthesized. Nature structural & molecular biology. 2012;19(11):1132-8. doi: 10.1038/nsmb.2393. PubMed PMID: PMC3562136.

30. Nikaido H. Molecular basis of bacterial outer membrane permeability revisited. Microbiology and molecular biology reviews : MMBR. 2003;67(4):593-656. doi: 10.1128/MMBR.67.4.593.

31. Fernandez L, Hancock RE. Adaptive and mutational resistance: role of porins and efflux pumps in drug resistance. Clin Microbiol Rev. 2012;25(4):661-81. Epub 2012/10/05. doi: 10.1128/cmr.00043-12. PubMed PMID: 23034325; PMCID: PMC3485749.

32. Tamber S, Hancock REW. The Outer Membranes of Pseudomonads. In: Ramos J-L, editor. Pseudomonas: Volume 1 Genomics, Life Style and Molecular Architecture. Boston, MA: Springer US; 2004. p. 575-601.

33. Murakami S. Structures and Transport Mechanisms of RND Efflux Pumps. Cham: Springer International Publishing; 2016. p. 3-28.

34. Seeger MA, van Veen HW. Molecular basis of multidrug transport by ABC transporters. Biochimica et Biophysica Acta (BBA) - Proteins and Proteomics. 2009;1794(5):725-37. doi: http://dx.doi.org/10.1016/j.bbapap.2008.12.004.

35. Fluman N, Bibi E. Bacterial multidrug transport through the lens of the major facilitator superfamily. Biochim Biophys Acta. 2009;1794(5):738-47. Epub 2008/12/24. doi: 10.1016/j.bbapap.2008.11.020. PubMed PMID: 19103310.

36. Schuldiner S. EmrE, a model for studying evolution and mechanism of ion-coupled transporters. Biochim Biophys Acta. 2009;1794(5):748-62. Epub 2009/01/27. doi: 10.1016/j.bbapap.2008.12.018. PubMed PMID: 19167526.

37. Kuroda T, Tsuchiya T. Multidrug efflux transporters in the MATE family. Biochim Biophys Acta. 2009;1794(5):763-8. Epub 2008/12/23. doi: 10.1016/j.bbapap.2008.11.012. PubMed PMID: 19100867.

38. Pos KM. Drug transport mechanism of the AcrB efflux pump. Biochim Biophys Acta. 2009;1794(5):782-93. Epub 01/27. doi: 10.1016/j.bbapap.2008.12.015 10.1016/j.bbapap.2008.12.015. Epub 2009 Jan 3.

39. Li X-Z, Plésiat P. Antimicrobial Drug Efflux Pumps in Pseudomonas aeruginosa. Cham: Springer International Publishing; 2016. p. 359-400.

40. Poole K, Krebes K, McNally C, Neshat S. Multiple antibiotic resistance in Pseudomonas aeruginosa: evidence for involvement of an efflux operon. Journal of Bacteriology. 1993;175(22):7363-72. PubMed PMID: PMC206881.

41. Jeannot K, Elsen S, Kohler T, Attree I, van Delden C, Plesiat P. Resistance and virulence of Pseudomonas aeruginosa clinical strains overproducing the MexCD-OprJ efflux pump. Antimicrob Agents Chemother. 2008;52(7):2455-62. Epub 2008/05/14. doi: 10.1128/aac.01107-07. PubMed PMID: 18474583; PMCID: PMC2443911.

42. Sobel ML, Neshat S, Poole K. Mutations in PA2491 (mexS) promote MexT-dependent mexEF-oprN expression and multidrug resistance in a clinical strain of Pseudomonas aeruginosa. J Bacteriol. 2005;187(4):1246-53. Epub 2005/02/03. doi: 10.1128/jb.187.4.1246-1253.2005. PubMed PMID: 15687188; PMCID: PMC545639.

43. Wolter DJ, Smith-Moland E, Goering RV, Hanson ND, Lister PD. Multidrug resistance associated with mexXY expression in clinical isolates of Pseudomonas aeruginosa from a Texas hospital. Diagnostic microbiology and infectious disease. 2004;50(1):43-50. Epub 2004/09/24. doi: 10.1016/j.diagmicrobio.2004.05.004. PubMed PMID: 15380277.

44. Abdali N, Parks JM, Haynes KM, Chaney JL, Green AT, Wolloscheck D, Walker JK, Rybenkov VV, Baudry J, Smith JC, Zgurskaya HI. Reviving Antibiotics:

Efflux Pump Inhibitors That Interact with AcrA, a Membrane Fusion Protein of the AcrAB-TolC Multidrug Efflux Pump. ACS Infectious Diseases. 2016:acsinfecdis.6b00167-acsinfecdis.6b. doi: 10.1021/acsinfecdis.6b00167.

45. Lomovskaya O, Warren MS, Lee A, Galazzo J, Fronko R, Lee M, Blais J, Cho D, Chamberland S, Renau T, Leger R, Hecker S, Watkins W, Hoshino K, Ishida H, Lee VJ. Identification and characterization of inhibitors of multidrug resistance efflux pumps in Pseudomonas aeruginosa: novel agents for combination therapy. Antimicrob Agents Chemother. 2001;45(1):105-16. Epub 2000/12/20. doi: 10.1128/aac.45.1.105-116.2001. PubMed PMID: 11120952; PMCID: PMC90247.

46. Tanabe M, Szakonyi G, Brown KA, Henderson PJF, Nield J, Byrne B. The multidrug resistance efflux complex, EmrAB from Escherichia coli forms a dimer in vitro. Biochemical and Biophysical Research Communications. 2009;380(2):338-42. doi: https://doi.org/10.1016/j.bbrc.2009.01.081.

47. Kobayashi N, Nishino K, Yamaguchi A. Novel macrolide-specific ABC-type efflux transporter in Escherichia coli. J Bacteriol. 2001;183(19):5639-44. Epub 2001/09/07. doi: 10.1128/jb.183.19.5639-5644.2001. PubMed PMID: 11544226; PMCID: PMC95455.

48. Du D, van Veen HW, Murakami S, Pos KM, Luisi BF. Structure, mechanism and cooperation of bacterial multidrug transporters. Current Opinion in Structural Biology. 2015;33:76-91. doi: http://dx.doi.org/10.1016/j.sbi.2015.07.015.

49. Lu M, Symersky J, Radchenko M, Koide A, Guo Y, Nie R, Koide S. Structures of a Na+-coupled, substrate-bound MATE multidrug transporter. Proc Natl Acad Sci U S A. 2013;110(6):2099-104. Epub 2013/01/24. doi: 10.1073/pnas.1219901110. PubMed PMID: 23341609; PMCID: PMC3568332.

50. Yin Y, He X, Szewczyk P, Nguyen T, Chang G. Structure of the multidrug transporter EmrD from Escherichia coli. Science. 2006;312(5774):741-4. Epub 2006/05/06. doi: 10.1126/science.1125629. PubMed PMID: 16675700; PMCID: PMC3152482.

51. Wang Z, Fan G, Hryc CF, Blaza JN, Serysheva, II, Schmid MF, Chiu W, Luisi BF, Du D. An allosteric transport mechanism for the AcrAB-TolC multidrug efflux pump. eLife. 2017;6. Epub 2017/03/30. doi: 10.7554/eLife.24905. PubMed PMID: 28355133.

52. Fitzpatrick AWP, Llabres S, Neuberger A, Blaza JN, Bai XC, Okada U, Murakami S, van Veen HW, Zachariae U, Scheres SHW, Luisi BF, Du D. Structure of the MacAB-TolC ABC-type tripartite multidrug efflux pump. Nature microbiology. 2017;2:17070. Epub 2017/05/16. doi: 10.1038/nmicrobiol.2017.70. PubMed PMID: 28504659; PMCID: PMC5447821.

53. Fleishman SJ, Harrington SE, Enosh A, Halperin D, Tate CG, Ben-Tal N. Quasi-symmetry in the cryo-EM structure of EmrE provides the key to modeling its

transmembrane domain. J Mol Biol. 2006;364(1):54-67. Epub 2006/09/29. doi: 10.1016/j.jmb.2006.08.072. PubMed PMID: 17005200.

54. Ma D, Cook DN, Alberti M, Pon NG, Nikaido H, Hearst JE. Genes acrA and acrB encode a stress-induced efflux system of Escherichia coli. Molecular Microbiology. 1995;16(1):45-55. doi: 10.1111/j.1365-2958.1995.tb02390.x.

55. Krishnamoorthy G, Tikhonova EB, Dhamdhere G, Zgurskaya HI. On the role of TolC in multidrug efflux: The function and assembly of AcrAB-TolC tolerate significant depletion of intracellular TolC protein. Molecular Microbiology. 2013;87(5):982-97. doi: 10.1111/mmi.12143.

56. Zgurskaya HI, Nikaido H. Cross-linked complex between oligomeric periplasmic lipoprotein AcrA and the inner-membrane-associated multidrug efflux pump AcrB from Escherichia coli. J Bacteriol. 2000;182(15):4264-7. doi: 10.1128/JB.182.15.4264-4267.2000.

57. Tikhonova EB, Zgurskaya HI. AcrA, AcrB, and TolC of Escherichia coli Form a Stable Intermembrane Multidrug Efflux Complex. The Journal of biological chemistry. 2004;279(31):32116-24. doi: 10.1074/jbc.M402230200.

58. Nikaido H, Takatsuka Y. Mechanisms of RND Multidrug Efflux Pumps. Biochimica et biophysica acta. 2009;1794(5):769-81. doi: 10.1016/j.bbapap.2008.10.004. PubMed PMID: PMC2696896.

59. Zgurskaya HI, Yamada Y, Tikhonova EB, Ge Q, Krishnamoorthy G. Structural and functional diversity of bacterial membrane fusion proteins. Biochim Biophys Acta. 2009;1794(5):794-807. Epub 12/02. doi: 10.1016/j.bbapap.2008.10.010.

60. Murakami S, Nakashima R, Yamashita E, Matsumoto T, Yamaguchi A. Crystal structures of a multidrug transporter reveal a functionally rotating mechanism. Nature. 2006;443(7108):173-9. Epub 08/18. doi: 10.1038/nature05076.

61. Cha HJ, Muller RT, Pos KM. Switch-loop flexibility affects transport of large drugs by the promiscuous AcrB multidrug efflux transporter. Antimicrob Agents Chemother. 2014;58(8):4767-72. Epub 2014/06/11. doi: 10.1128/aac.02733-13. PubMed PMID: 24914123; PMCID: PMC4136034.

62. Nakashima R, Sakurai K, Yamasaki S, Nishino K, Yamaguchi A. Structures of the multidrug exporter AcrB reveal a proximal multisite drug-binding pocket. Nature. 2011;480(7378):565-9. Epub 11/29. doi: 10.1038/nature10641 10.1038/nature10641.

63. Seeger MA, Schiefner A, Eicher T, Verrey F, Diederichs K, Pos KM. Structural asymmetry of AcrB trimer suggests a peristaltic pump mechanism. Science. 2006;313(5791):1295-8. Epub 2006/09/02. doi: 10.1126/science.1131542. PubMed PMID: 16946072.

64. Symmons MF, Marshall RL, Bavro VN. Architecture and roles of periplasmic adaptor proteins in tripartite efflux assemblies. Frontiers in Microbiology. 2015;6:513. doi: 10.3389/fmicb.2015.00513. PubMed PMID: PMC4446572.

65. Ge Q, Yamada Y, Zgurskaya H. The C-terminal domain of AcrA is essential for the assembly and function of the multidrug efflux pump AcrAB-TolC. J Bacteriol. 2009;191(13):4365-71. Epub 2009/05/05. doi: 10.1128/jb.00204-09. PubMed PMID: 19411330; PMCID: PMC2698478.

66. Mikolosko J, Bobyk K, Zgurskaya HI, Ghosh P. Conformational flexibility in the multidrug efflux system protein AcrA. Structure. 2006;14(3):577-87. doi: 10.1016/j.str.2005.11.015.

67. Weeks JW, Celaya-Kolb T, Pecora S, Misra R. AcrA suppressor alterations reverse the drug hypersensitivity phenotype of a TolC mutant by inducing TolC aperture opening. Molecular microbiology. 2010;75(6):1468-83. doi: 10.1111/j.1365-2958.2010.07068.x. PubMed PMID: PMC2875072.

68. Ntreh AT, Weeks JW, Nickels LM, Zgurskaya HI. Opening the Channel: the Two Functional Interfaces of Pseudomonas aeruginosa OpmH with the Triclosan Efflux Pump TriABC. J Bacteriol. 2016;198(23):3176-85. Epub 2016/09/21. doi: 10.1128/jb.00535-16. PubMed PMID: 27645384; PMCID: PMC5105898.

69. Xu Y, Lee M, Moeller A, Song S, Yoon BY, Kim HM, Jun SY, Lee K, Ha NC. Funnel-like hexameric assembly of the periplasmic adapter protein in the tripartite multidrug efflux pump in gram-negative bacteria. J Biol Chem. 2011;286(20):17910-20. Epub 2011/04/02. doi: 10.1074/jbc.M111.238535. PubMed PMID: 21454662; PMCID: PMC3093866.

70. Zgurskaya HI, Weeks JW, Ntreh AT, Nickels LM, Wolloscheck D. Mechanism of coupling drug transport reactions located in two different membranes. Frontiers in Microbiology. 2015;6(FEB). doi: 10.3389/fmicb.2015.00100.

71. Xu Y, Lee M, Moeller A, Song S, Yoon B-Y, Kim H-M, Jun S-Y, Lee K, Ha N-C. Funnel-like Hexameric Assembly of the Periplasmic Adapter Protein in the Tripartite Multidrug Efflux Pump in Gram-negative Bacteria. The Journal of Biological Chemistry. 2011;286(20):17910-20. doi: 10.1074/jbc.M111.238535. PubMed PMID: PMC3093866.

72. Rosner JL, Martin RG. Reduction of cellular stress by TolC-dependent efflux pumps in Escherichia coli indicated by BaeSR and CpxARP activation of spy in efflux mutants. J Bacteriol. 2013;195(5):1042-50. Epub 2012/12/25. doi: 10.1128/jb.01996-12. PubMed PMID: 23264577; PMCID: PMC3571319.

73. Bavro VN, Pietras Z, Furnham N, Pérez-Cano L, Fernández-Recio J, Pei XY, Misra R, Luisi B. Assembly and Channel Opening in a Bacterial Drug Efflux Machine. Molecular Cell. 2008;30(1):114-21. doi: 10.1016/j.molcel.2008.02.015.

74. Du D, Wang Z, James NR, Voss JE, Klimont E, Ohene-Agyei T, Venter H, Chiu W, Luisi BF. Structure of the AcrAB-TolC multidrug efflux pump. Nature. 2014;509(7501):512-5. doi: 10.1038/nature13205.

75. Lu S, Zgurskaya HI. MacA, a periplasmic membrane fusion protein of the macrolide transporter MacAB-TolC, binds lipopolysaccharide core specifically and with high affinity. J Bacteriol. 2013;195(21):4865-72. Epub 2013/08/27. doi: 10.1128/jb.00756-13. PubMed PMID: 23974027; PMCID: PMC3807484.

76. Rutherford ST, Bassler BL. Bacterial quorum sensing: its role in virulence and possibilities for its control. Cold Spring Harbor Perspect Med. 2012;2(11):a012427/1-a/25. doi: 10.1101/cshperspect.a012427.

77. Ng W-L, Bassler BL. Bacterial quorum-sensing network architectures. Annu Rev Genet. 2009;43:197-222. doi: 10.1146/annurev-genet-102108-134304.

78. Welch M, Mikkelsen H, Swatton JE, Smith D, Thomas GL, Glansdorp FG, Spring DR. Cell-cell communication in Gram-negative bacteria. Molecular BioSystems. 2005;1(3):196-202. doi: 10.1039/B505796P.

79. Evans K, Passador L, Srikumar R, Tsang E, Nezezon J, Poole K. Influence of the MexAB-OprM multidrug efflux system on quorum sensing in Pseudomonas aeruginosa. J Bacteriol. 1998;180(20):5443-7. Epub 1998/10/10. PubMed PMID: 9765578; PMCID: PMC107595.

80. Minagawa S, Inami H, Kato T, Sawada S, Yasuki T, Miyairi S, Horikawa M, Okuda J, Gotoh N. RND type efflux pump system MexAB-OprM of Pseudomonas aeruginosa selects bacterial languages, 3-oxo-acyl-homoserine lactones, for cell-to-cell communication. BMC Microbiol. 2012;12:70. Epub 2012/05/12. doi: 10.1186/1471-2180-12-70. PubMed PMID: 22574700; PMCID: PMC3460771.

81. Lamarche MG, Deziel E. MexEF-OprN efflux pump exports the Pseudomonas quinolone signal (PQS) precursor HHQ (4-hydroxy-2-heptylquinoline). PLoS One. 2011;6(9):e24310. Epub 2011/10/01. doi: 10.1371/journal.pone.0024310. PubMed PMID: 21957445; PMCID: PMC3177830.

82. Olivares J, Alvarez-Ortega C, Linares JF, Rojo F, Kohler T, Martinez JL. Overproduction of the multidrug efflux pump MexEF-OprN does not impair Pseudomonas aeruginosa fitness in competition tests, but produces specific changes in bacterial regulatory networks. Environ Microbiol. 2012;14(8):1968-81. Epub 2012/03/16. doi: 10.1111/j.1462-2920.2012.02727.x. PubMed PMID: 22417660.

83. Aendekerk S, Diggle SP, Song Z, Hoiby N, Cornelis P, Williams P, Camara M, Høiby N, Cornelis P, Williams P, Cámara M. The MexGHI-OpmD multidrug efflux pump controls growth, antibiotic susceptibility and virulence in Pseudomonas aeruginosa via 4-quinolone-dependent cell-to-cell communication. Microbiology (Reading, U K). 2005;151(4):1113-25. doi: 10.1099/mic.0.27631-0.

84. Sakhtah H, Koyama L, Zhang Y, Morales DK, Fields BL, Price-Whelan A, Hogan DA, Shepard K, Dietrich LEP. The Pseudomonas aeruginosa efflux pump MexGHI-OpmD transports a natural phenazine that controls gene expression and biofilm development. Proceedings of the National Academy of Sciences of the United States of America. 2016;113(25):E3538-47. doi: 10.1073/pnas.1600424113.

85. Hirakata Y, Srikumar R, Poole K, Gotoh N, Suematsu T, Kohno S, Kamihira S, Hancock RE, Speert DP. Multidrug efflux systems play an important role in the invasiveness of Pseudomonas aeruginosa. The Journal of experimental medicine. 2002;196(1):109-18. Epub 2002/07/03. PubMed PMID: 12093875; PMCID: PMC2194012.

86. Alcalde-Rico M, Hernando-Amado S, Blanco P, Martinez JL. Multidrug efflux pumps at the crossroad between antibiotic resistance and bacterial virulence. Frontiers in Microbiology. 2016;7(SEP):1-14. doi: 10.3389/fmicb.2016.01483.

87. Maseda H, Sawada I, Saito K, Uchiyama H, Nakae T, Nomura N. Enhancement of the mexAB-oprM efflux pump expression by a quorum-sensing autoinducer and its cancellation by a regulator, MexT, of the mexEF-oprN efflux pump operon in Pseudomonas aeruginosa. Antimicrob Agents Chemother. 2004;48(4):1320-8. Epub 2004/03/30. PubMed PMID: 15047536; PMCID: PMC375252.

88. Aendekerk S, Ghysels B, Cornelis P, Baysse C. Characterization of a new efflux pump, MexGHI-OpmD, from Pseudomonas aeruginosa that confers resistance to vanadium. Microbiology. 2002;148(8):2371-81. doi: 10.1099/00221287-148-8-2371.

89. Masuda N, Sakagawa E, Ohya S, Gotoh N, Tsujimoto H, Nishino T. Substrate specificities of MexAB-OprM, MexCD-OprJ, and MexXY-oprM efflux pumps in Pseudomonas aeruginosa. Antimicrob Agents Chemother. 2000;44(12):3322-7. Epub 2000/11/18. PubMed PMID: 11083635; PMCID: PMC90200.

90. Minagawa S, Inami H, Kato T, Sawada S, Yasuki T, Miyairi S, Horikawa M, Okuda J, Gotoh N. RND type efflux pump system MexAB-OprM of pseudomonas aeruginosa selects bacterial languages, 3-oxo-acyl-homoserine lactones, for cell-to-cell communication. BMC Microbiology. 2012;12(1):70-. doi: 10.1186/1471-2180-12-70.

91. Fetar H, Gilmour C, Klinoski R, Daigle DM, Dean CR, Poole K. mexEF-oprN multidrug efflux operon of Pseudomonas aeruginosa: regulation by the MexT activator in response to nitrosative stress and chloramphenicol. Antimicrob Agents Chemother. 2011;55(2):508-14. Epub 2010/11/17. doi: 10.1128/aac.00830-10. PubMed PMID: 21078928; PMCID: PMC3028769.

92. Maseda H, Yoneyama H, Nakae T. Assignment of the substrate-selective subunits of the MexEF-OprN multidrug efflux pump of Pseudomonas aeruginosa. Antimicrob Agents Chemother. 2000;44(3):658-64. Epub 2000/02/19. PubMed PMID: 10681335; PMCID: PMC89743.

93. Sekiya H, Mima T, Morita Y, Kuroda T, Mizushima T, Tsuchiya T. Functional Cloning and Characterization of a Multidrug Efflux Pump , MexHI-OpmD , from a Pseudomonas aeruginosa Mutant Functional Cloning and Characterization of a Multidrug Efflux Pump , MexHI-OpmD , from a Pseudomonas aeruginosa Mutant. Antimicrobial Agents and Chemotherapy. 2003;47(9):2990-2. doi: 10.1128/AAC.47.9.2990.

94. Chuanchuen R, Murata T, Gotoh N, Schweizer HP. Substrate-dependent utilization of OprM or OpmH by the Pseudomonas aeruginosa MexJK efflux pump. Antimicrob Agents Chemother. 2005;49(5):2133-6. Epub 2005/04/28. doi: 10.1128/aac.49.5.2133-2136.2005. PubMed PMID: 15855547; PMCID: PMC1087666.

95. Chuanchuen R, Narasaki CT, Schweizer HP. The MexJK efflux pump of Pseudomonas aeruginosa requires OprM for antibiotic efflux but not for efflux of triclosan. J Bacteriol. 2002;184(18):5036-44. Epub 2002/08/24. PubMed PMID: 12193619; PMCID: PMC135324.

96. Mima T, Sekiya H, Mizushima T, Kuroda T, Tsuchiya T. Gene cloning and properties of the RND-type multidrug efflux pumps MexPQ-OpmE and MexMN-OprM from Pseudomonas aeruginosa. Microbiology and immunology. 2005;49(11):999-1002. Epub 2005/11/23. PubMed PMID: 16301811.

97. Li Y, Mima T, Komori Y, Morita Y, Kuroda T, Mizushima T, Tsuchiya T. A new member of the tripartite multidrug efflux pumps, MexVW-OprM, in Pseudomonas aeruginosa. The Journal of antimicrobial chemotherapy. 2003;52(4):572-5. Epub 2003/09/03. doi: 10.1093/jac/dkg390. PubMed PMID: 12951344.

98. Mima T, Kohira N, Li Y, Sekiya H, Ogawa W, Kuroda T, Tsuchiya T. Gene cloning and characteristics of the RND-type multidrug efflux pump MuxABC-OpmB possessing two RND components in Pseudomonas aeruginosa. Microbiology. 2009;155(Pt 11):3509-17. Epub 2009/08/29. doi: 10.1099/mic.0.031260-0. PubMed PMID: 19713238.

99. Mima T, Joshi S, Gomez-Escalada M, Schweizer HP. Identification and Characterization of TriABC-OpmH, a Triclosan Efflux Pump of Pseudomonas aeruginosa Requiring Two Membrane Fusion Proteins. Journal of Bacteriology. 2007;189(21):7600-9. doi: 10.1128/JB.00850-07. PubMed PMID: PMC2168734.

100. Hassan MT, van der Lelie D, Springael D, Romling U, Ahmed N, Mergeay M. Identification of a gene cluster, czr, involved in cadmium and zinc resistance in Pseudomonas aeruginosa. Gene. 1999;238(2):417-25. Epub 1999/11/26. PubMed PMID: 10570969.

101. Rensing C, Pribyl T, Nies DH. New functions for the three subunits of the CzcCBA cation-proton antiporter. J Bacteriol. 1997;179(22):6871-9. Epub 1997/11/26. PubMed PMID: 9371429; PMCID: PMC179623.

102. Vaara M. Agents that increase the permeability of the outer membrane. Microbiological reviews. 1992;56(3):395-411. Epub 1992/09/01. PubMed PMID: 1406489; PMCID: PMC372877.

103. Storm DR, Rosenthal KS, Swanson PE. Polymyxin and related peptide antibiotics. Annual review of biochemistry. 1977;46:723-63. Epub 1977/01/01. doi: 10.1146/annurev.bi.46.070177.003451. PubMed PMID: 197881.

104. Datsenko KA, Wanner BL. One-step inactivation of chromosomal genes in Escherichia coli K-12 using PCR products. Proceedings of the National Academy of Sciences. 2000;97(12):6640-5.

105. Dhamdhere G, Zgurskaya HI. Metabolic shutdown in Escherichia coli cells lacking the outer membrane channel TolC. Molecular Microbiology. 2010;77(3):743-54. doi: 10.1111/j.1365-2958.2010.07245.x.

106. Krishnamoorthy G, Wolloscheck D, Weeks JW, Croft C, Rybenkov VV, Zgurskaya HI. Breaking the Permeability Barrier of Escherichia coli by Controlled Hyperporination of the Outer Membrane. Antimicrobial agents and chemotherapy. 2016;60(12):7372-81. doi: 10.1128/AAC.01882-16.

107. Wolloscheck D, Krishnamoorthy G, Nguyen J, Zgurskaya HI. Kinetic control of quorum sensing in Pseudomonas aeruginosa by multidrug efflux pumps. 2017.

108. Schweizer HP, Hoang TT, Propst KL, Ornelas HR, Karkhoff-Schweizer RR. Vector Design and Development of Host Systems for Pseudomonas. In: Setlow JK, editor. Genetic Engineering: Principles and Methods: Principles and Methods. Boston, MA: Springer US; 2001. p. 69-81.

109. Hoang TT, Karkhoff-Schweizer RR, Kutchma AJ, Schweizer HP. A broad-host-range Flp-FRT recombination system for site-specific excision of chromosomally-located DNA sequences: Application for isolation of unmarked Pseudomonas aeruginosa mutants. Gene. 1998;212(1):77-86. doi: 10.1016/S0378-1119(98)00130-9.

110. Choi K-H, Schweizer HP. mini-Tn7 insertion in bacteria with single attTn7 sites: example Pseudomonas aeruginosa. Nature protocols. 2006;1(1):153-61. doi: 10.1038/nprot.2006.24.

111. Choi KH, Gaynor JB, White KG, Lopez C, Bosio CM, Karkhoff-Schweizer RR, Schweizer HP. A Tn7-based broad-range bacterial cloning and expression system. Nature methods. 2005;2(6):443-8. Epub 2005/05/24. doi: 10.1038/nmeth765. PubMed PMID: 15908923.

112. Vogel HJ, Bonner DM. Acetylornithinase of Escherichia coli: partial purification and some properties. J Biol Chem. 1956;218(1):97-106. Epub 1956/01/01. PubMed PMID: 13278318.

113. Wiegand I, Hilpert K, Hancock REW. Agar and broth dilution methods to determine the minimal inhibitory concentration (MIC) of antimicrobial substances. Nat Protocols. 2008;3(2):163-75.

114. Tikhonova EB, Wang Q, Zgurskaya HI. Chimeric analysis of the multicomponent multidrug efflux transporters from gram-negative bacteria. J Bacteriol. 2002;184(23):6499-507. Epub 2002/11/12. PubMed PMID: 12426337; PMCID: PMC135444.

115. Guendouze A, Plener L, Bzdrenga J, Jacquet P, Rémy B, Elias M, Lavigne J-P, Daudé D, Chabrière E. Effect of Quorum Quenching Lactonase in Clinical Isolates of Pseudomonas aeruginosa and Comparison with Quorum Sensing Inhibitors. Frontiers in Microbiology. 2017;8:227-.

116. Cox CD, Adams P. Siderophore activity of pyoverdin for Pseudomonas aeruginosa. Infection and Immunity. 1985;48(1):130-8. PubMed PMID: PMC261925.

117. O'Toole GA, Kolter R. Initiation of biofilm formation in Pseudomonas fluorescens WCS365 proceeds via multiple, convergent signalling pathways: a genetic analysis. Mol Microbiol. 1998;28(3):449-61. Epub 1998/06/19. PubMed PMID: 9632250.

118. Eftink MR. Fluorescence methods for studying equilibrium macromolecule-ligand interactions. Methods in enzymology. 1997;278:221-57. doi: 10.1016/S0076-6879(97)78013-3.

119. Niedzwiecka A, Stepinski J, Antosiewicz JM, Darzynkiewicz E, Stolarski R. Biophysical approach to studies of cap-eIF4E interaction by synthetic cap analogs. Methods in enzymology. 2007;430:209-45. Epub 2007/10/05. doi: 10.1016/s0076-6879(07)30009-8. PubMed PMID: 17913640.

120. Braun V. FhuA (TonA), the career of a protein. J Bacteriol. 2009;191(11):3431-6. Epub 2009/03/31. doi: 10.1128/jb.00106-09. PubMed PMID: 19329642; PMCID: PMC2681897.

121. Ferguson AD, Hofmann E, Coulton JW, Diederichs K, Welte W. Siderophore-mediated iron transport: crystal structure of FhuA with bound lipopolysaccharide. Science. 1998;282(5397):2215-20. Epub 1998/12/18. PubMed PMID: 9856937.

122. Mohammad MM, Howard KR, Movileanu L. Redesign of a plugged β-barrel membrane protein. Journal of Biological Chemistry. 2011;286(10):8000-13. doi: 10.1074/jbc.M110.197723.

123. Niedzwiecki DJ, Mohammad MM, Movileanu L. Inspection of the Engineered FhuA Δc/Δ4L Protein Nanopore by Polymer Exclusion. Biophysical Journal. 2012;103(10):2115-24. doi: 10.1016/j.bpj.2012.10.008.

124. Locher KP, Rees B, Koebnik R, Mitschler A, Moulinier L, Rosenbusch JP, Moras D. Transmembrane signaling across the ligand-gated FhuA receptor: crystal structures of free and ferrichrome-bound states reveal allosteric changes. Cell. 1998;95(6):771-8. Epub 1998/12/29. PubMed PMID: 9865695.

125. Parsek MR, Greenberg EP. Sociomicrobiology: the connections between quorum sensing and biofilms. Trends Microbiol. 2005;13(1):27-33. Epub 2005/01/11. doi: 10.1016/j.tim.2004.11.007. PubMed PMID: 15639629.

126. Juhas M, Eberl L, Tümmler B, Tummler B. Quorum sensing: the power of cooperation in the world of Pseudomonas. Environ Microbiol. 2005;7(4):459-71. Epub 04/09. doi: 10.1111/j.1462-2920.2005.00769.x.

127. Dietrich LEP, Price-Whelan A, Petersen A, Whiteley M, Newman DK. The phenazine pyocyanin is a terminal signalling factor in the quorum sensing network of Pseudomonas aeruginosa. Mol Microbiol. 2006;61(5):1308-21. Epub 08/02. doi: 10.1111/j.1365-2958.2006.05306.x.

128. Kohler T, Van DC, Curty LK, Hamzehpour MM, Pechere J-C. Overexpression of the MexEF-OprN multidrug efflux system affects cell-to-cell signaling in Pseudomonas aeruginosa. J Bacteriol. 2001;183(18):5213-22. doi: 10.1128/JB.183.18.5213-5222.2001.

129. Stintzi A, Evans K, Meyer JM, Poole K. Quorum-sensing and siderophore biosynthesis in Pseudomonas aeruginosa: lasR/lasI mutants exhibit reduced pyoverdine biosynthesis. FEMS Microbiol Lett. 1998;166(2):341-5. Epub 1998/10/14. PubMed PMID: 9770291.

130. Schalk IJ, Guillon L. Pyoverdine biosynthesis and secretion in Pseudomonas aeruginosa: implications for metal homeostasis. Environ Microbiol. 2013;15(6):1661-73. Epub 2012/11/07. doi: 10.1111/1462-2920.12013. PubMed PMID: 23126435.

131. Hocquet D, Roussel-Delvallez M, Cavallo JD, Plesiat P. MexAB-OprM- and MexXY-overproducing mutants are very prevalent among clinical strains of Pseudomonas aeruginosa with reduced susceptibility to ticarcillin. Antimicrob Agents Chemother. 2007;51(4):1582-3. Epub 2007/01/16. doi: 10.1128/aac.01334-06. PubMed PMID: 17220417; PMCID: PMC1855456.

132. Bohnert JA, Karamian B, Nikaido H. Optimized Nile Red efflux assay of AcrAB-TolC multidrug efflux system shows competition between substrates. Antimicrob Agents Chemother. 2010;54(9):3770-5. Epub 2010/07/08. doi: 10.1128/aac.00620-10. PubMed PMID: 20606071; PMCID: PMC2934970.

133. Helander IM, Mattila-Sandholm T. Fluorometric assessment of gram-negative bacterial permeabilization. Journal of applied microbiology. 2000;88(2):213-9. Epub 2000/03/29. PubMed PMID: 10735988.

134. Blair JM, Piddock LJ. How to Measure Export via Bacterial Multidrug Resistance Efflux Pumps. MBio. 2016;7(4). Epub 2016/07/07. doi: 10.1128/mBio.00840-16. PubMed PMID: 27381291; PMCID: PMC4958252.

135. Coldham NG, Webber M, Woodward MJ, Piddock LJV. A 96-well plate fluorescence assay for assessment of cellular permeability and active efflux in Salmonella enterica serovar Typhimurium and Escherichia coli. Journal of Antimicrobial Chemotherapy. 2010;65(8):1655-63. doi: 10.1093/jac/dkq169.

136. BNID: 111490, BioNumbers—the database of key numbers in molecular and cell biology [Internet]. Oxford University Press. 2010 [cited 10/23
07/16/received
10/02/accepted]. Available from:
http://www.ncbi.nlm.nih.gov/pmc/articles/PMC2808940/.

137. ThermoFisher. Macromolecular Components of E. coli and HeLa Cells www.thermofisher.com. Available from:
https://www.thermofisher.com/us/en/home/references/ambion-tech-support/rna-tools-and-calculators/macromolecular-components-of-e.html.

138. Westfall D, Krishnamoorthy G, Wolloscheck D, Sarkar R, Zgurskaya HI, Rybenkov VV. Bifurcation kinetics of drug uptake - submitted2017.

139. Hancock RE, Farmer SW, Li ZS, Poole K. Interaction of aminoglycosides with the outer membranes and purified lipopolysaccharide and OmpF porin of Escherichia coli. Antimicrobial Agents and Chemotherapy. 1991;35(7):1309-14. PubMed PMID: PMC245163.

140. Lewis K. Antibiotics: Recover the lost art of drug discovery. Nature. 2012;485(7399):439-40.

141. CDC. Antibiotic resistance threats in the United States, 2013. Current. 2013:114-. doi: CS239559-B.

142. Kojima S, Nikaido H. Permeation rates of penicillins indicate that Escherichia coli porins function principally as nonspecific channels. Proc Natl Acad Sci U S A. 2013;110(28):E2629-34. Epub 2013/06/27. doi: 10.1073/pnas.1310333110. PubMed PMID: 23798411; PMCID: PMC3710850.

143. Aires JR, Kohler T, Nikaido H, Plesiat P. Involvement of an active efflux system in the natural resistance of Pseudomonas aeruginosa to aminoglycosides. Antimicrob Agents Chemother. 1999;43(11):2624-8. Epub 1999/10/30. PubMed PMID: 10543738; PMCID: PMC89534.

144. Hocquet D, Vogne C, El Garch F, Vejux A, Gotoh N, Lee A, Lomovskaya O, Plesiat P. MexXY-OprM efflux pump is necessary for a adaptive resistance of Pseudomonas aeruginosa to aminoglycosides. Antimicrob Agents Chemother.

2003;47(4):1371-5. Epub 2003/03/26. PubMed PMID: 12654672; PMCID: PMC152483.

145. Shaw KJ, Rather PN, Hare RS, Miller GH. Molecular genetics of aminoglycoside resistance genes and familial relationships of the aminoglycoside-modifying enzymes. Microbiological reviews. 1993;57(1):138-63. Epub 1993/03/01. PubMed PMID: 8385262; PMCID: PMC372903.

146. Bellido F, Martin NL, Siehnel RJ, Hancock RE. Reevaluation, using intact cells, of the exclusion limit and role of porin OprF in Pseudomonas aeruginosa outer membrane permeability. J Bacteriol. 1992;174(16):5196-203. Epub 1992/08/01. PubMed PMID: 1322882; PMCID: PMC206352.

147. Islam S, Jalal S, Wretlind B. Expression of the MexXY efflux pump in amikacin-resistant isolates of Pseudomonas aeruginosa. Clinical Microbiology and Infection. 2004;10(10):877-83. doi: http://dx.doi.org/10.1111/j.1469-0691.2004.00991.x.

148. Ntreh AT, Weeks JW, Nickels LM, Zgurskaya HI. Opening the Channel: the Two Functional Interfaces of Pseudomonas aeruginosa OpmH with the Triclosan Efflux Pump TriABC. Journal of bacteriology. 2016;198(23):3176-85. doi: 10.1128/JB.00535-16.

149. Weeks JW, Nickels LM, Ntreh AT, Zgurskaya HI. Non-equivalent roles of two periplasmic subunits in the function and assembly of triclosan pump TriABC from Pseudomonas aeruginosa. Molecular microbiology. 2015;98(2):343-56. doi: 10.1111/mmi.13124. PubMed PMID: PMC4690728.

150. World Health O. Global priority list of antibiotic-resistant bacteria to guide research, discovery, and development of new antibiotics2017.

151. Dreier J, Ruggerone P. Interaction of antibacterial compounds with RND efflux pumps in Pseudomonas aeruginosa. Frontiers in Microbiology. 2015;6:660. doi: 10.3389/fmicb.2015.00660. PubMed PMID: PMC4495556.

152. Kumar A, Schweizer HP. Bacterial resistance to antibiotics: Active efflux and reduced uptake. Advanced Drug Delivery Reviews. 2005;57(10):1486-513. doi: https://doi.org/10.1016/j.addr.2005.04.004.

153. Kohler T, Michea-Hamzehpour M, Henze U, Gotoh N, Curty LK, Pechere JC. Characterization of MexE-MexF-OprN, a positively regulated multidrug efflux system of Pseudomonas aeruginosa. Mol Microbiol. 1997;23(2):345-54. Epub 1997/01/01. PubMed PMID: 9044268.

154. Kohler T, van Delden C, Curty LK, Hamzehpour MM, Pechere JC. Overexpression of the MexEF-OprN multidrug efflux system affects cell-to-cell signaling in Pseudomonas aeruginosa. J Bacteriol. 2001;183(18):5213-22. Epub 2001/08/22. PubMed PMID: 11514502; PMCID: PMC95401.

155. Nagakubo S, Nishino K, Hirata T, Yamaguchi A. The putative response regulator BaeR stimulates multidrug resistance of Escherichia coli via a novel multidrug exporter system, MdtABC. J Bacteriol. 2002;184(15):4161-7. Epub 07/11.

156. Mima T, Joshi S, Gomez-Escalada M, Schweizer HP. Identification and characterization of TriABC-OpmH, a triclosan efflux pump of Pseudomonas aeruginosa requiring two membrane fusion proteins. J Bacteriol. 2007;189(21):7600-9. Epub 2007/08/28. doi: JB.00850-07 [pii]
10.1128/JB.00850-07. PubMed PMID: 17720796; PMCID: 2168734.

157. Hobbs EC, Yin X, Paul BJ, Astarita JL, Storz G. Conserved small protein associates with the multidrug efflux pump AcrB and differentially affects antibiotic resistance. Proceedings of the National Academy of Sciences. 2012;109(41):16696-701. doi: 10.1073/pnas.1210093109.

158. Hodgkinson JT, Gross J, Baker YR, Spring DR, Welch M. A new Pseudomonas quinolone signal (PQS) binding partner: MexG. Chem Sci. 2016;7(4):2553-62. doi: 10.1039/C5SC04197J.

159. Krishnamoorthy G, Leus IV, Weeks JW, Wolloscheck D, Rybenkov VV, Zgurskaya HI. Synergy between active efflux and outer membrane diffusion defines rules of antibiotic permeation into Gram-negative bacteria. submitted. 2017.

160. Krishnamoorthy G, Wolloscheck D, Weeks JW, Croft C, Rybenkov VV, Zgurskaya HI. Breaking the Permeability Barrier of Escherichia coli by Controlled Hyperporination of the Outer Membrane. Antimicrob Agents Chemother. 2016;60(12):7372-81. doi: 10.1128/AAC.01882-16. PubMed PMID: 27697764; PMCID: PMC5119019.

161. Krishnamoorthy G, Wolloscheck D, Weeks JW, Zgurskaya HI. When the permeability barrier is broken: physiology of hyperporinated Pseudomonas aeruginosa strains. Mol Microbiol. 2017;submitted.

162. Rada B, Leto TL. Pyocyanin effects on respiratory epithelium: relevance in Pseudomonas aeruginosa airway infections. Trends in microbiology. 2013;21(2):73-81. doi: 10.1016/j.tim.2012.10.004.

163. Rada B, Leto TL. Redox warfare between airway epithelial cells and Pseudomonas: dual oxidase versus pyocyanin. Immunologic research. 2009;43(1-3):198-209. Epub 2008/11/04. doi: 10.1007/s12026-008-8071-8. PubMed PMID: 18979077; PMCID: PMC2776630.

164. Schwarzer C, Fischer H, Kim EJ, Barber KJ, Mills AD, Kurth MJ, Gruenert DC, Suh JH, Machen TE, Illek B. Oxidative stress caused by pyocyanin impairs CFTR Cl(-) transport in human bronchial epithelial cells. Free radical biology & medicine. 2008;45(12):1653-62. Epub 2008/10/11. doi: 10.1016/j.freeradbiomed.2008.09.011. PubMed PMID: 18845244; PMCID: PMC2628806.

165. Lau GW, Hassett DJ, Ran H, Kong F. The role of pyocyanin in Pseudomonas aeruginosa infection. Trends in Molecular Medicine. 2004;10(12):599-606. doi: http://dx.doi.org/10.1016/j.molmed.2004.10.002.

166. Baron SS, Rowe JJ. Antibiotic action of pyocyanin. Antimicrob Agents Chemother. 1981;20(6):814-20. Epub 1981/12/01. PubMed PMID: 6798928; PMCID: PMC181804.

167. Kerr JR, Taylor GW, Rutman A, Høiby N, Cole PJ, Wilson R. Pseudomonas aeruginosa pyocyanin and 1-hydroxyphenazine inhibit fungal growth. Journal of Clinical Pathology. 1999;52(5):385.

168. Price-Whelan A, Dietrich LE, Newman DK. Pyocyanin alters redox homeostasis and carbon flux through central metabolic pathways in Pseudomonas aeruginosa PA14. J Bacteriol. 2007;189(17):6372-81. Epub 2007/05/29. doi: 10.1128/jb.00505-07. PubMed PMID: 17526704; PMCID: PMC1951912.

169. Schweizer HP, Hoang TT, Propst KL, Ornelas HR, Karkhoff-Schweizer RR. Vector design and development of host systems for Pseudomonas. Genetic engineering. 2001;23:69-81. Epub 2001/09/26. PubMed PMID: 11570107.

170. Chen AY, Yu C, Gatto B, Liu LF. DNA minor groove-binding ligands: a different class of mammalian DNA topoisomerase I inhibitors. Proceedings of the National Academy of Sciences of the United States of America. 1993;90(17):8131-5. PubMed PMID: PMC47302.

171. Meletiadis J, Pournaras S, Roilides E, Walsh TJ. Defining fractional inhibitory concentration index cutoffs for additive interactions based on self-drug additive combinations, Monte Carlo simulation analysis, and in vitro-in vivo correlation data for antifungal drug combinations against Aspergillus fumigatus. Antimicrob Agents Chemother. 2010;54(2):602-9. Epub 2009/12/10. doi: 10.1128/aac.00999-09. PubMed PMID: 19995928; PMCID: PMC2812160.

172. Te Dorsthorst DT, Verweij PE, Meis JF, Punt NC, Mouton JW. Comparison of fractional inhibitory concentration index with response surface modeling for characterization of in vitro interaction of antifungals against itraconazole-susceptible and -resistant Aspergillus fumigatus isolates. Antimicrob Agents Chemother. 2002;46(3):702-7. Epub 2002/02/19. PubMed PMID: 11850251; PMCID: PMC127491.

173. Botelho MG. Fractional inhibitory concentration index of combinations of antibacterial agents against cariogenic organisms. Journal of Dentistry. 2000;28(8):565-70. doi: http://dx.doi.org/10.1016/S0300-5712(00)00039-7.

174. Chaturvedi V, Ramani R, Andes D, Diekema DJ, Pfaller MA, Ghannoum MA, Knapp C, Lockhart SR, Ostrosky-Zeichner L, Walsh TJ, Marchillo K, Messer S, Welshenbaugh AR, Bastulli C, Iqbal N, Paetznick VL, Rodriguez J, Sein T. Multilaboratory testing of two-drug combinations of antifungals against Candida albicans, Candida glabrata, and Candida parapsilosis. Antimicrob Agents Chemother.

2011;55(4):1543-8. Epub 2011/02/02. doi: 10.1128/aac.01510-09. PubMed PMID: 21282457; PMCID: PMC3067183.

Appendix A: List of primers

Primer Name	Sequence (5' – 3')
EFNpbspFWD	ATGCGGTACCAGGAGGAATTCACCATGGAA CAGTCATCCCACTTCTCC
EFNpbspREV	TATTAAGCTTAATGGTGATGGTGATGGTGGG CGCTGGGTTGCCAGCCACC
GHIDpbspFWD	TTAGAAGCTTAGGAGGAATTCACCATGCAG CGCTTCATCGATAAC
GHIDpbspREVhis	ATATGGATCCTCAATGGTGATGGTGATGGTG ACGGTTGGCCCCGGCGG
GpbspREVhis	ATATGGATCCTCAATGATGATGATGATGATG GGCCTTCTGGTAGGTGGC
GHpbspREVhis	ATATGGATCCTCAATGATGATGATGATGATG GCGGCCGGCGACCGGCAC
GHIpbspREVhis	ATATGGATCCTCAATGATGATGATGATGATG ATGATGATGATGTGCCTTGTTCACCAGCAGA TCGG
HIDpbspFWDhis	TTAGAAGCTTAGGAGGAATTCACCATGCAG AAACCCGTCCTGATC
GpbspFWDflag	TTAGAAGCTTAGGAGGAATTCACCATGGACT ACAAAGACGATGACGACAAGGGAGGACAGC GCTTCATCGATAACTCG

GHIDnestedFWD	ATATGGTACCTAAGCGGTCATCCGCACTAC
GHIDnestedREV	ATATAAGCTTCGATGAAGGCGAGCAA
GHIDupFWD	ATATGAATTCCGAATAACGCCAGGGGCGTTATC
GHIDupREV	ATATGGTACCGGGTCGTTCCTTGTGCTGGTC
GHIDdownFWD	ATATCTGCAGCCTGGGCGGCTTCATCGGTTTC
GHIDdownREV	ATATAAGCTTTCAACGGTTGGCCCCGGCGG
SalIfrtGMfrtFWD	ATATGTCGACCTTGCGGCCCGGACGATCGAATTGG
SalIfrtGMfrtREV	ATATGTCGACGTGAGCGCAACGCAATGCATGATCG
GdHWfwd	CGCCGGTCTTGCTCGCGAAGGTGGCGACGATGAGGATGG
GdHWrev	CCATCCTCATCGTCGCCACCTTCGCGAGCAA

	GACCGGCG
Greg1FWD	GCCAGGCAGATCGCGGCGGTCAGCGCGAGC
	GCGTTGCTTTCGAG
Greg1REV	CTCGAAAGCAACGCGCTCGCGCTGACCGCC
	GCGATCTGCCTGGC
Greg2FWD	GCGCGCATTTCCTCCAGGGCGGCCGCAGCGT
	CGAACAGCTTCGCCAG
Greg2REV	CTGGCGAAGCTGTTCGACGCTGCGGCCGCCC
	TGGAGGAAATGCGCGC
Greg3FWD	GGCGGTGGCGATGGCGAACAGCGCGGCCGG
	CTCCAGG
Greg3REV	CCTGGAGCCGGCCGCGCTGTTCGCCATCGCC
	ACCGCC
Greg4FWD	GGCGCCGAGCGCTAGCTTGCGGTCCAGCAG
Greg4REV	CTGCTGGACCGCAAGCTAGCGCTCGGCGCC
Greg6FWD	GCCGATCACCGCGATGGCTGCGAGGGCGAA
	GAACAT
Greg6REV	ATGTTCTTCGCCCTCGCAGCCATCGCGGTGA
	TCGGC
GHIDayFWD	TTAGGAGCTCAGGAGGaattcaccATGCAGCGCT

	TCATCGATAAC
GHIDayREV	ATATAAGCTTTCAATGGTGATGGTGATGGTG
	ACGGTTGGCCCCGGCGG

Appendix B: Drug library results *E. coli*

MICs in μM

Cephalosporins	Molecular weight (g/mol)	WT	WT-Pore	ΔTolC	ΔTolC-Pore
ceftriaxone sodium trihydrate	554.58	0.10	0.02	0.10	0.00
ceftibuten	410.425	1.56	0.39	1.56	0.39
cefdinir	395.414	0.39	0.10	0.39	0.10
cefepime hydrochloride	481.568	0.10	0.10	0.10	0.10
cefmenoxime hydrochloride	511.558	2000.00	1000.00	250.00	250.00
ceforanide	519.554	3.91	3.91	3.91	3.91
cefotetan	575.619	0.98	0.24	0.98	0.24
cefamandole sodium	462.503	1.56	0.39	0.39	0.10
cefmetazole sodium	471.534	1000.00	250.00	250.00	250.00
cefamandole nafate	490.513	3.91	3.91	3.91	0.98
cefoperazone	645.667	0.39	0.02	0.02	0.00
cephalexin	347.389	62.50	62.50	62.50	62.50
cefsulodin sodium	531.539	250.00	250.00	62.50	62.50
cefoxitin sodium	427.452	6.25	1.56	6.25	1.56
cefuroxime sodium	424.385	15.63	0.98	0.98	0.24
cephalosporin c zn	415.418	1000.00	1000.00	1000.00	1000.00
cefaclor	367.807	3.91	3.91	3.91	3.91
cephradine	349.405	2000.00	2000.00	1000.00	1000.00
cefadroxil	363.388	62.50	62.50	62.50	62.50
cefazolin sodium	454.507	6.25	6.25	6.25	6.25
cefotaxime sodium	455.465	0.10	0.01	0.02	0.01
cephalothin sodium	396.438	15.63	3.91	15.63	3.91
cephapirin sodium	423.463	62.50	15.63	62.50	15.63
cefonicid sodium	542.566	25.00	1.56	25.00	1.56
cefprozil	389.426	25.00	6.25	25.00	6.25
ceftazidime	546.576	1.56	0.39	1.56	0.39
cefalonium	458.511	6.25	6.25	6.25	6.25
cefpiramide	612.637	2000.00	2000.00	2000.00	2000.00

Beta-Lactams	Molecular weight (g/mol)	WT	WT-Pore	ΔTolC	ΔTolC-Pore
azlocillin sodium	461.492	62.50	0.98	15.63	0.24
meropenem	383.463	0.39	0.39	0.39	0.39
oxacillin sodium	401.436	2000.00	62.50	0.98	0.98
penicillin g potassium	334.39	250.00	3.91	62.50	3.91
penicillin v potassium	350.39	1000.00	62.50	62.50	3.91
piperacillin sodium	517.555	25.00	6.25	1.56	0.02
cloxacillin sodium, cloxacillin	435.881	1000.00	250.00	0.98	0.98
dicloxacillin sodium	470.326	1000.00	62.50	0.98	0.98
hetacillin potassium	389.469	15.63	3.91	15.63	0.98
methicillin sodium	380.415	2000.00	250.00	15.63	15.63
moxalactam disodium	520.473	3.91	3.91	3.91	0.98
nafcillin sodium	414.475	1000.00	62.50	3.91	0.98
amoxicillin	365.404	62.50	15.63	62.50	15.63
ampicillin sodium, ampicillin	349.405	2000.00	250.00	1000.00	15.63
carbenicillin disodium, carbenicillin	378.4	250.00	15.63	62.50	15.63
ticarcillin disodium	384.427	2000	2000	1000	1000

Fluoroquinolones	Molecular weight (g/mol)	WT	WT-Pore	ΔTolC	ΔTolC-Pore
ciprofloxacin	331.342	0.39	0.1	0.1	0.02
enrofloxacin	359.395	1	0.25	0.25	0.02
levofloxacin	361.368	1	0.25	0.25	0.02
gatifloxacin	375.394	1	0.25	0.25	0.02
moxifloxacin hydrochloride	429.484	6.25	0.39	0.39	0.02
prulifloxacin	443.425	0.25	0.06	0.02	0
sparfloxacin	392.4	1	0.25	0.25	0.02
difloxacin hydrochloride	399.391	1.56	0.39	0.39	0.1
lomefloxacin	351.348	1.56	1.56	0.39	0.1
ofloxacin	361.368	1.56	0.39	0.39	0.1
pazufloxacin mesylate	318.3	1	0.25	0.25	0.02
oxolinic acid	261.23	100	25	6.25	1.56
flumequine	261.248	1	1	0.25	0.06
norfloxacin	319.331	1	0.25	0.06	0.02
pefloxacine mesylate	333.357	0.39	0.39	0.1	0.02
sarafloxacin hydrochloride	385.364	6.25	0.39	0.1	0.02
nadifloxacin	360.38	1.56	0.39	0.39	0.1

orbifloxacin	395.38	0.39	0.1	0.1	0.02

Sulfonamides	Molecular weight (g/mol)	WT	WT-Pore	ΔTolC	ΔTolC-Pore
sulfameter	280.303	1000	1000	1000	1000
sulfamethoxypyridazine	280.303	1000	1000	2000	1000
phthalylsulfathiazole	403.432	1000	1000	1000	1000
sulfachlorpyridazine	284.722	1000	1000	1000	1000
sulfaphenazole	314.362	2000	1000	1000	1000
sulfadimethoxine	310.329	2000	2000	2000	2000
sulfaquinoxaline sodium	300.336	2000	1000	250	1000
sulfaguanidine	214.245	2000	1000	2000	2000
sulfamonomethoxine	280.303	1000	250	250	250
sulfamethazine	278.33	2000	2000	2000	2000
sulfamethizole	270.331	2000	2000	250	250
sulfamethoxazole	253.278	1000	250	1000	1000
sulfapyridine	249.289	2000	2000	2000	1000
sulfathiazole	255.317	2000	2000	250	250
sulfisoxazole	267.304	2000	2000	250	250
sulfanilamide	172.205	2000	2000	2000	2000
sulfabenzamide	276.311	1000	1000	1000	1000
sulfacetamide	214.242	2000	2000	2000	2000
sulfadiazine	250.277	1000	2000	2000	2000
sulfamerazine	264.304	1000	1000	1000	1000
sulfisoxazole acetyl	309.341	2000	2000	250	250
sulfacarbamide	215.23	2000	2000	250	250
sulfadoxine	310.329	1000	1000	1000	1000

Appendix C: Drug library results *P. aeruginosa*

MICs in μM

Cephalosporins	Molecular weight (g/mol)	PAO1	PAO1-Pore	PΔ3	PΔ3-Pore	PΔ6	PΔ6-Pore
ceftriaxone sodium trihydrate	554.58	15.6	0.97	3.9	0.015	3.9	0.061
ceftibuten	410.425	4000	2000	1000	1000	1000	62.5
cefdinir	395.414	1000	1000	1000	1000	1000	62.5
cefepime hydrochloride	481.568	3.9	0.24	0.24	0.061	0.24	0.061
cefmenoxime hydrochloride	511.558	15.6	0.97	0.97	0.0152	0.24	0.0152
ceforanide	519.554	2000	2000	2000	2000	2000	250
cefotetan	575.619	1000	62.5	1000	62.5	250	62.5
cefamandole sodium	462.503	2000	2000	2000	1000	1000	250
cefmetazole sodium	471.534	2000	2000	1000	250	1000	250
cefamandole nafate	490.513	2000	2000	2000	1000	1000	250
cefoperazone	645.667	3.9	0.24	0.97	0.97	0.97	0.97
cephalexin	347.389	4000	4000	4000	4000	4000	250
cefsulodin sodium	531.539	3.9	0.97	0.97	0.24	0.97	0.24
cefoxitin sodium	427.452	2000	1000	2000	250	1000	62.5
cefuroxime sodium	424.385	1000	250	1000	250	1000	250
cephalosporin c zn	415.418	1000	1000	1000	1000	1000	1000
cefaclor	367.807	2000	2000	2000	250	1000	62.5
cephradine	349.405	2000	2000	2000	2000	2000	2000
cefadroxil	363.388	2000	2000	2000	2000	2000	2000
cefazolin sodium	454.507	2000	2000	2000	2000	2000	2000
cefotaxime sodium	455.465	62.5	3.9	3.9	3.9	3.9	3.9
cephalothin sodium	396.438	2000	2000	2000	2000	2000	1000
cephapirin sodium	423.463	2000	2000	2000	2000	2000	1000
cefprozil	389.426	1000	1000	1000	1000	1000	250
ceftazidime	546.576	3.9	0.24	3.9	0.24	3.9	0.24
cefalonium	458.511	1000	1000	1000	1000	1000	250
cefpiramide	360.38	2000	2000	2000	2000	2000	250

Beta-Lactams	Molecular weight (g/mol)	PAO1	PAO1-Pore	PΔ3	PΔ3-Pore	PΔ6	PΔ6-Pore
azlocillin sodium	461.492	62.5	3.9	3.9	0.24	3.9	0.061
ofloxacin	361.368	1.56	0.39	0.39	0.097	0.097	0.024
meropenem	383.463	6.25	1.56	0.39	0.097	0.39	0.097
oxacillin sodium	401.436	2000	250	250	3.90625	62.5	0.97
penicillin g potassium	334.39	2000	2000	2000	250	1000	250
penicillin v potassium	350.39	2000	2000	2000	250	2000	250
piperacillin sodium	517.555	15.625	0.97	0.97	0.97	3.9	0.061
cloxacillin sodium, cloxacillin	435.881	8000	1000	1000	62.5	1000	3.9
dicloxacillin sodium	470.326	2000	1000	62.5	3.9	62.5	3.9
hetacillin potassium	389.469	2000	250	1000	15.6	1000	15.6
methicillin sodium	380.415	2000	250	15.6	3.9	15.6	0.24
moxalactam disodium	520.473	62.5	15.625	62.5	0.97	62.5	0.97
nafcillin sodium	414.475	1000	62.5	62.5	0.24	3.9	0.24
amoxicillin	365.404	1000	1000	1000	62.5	1000	15.6
ampicillin sodium, ampicillin	349.405	4000	62.5	1000	62.5	250	62.5
carbenicillin disodium, carbenicillin	378.4	1000	250	15.6	0.97	15.6	0.24
ticarcillin disodium	384.427	4000	4000	4000	2000	2000	500

Fluoroquinolones	Molecular weight (g/mol)	PAO1	PAO1-Pore	PΔ3	PΔ3-Pore	PΔ6	PΔ6-Pore
ciprofloxacin	331.342	0.39	0.1	0.1	0.02	0.02	0.006
enrofloxacin	359.395	1	0.25	0.25	0.02	0.06	0.004
levofloxacin	361.368	1	0.25	0.25	0.02	0.02	0.004
gatifloxacin	375.394	1	0.25	0.25	0.02	0.06	0.004
moxifloxacin hydrochloride	429.484	6.25	0.39	0.39	0.02	0.1	0.024
prulifloxacin	443.425	0.25	0.06	0.02	0	0.02	0.004
sparfloxacin	392.4	1	0.25	0.25	0.02	0.02	0.004
difloxacin hydrochloride	399.391	1.56	0.39	0.39	0.1	0.39	0.097
lomefloxacin	351.348	1.56	1.56	0.39	0.1	0.1	0.024
ofloxacin	361.368	1.56	0.39	0.39	0.1	0.1	0.024
pazufloxacin mesylate	318.3	1	0.25	0.25	0.02	0.02	0.016
flumequine	261.248	100	25	6.25	1.56	1.56	0.097
norfloxacin	319.331	1	1	0.25	0.06	0.06	0.016
pefloxacine mesylate	333.357	1	0.25	0.06	0.02	0.02	0.004
sarafloxacin hydrochloride	385.364	0.39	0.39	0.1	0.02	0.02	0.006
nadifloxacin	612.6375	6.25	0.39	0.1	0.02	0.1	0.002
orbifloxacin	395.38	1.56	0.39	0.39	0.1	0.1	0.006

Sulfonamides	Molecular weight (g/mol)	PAO1	PAO1-Pore	PΔ3	PΔ3-Pore	PΔ6	PΔ6-Pore
sulfameter	280.303	1000	1000	250	250	250	62.5
sulfamethoxypyridazine	280.303	1000	1000	250	250	250	62.5
phthalylsulfathiazole	403.432	1000	1000	1000	1000	1000	1000
sulfachlorpyridazine	284.722	1000	1000	250	250	250	250
sulfaphenazole	314.362	1000	1000	1000	250	1000	250
sulfadimethoxine	310.329	1000	1000	1000	250	1000	250
sulfaquinoxaline sodium	300.336	1000	1000	1000	4000	1000	250
sulfaguanidine	214.245	4000	4000	4000	4000	4000	4000
sulfamonomethoxine	280.303	1000	1000	250	250	250	62.5

sulfamethazine	278.33	1000	1000	250	250	250	250
sulfamethizole	270.331	250	250	250	250	250	250
sulfamethoxazole	253.278	1000	250	250	62.5	250	62.5
sulfapyridine	249.289	1000	1000	250	250	250	250
sulfathiazole	255.317	250	250	62.5	62.5	250	62.5
sulfisoxazole	267.304	250	250	250	62.5	250	62.5
sulfanilamide	172.205	4000	4000	4000	4000	4000	4000
sulfabenzamide	276.311	1000	1000	1000	1000	1000	1000
sulfacetamide	214.242	4000	4000	1000	1000	4000	1000
sulfadiazine	250.277	1000	1000	250	250	1000	250

Appendix D: LN(OD_{600}) vs time plots of growth curves

LN(OD) vs time plots of growth measurements. The steepest part of the curve was used to calculate growth rates using linear regression. Six time points were used to determine the rates and were selected based on the highest coefficient of determination (r^2).

E. coli:

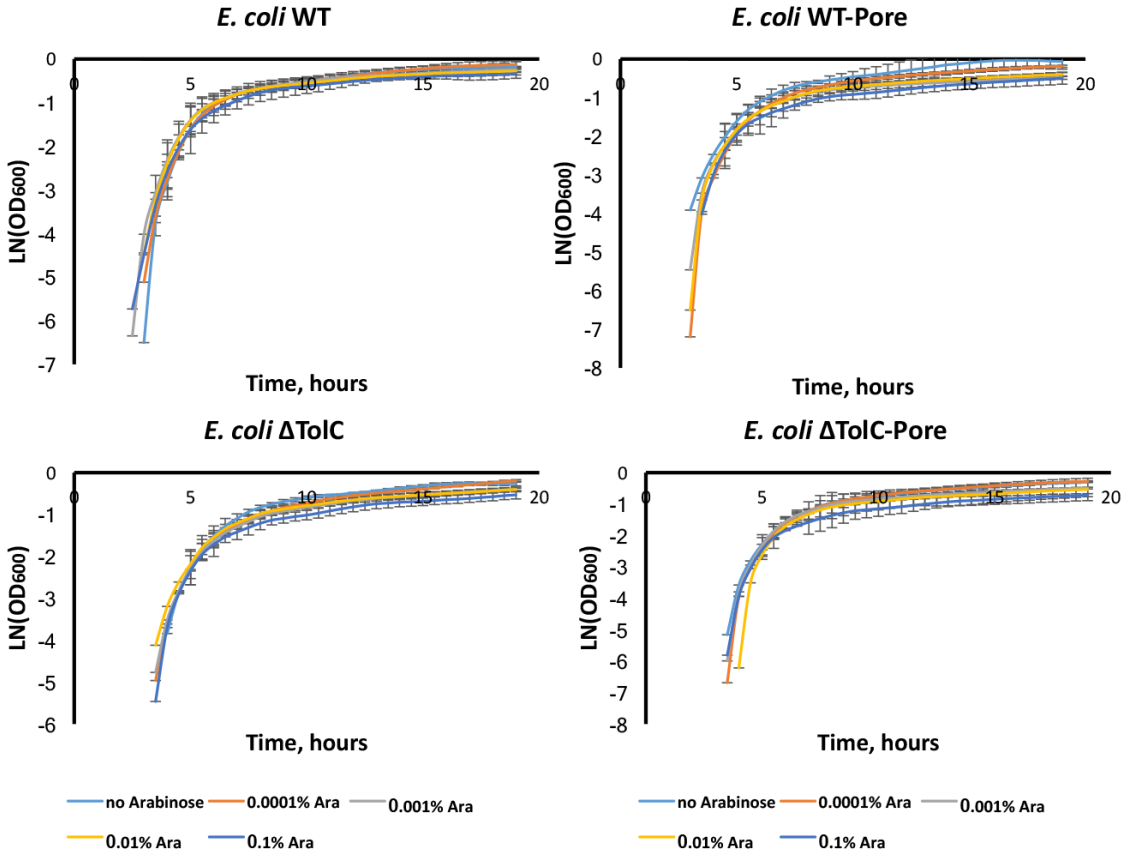

P. aeruginosa: